A STUDY OF THE EXTERNAL WIND PRESSURE DISTRIBUTIONS AND INDUCED INTERNAL VENTILATION FLOW IN LOW-RISE INDUSTRIAL AND DOMESTIC STRUCTURES

By

B. J. VICKERY
R. E. BADDOUR
C. A. KARAKATSANIS

For Florida Solar Energy Centre
300 State Road 401
Cape Canaveral, Florida
U.S.A. 32920

JANUARY 1983

BLWT-SS2-1983

BOUNDARY LAYER WIND TUNNEL LABORATORY
THE UNIVERSITY OF WESTERN ONTARIO
FACULTY OF ENGINEERING SCIENCE
LONDON, ONTARIO, CANADA
N6A 5B9

A STUDY OF THE EXTERNAL WIND PRESSURE DISTRIBUTONS AND INDUCED INTERNAL VENTILATION FLOWS IN LOW-RISE INDUSTRIAL AND DOMESTIC STRUCTURES

B. J. Vickery, R. E. Baddour, C. A. Karakatsanis

BLWT-SS2-1983

TABLE OF CONTENTS

TABLE OF CONTENTS (Cont'd)

1.0 INTRODUCTION

1.1 Background

A prime force producing internal flows in a naturally ventilated structure is the external wind pressure field. Even in comparatively light winds these pressures will exceed those generated by thermal or "stack" effects. For a building height of 30 feet the pressure difference created by a 10^{o}F temperature difference between the interior and exterior is of the same order as those created by wind at a speed of about 4 mph.

If the external pressure distribution is known together with the size, shape and disposition of both the external openings and the internal flow paths, then the internal flows can be computed by established procedures. The procedures involved have been described by Vickery (1) and have been applied in a feasilility study related to the provision of a natural ventilation system in a 600 ft. office building. A difficulty which arises in the computation of these flows is the possible interaction between the pressure field and the flow through the building. If the openings are comparatively small the flow through the building from high to low pressure regions will not influence the external pressure field but as the openings increase in size the flow will eventually modify the pressure field and computations based upon the pressures measured on a sealed structure will be in error. It has been suggested (2) that if the openings do not exceed 10% to 20% of the wall area then the errors will not be significant but the data available on this point are extremely limited. An evaluation of the accuracy of internal flow estimates deduced from the external pressure distribution measured on sealed models is one of the aims of the proposed study.

Central to the computation of internal flow rates is a knowledge of the external pressure distribution. Although the pressure distributions on low-rise buildings have been studied extensively, the object, in the main, has been the determination of wind loads for use in the structural design of the building. With this end in mind, the attention has been concentrated on maximum (or minimum) values and the data gathered have been presented in forms which greatly exaggerates the pressure differences which exist at some arbitrary wind direction. Because of the emphasis on maximum values, much of the published data is quite unsuitable to the computation of ventilation rates.

The most comprehensive study of wind pressures on low-rise buildings is that conducted at the Boundary Layer Wind Tunnel Laboratory, The University of Western Ontario and sponsored by the Metal Building Manufacturers Association, the American Iron and Steel Institute and the Canadian Steel Industries Construction Council. The results of this study have been published (3,4) and have provided the basis for recent revisions in American (ANSI) and Canadian (NBC) building codes. Although the published data are directed towards structural design applications, all the measured data have been archived in a computer compatible form. The second aim of this study is to develop computer programs to analyse these data and present the results in a form in which they will be readily usable in the computation of internal flow rates and in the evaluation of proposed systems of natural ventilation.

1.2 Description of Program of Study

The study can be considered in three major phases as follows:

Phase I:	Comparison of computed and measured internal flows.
Phase II:	Preparation of a data base for external pressures on low-rise buildings.
Phase III:	The development of design aids.

The aim of Phase I was to establish the conditions under which the external distribution of pressure can be used to obtain reliable estimates of internal flows. It can be anticipated that, for small openings, the flow field and hence the external pressure field will be unchanged by flow through the structure. In such cases the induced flows can be computed from the pressures measured on a sealed model provided that the size and the pressure loss characteristics of the external openings and internal flow paths are known. As the opening size is increased the "through flows" will distort the pressure field and lead to eroneous predictions. The magnitude of these errors and the dependency on the size and position of the openings is presently poorly defined. To evaluate these errors the pressure distribution on two 1:100 models of simple domestic structures was measured in turbulent shear flow. These distributions were employed to compute internal flows. An additional two models with the same external dimensions were constructed with a variety of external openings varying from almost 100% of the face to only a few percent of the face. The latter models were fitted with a flow meter to measure internal flows to be compared with those computed from the pressures. The test procedures for Phase I are described in detail in Section 2 and the measured and computed flows are compared and the results discussed in Section 3.

The aim of Phase II was to collect the pressure data obtained in a comprehensive study of wind loads on low-rise buildings and re-arrange it in a form more suited to the computation of internal flows. The method adopted was to divide each wall surface into equal rectangular areas and, using the available data, to compute the average (spatial) mean (time average) pressure coefficient for each. A similar approach was adopted for a series of rectangular regions located along the ridge line. The coefficients so determined were then presented in a semi-pictorial format for a range of wind directions, roof slopes and terrain roughness. The origins of the data base, the methods employed in the reformulation and the results obtained are presented and discussed in Section 4.

While the data presented in Section 4 can be used to compute internal flows this procedure does entail computations best completed with the aid of a computer code. In order to eliminate or at least minimize the need for this procedure, Phase III was planned with the aim of developing design aids from which flow estimates could be made by simple hand calculations. Because of time limitations on the study it was clear that Phase III would not be completed in its entirety but that sample design charts would be produced. The development of the design aids is discussed in Section 5 and some sample charts are presented. Work on this Phase is continuing with support from other funding sources and a separate report will be prepared at a later date.

The overall conclusions derived from the study are summarized in Section 6.

2.0 A STUDY OF THE EXTERNAL PRESSURES AND INTERNAL FLOWS FOR A MODEL DOMESTIC DWELLING

2.1 The Models

The model employed in the external pressure studies is shown in Fig. 2.1, which gives the detailed measurements, and in the photograph in Fig. 2.2. The basic shell was fitted with a total of 80 pressure taps located as shown in Fig. 2.3. The model was tested with and without the end wall extensions or "wing" walls.

The models employed in the flow studies are shown in Fig. 2.4 which gives the detailed dimensions. The models were designed with removeable wall panels and a removeable leeward roof panel. A set of walls with openings of:

i)	No walls	;	% of front wall	=	89
ii)	4" x 1" rectangle	;	% of front wall	=	71
iii)	3.2" x 0.8" rectangle	;	% of front wall	=	46
iv)	24, 3/8" holes	;	% of front wall	=	47
v)	24, 1/4" holes	;	% of front wall	=	21
vi)	24, 3/16" holes	;	% of front wall	=	12
vii)	24, 1/8" holes	;	% of front wall	=	5
viii)	24, 3/32" holes	;	% of front wall	=	3

The roof panels were prepared to produce a slit just downstream of the ridge of the roof. The slit length was 4.0" or 89% of the full width and the widths were 1/8", 1/4" and 1/2" which produced open areas equal to 9%; 18% and 36% of the frontal wall area.

The flow through the model was measured by calibrating the bend in the ducting (see Fig. 2.4) as a flow meter. The average pressure difference between the group of five taps on the inside of the bend and the five taps on the outside was measured with a precision electronic manometer. This pressure difference was related to the flow through the building by the calibration procedure described in Section 2.2. The pressure loss through the flow meter can be expressed in the form;

$$\frac{\Delta p_{loss}}{\frac{1}{2}\rho V^2} = C_L \qquad (2.1)$$

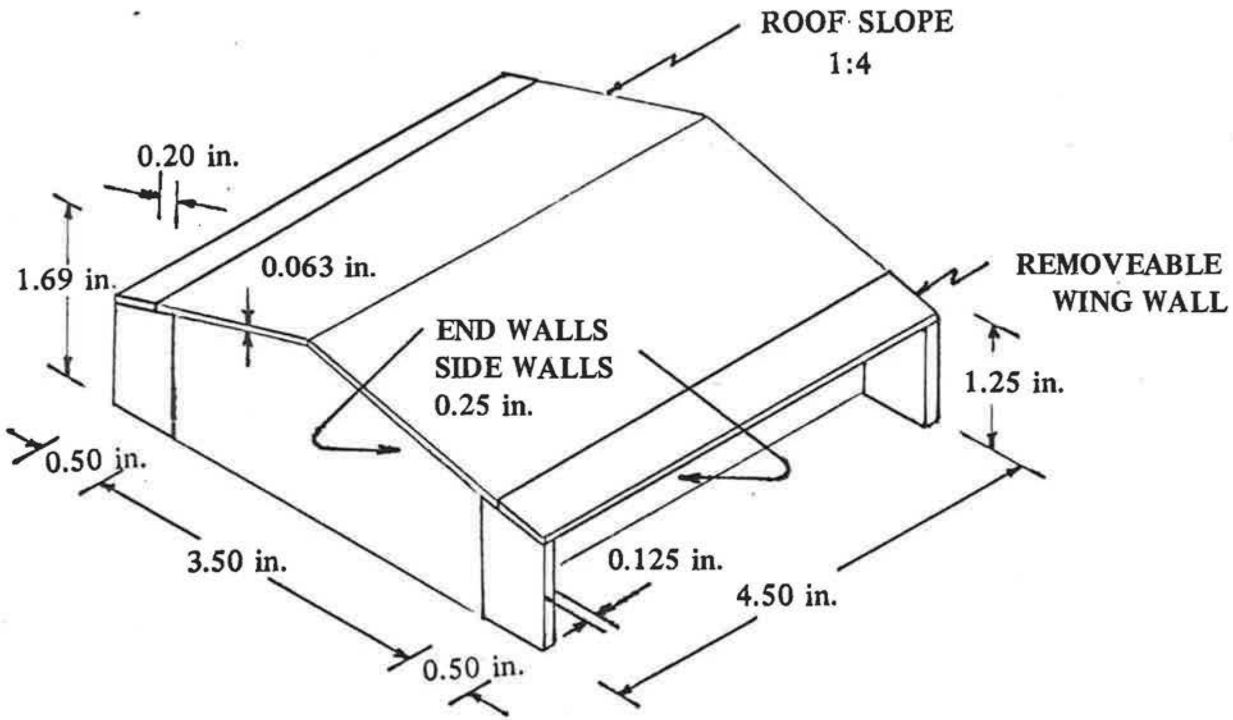

FIG. 2.1 1:100 MODEL EMPLOYED IN THE MEASUREMENT OF SURFACE PRESSURES

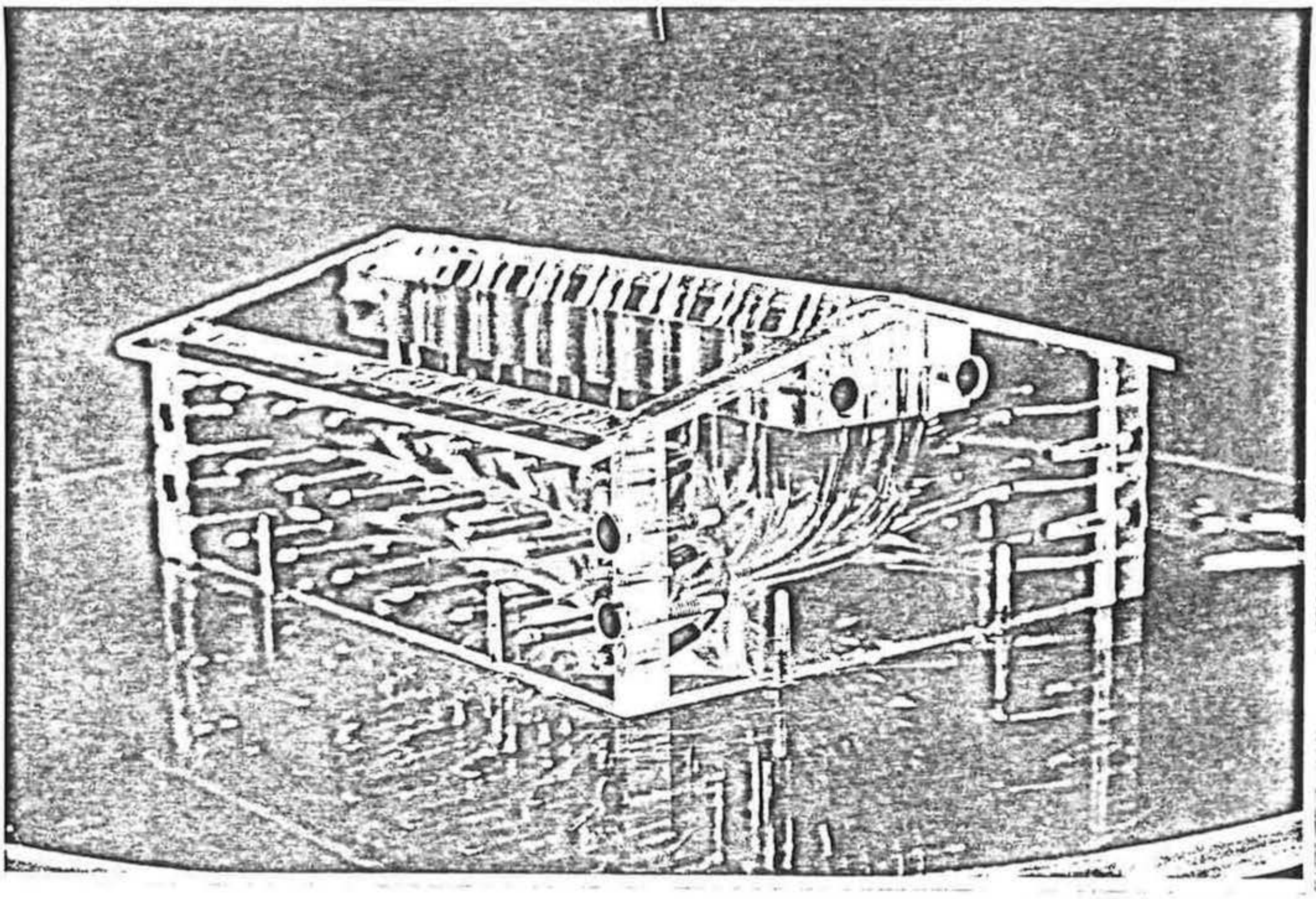

FIG. 2.2 1:100 MODEL EMPLOYED IN THE MEASUREMENT OF SURFACE PRESSURES

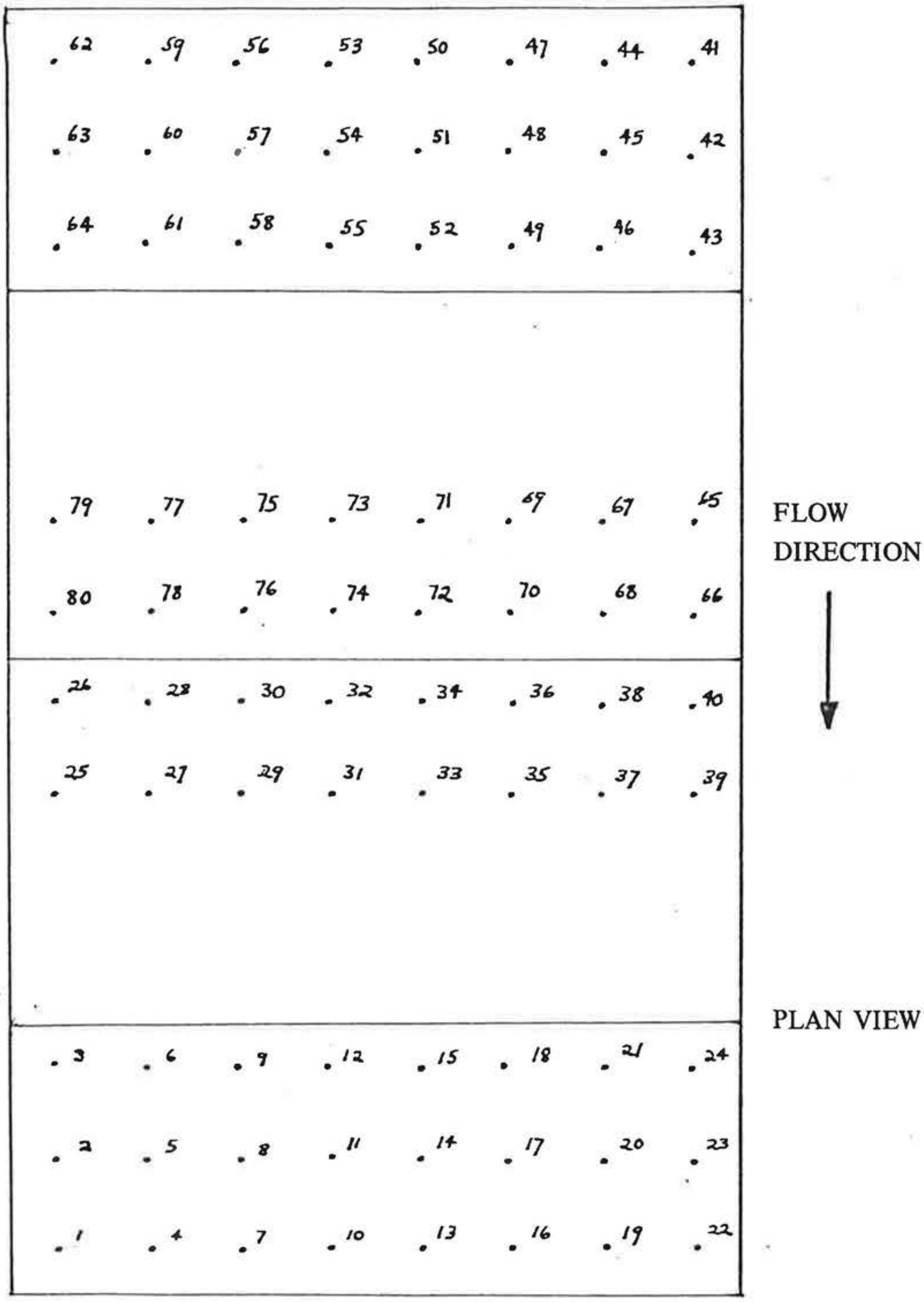

FIG. 2.3 LOCATION OF PRESSURE TAPPINGS ON 1:100 MODEL

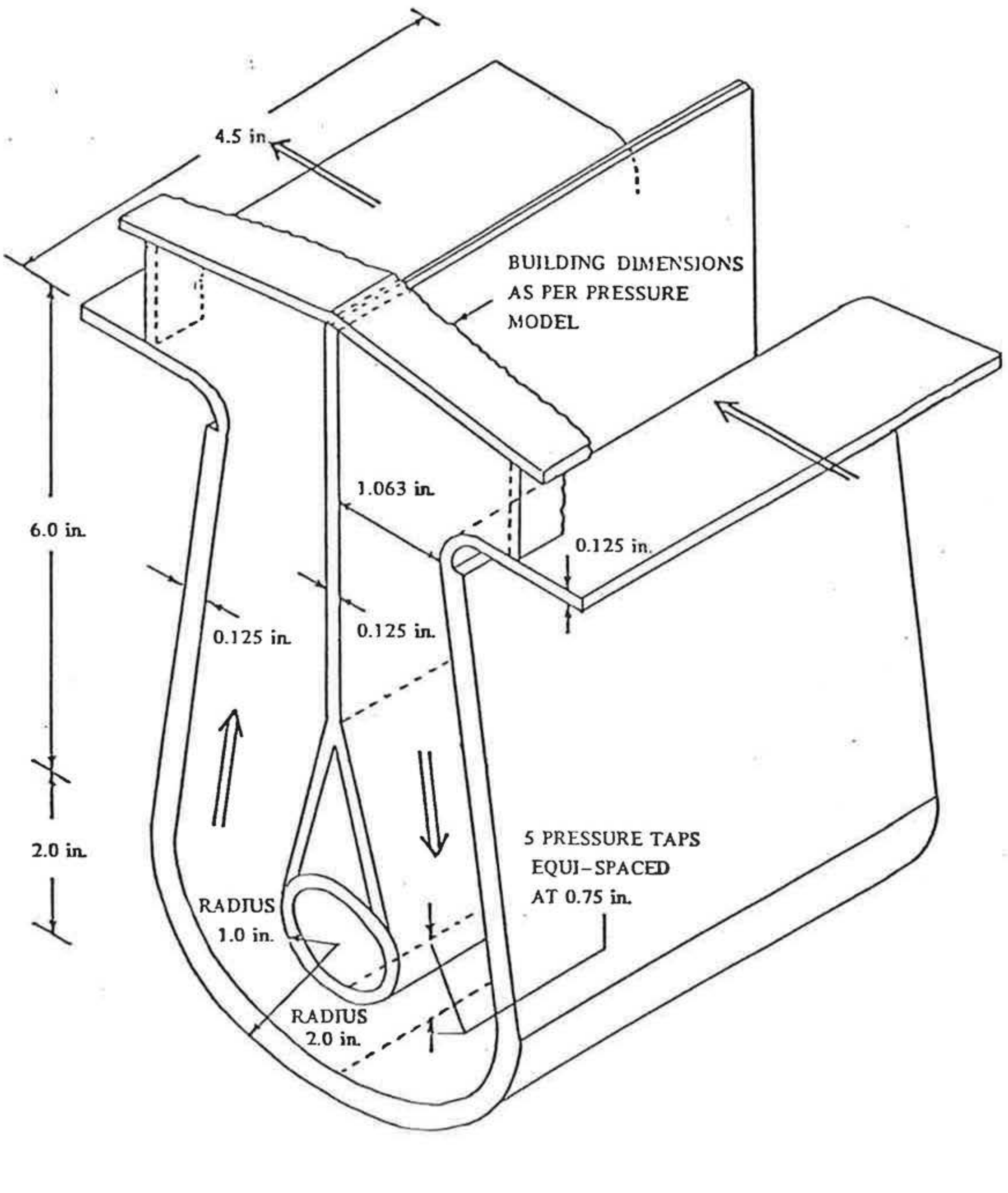

FIG. 2.4 1:100 MODEL WITH FLOWMETER FOR THE MEASUREMENT OF INTERNAL FLOWS

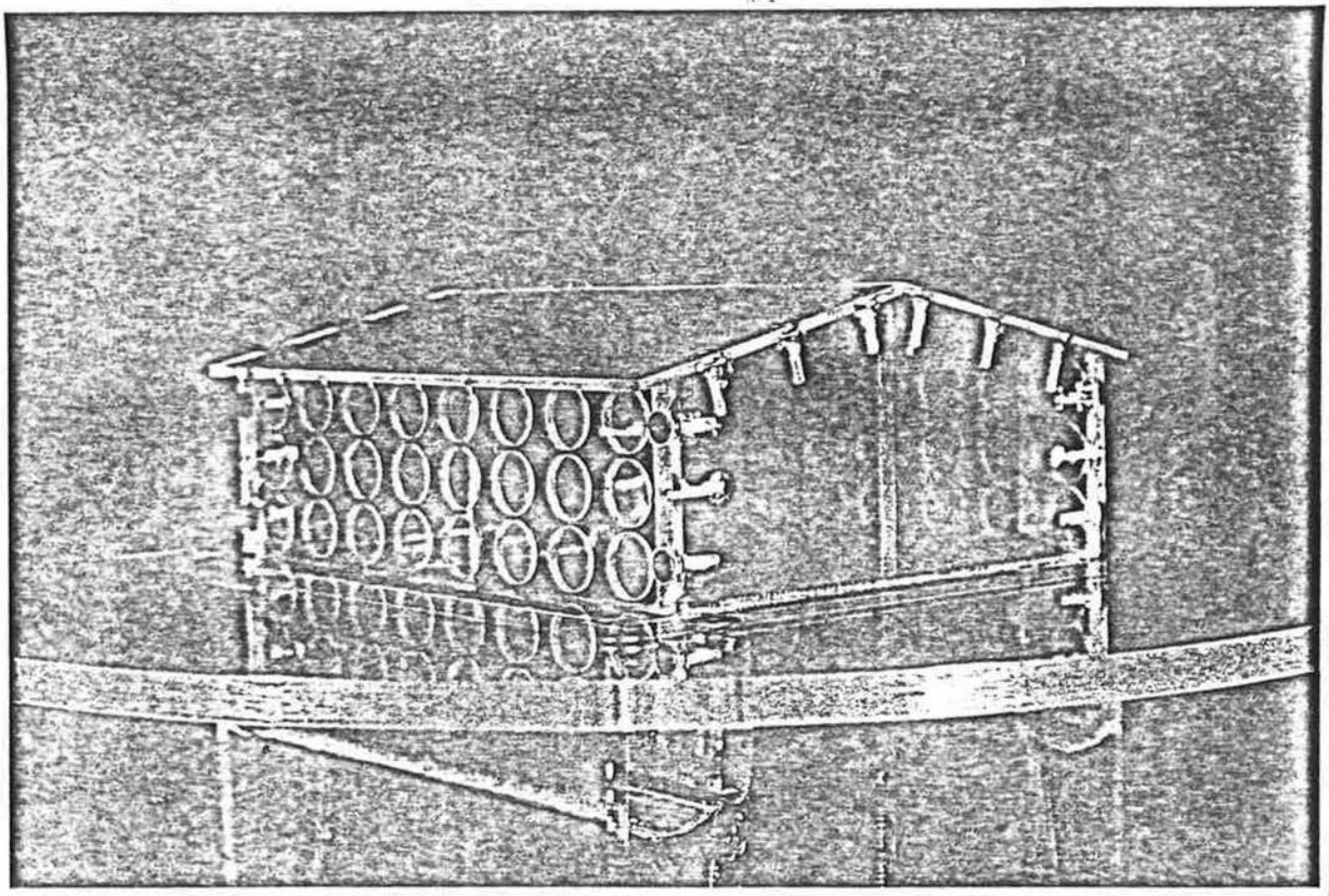

FIG. 2.5 1:100 MODEL VENTED BY 24, 3/8" DIAMETER HOLES IN EACH OF THE FRONT AND REAR WALLS

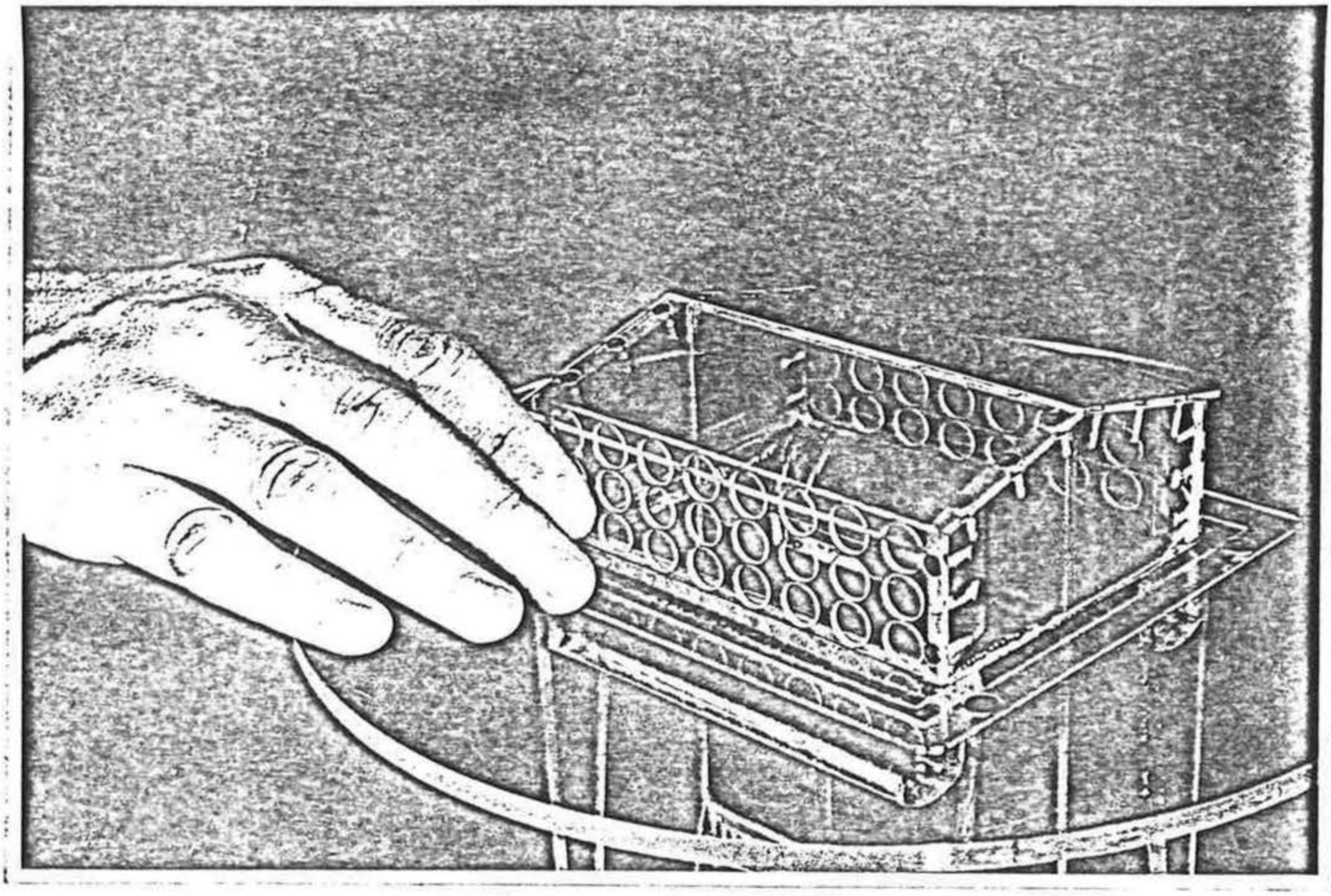

FIG. 2.6 1:100 MODEL VENTED BY 24, 3/8" DIAMETER HOLES IN EACH OF THE FRONT AND REAR WALLS

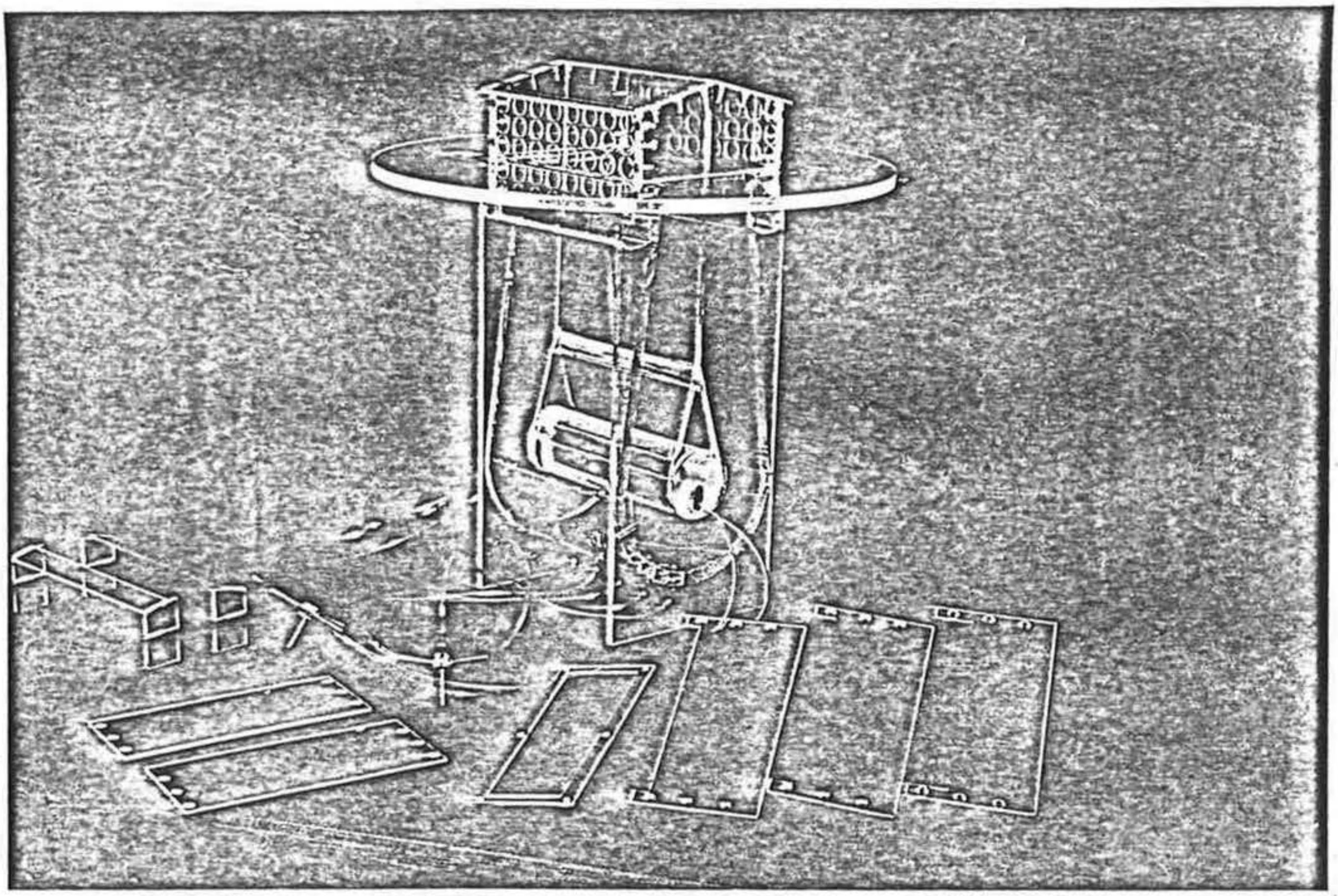

FIG. 2.7 1:100 MODEL WITH REMOVEABLE ROOF PANELS AND WING WALLS

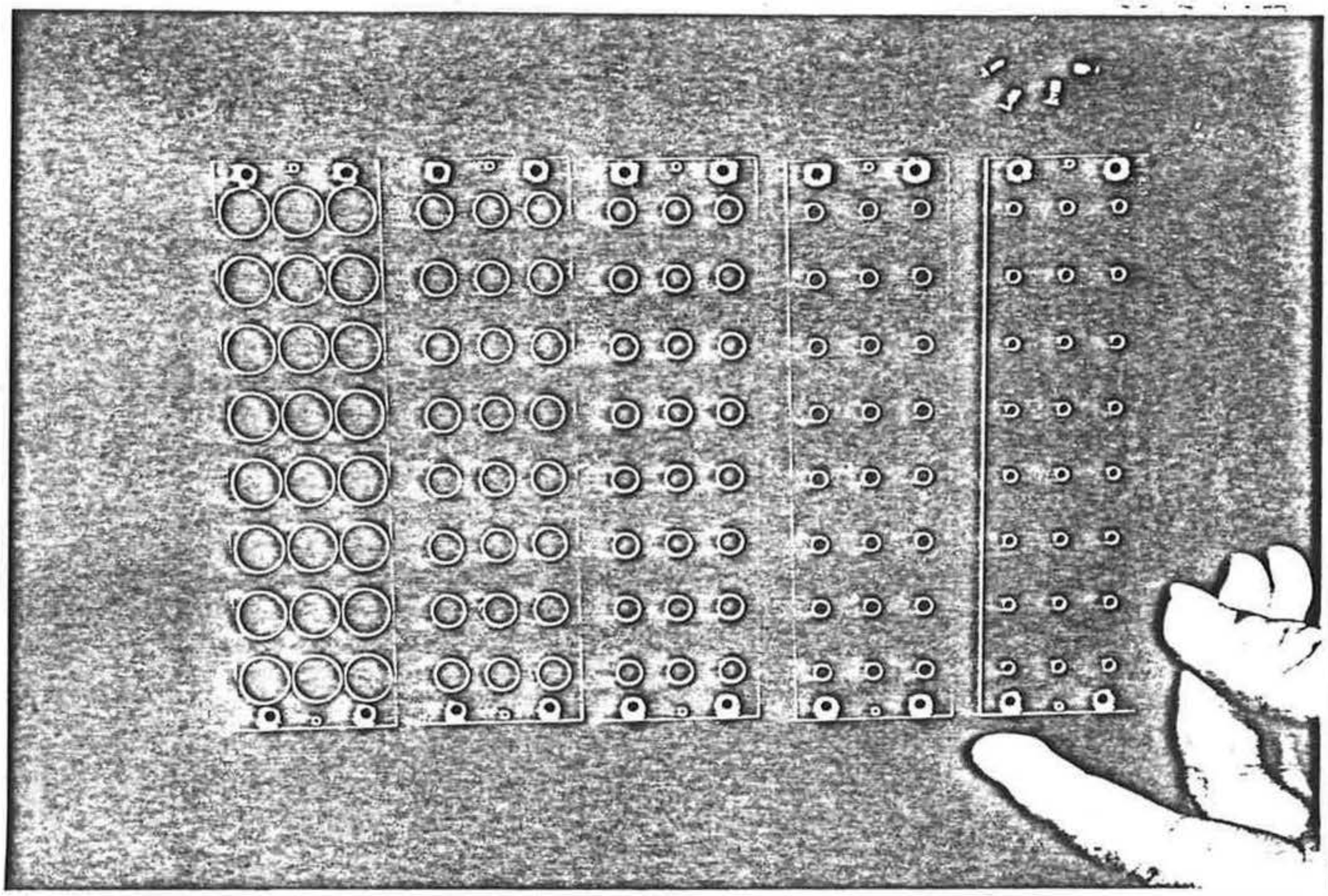

FIG. 2.8 VENTED WALL SEGMENTS WITH 3/8", 1/4", 3/16", 1/8" and 3/32" DIAMETER HOLES

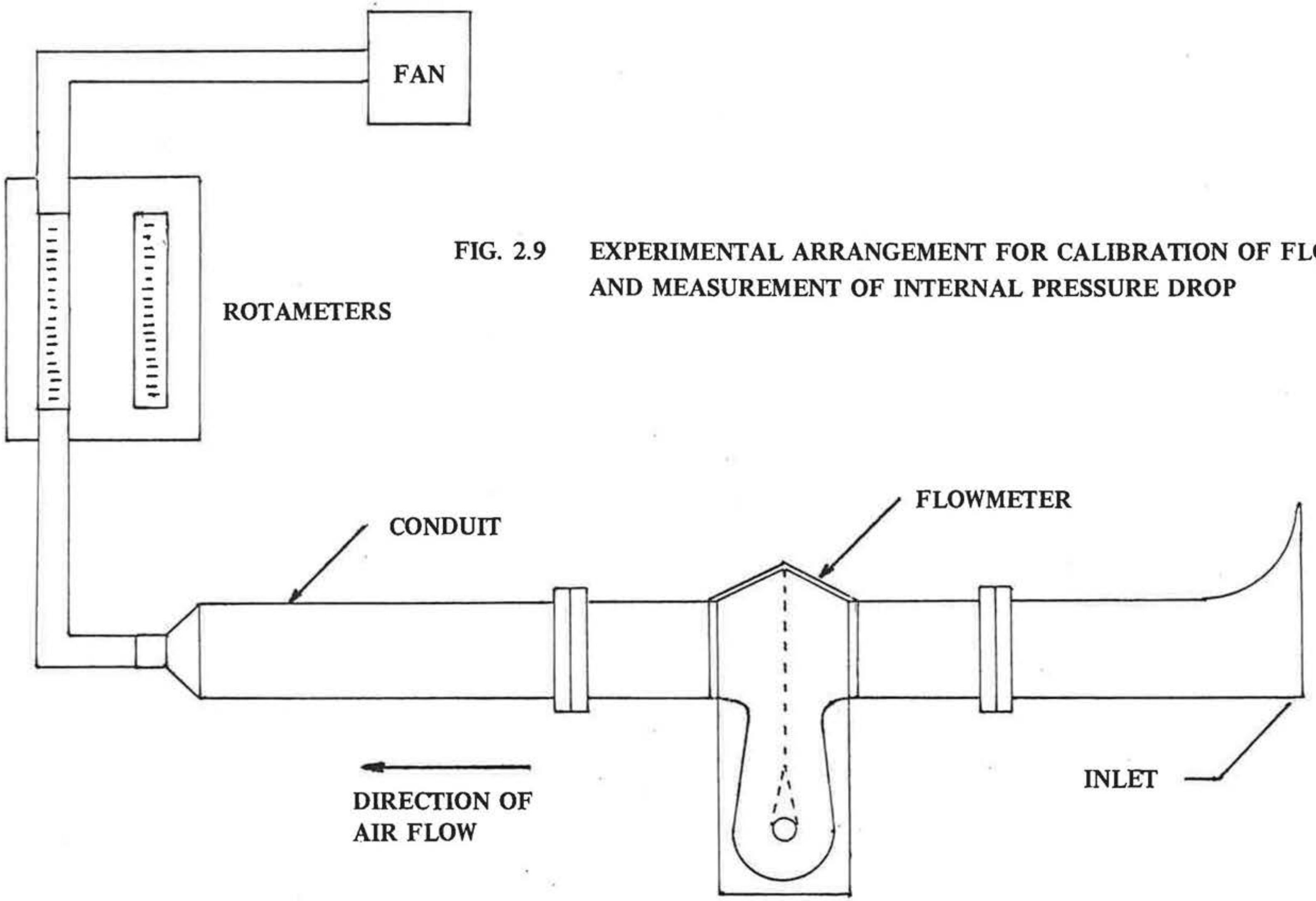

FIG. 2.9 EXPERIMENTAL ARRANGEMENT FOR CALIBRATION OF FLOW METER AND MEASUREMENT OF INTERNAL PRESSURE DROP

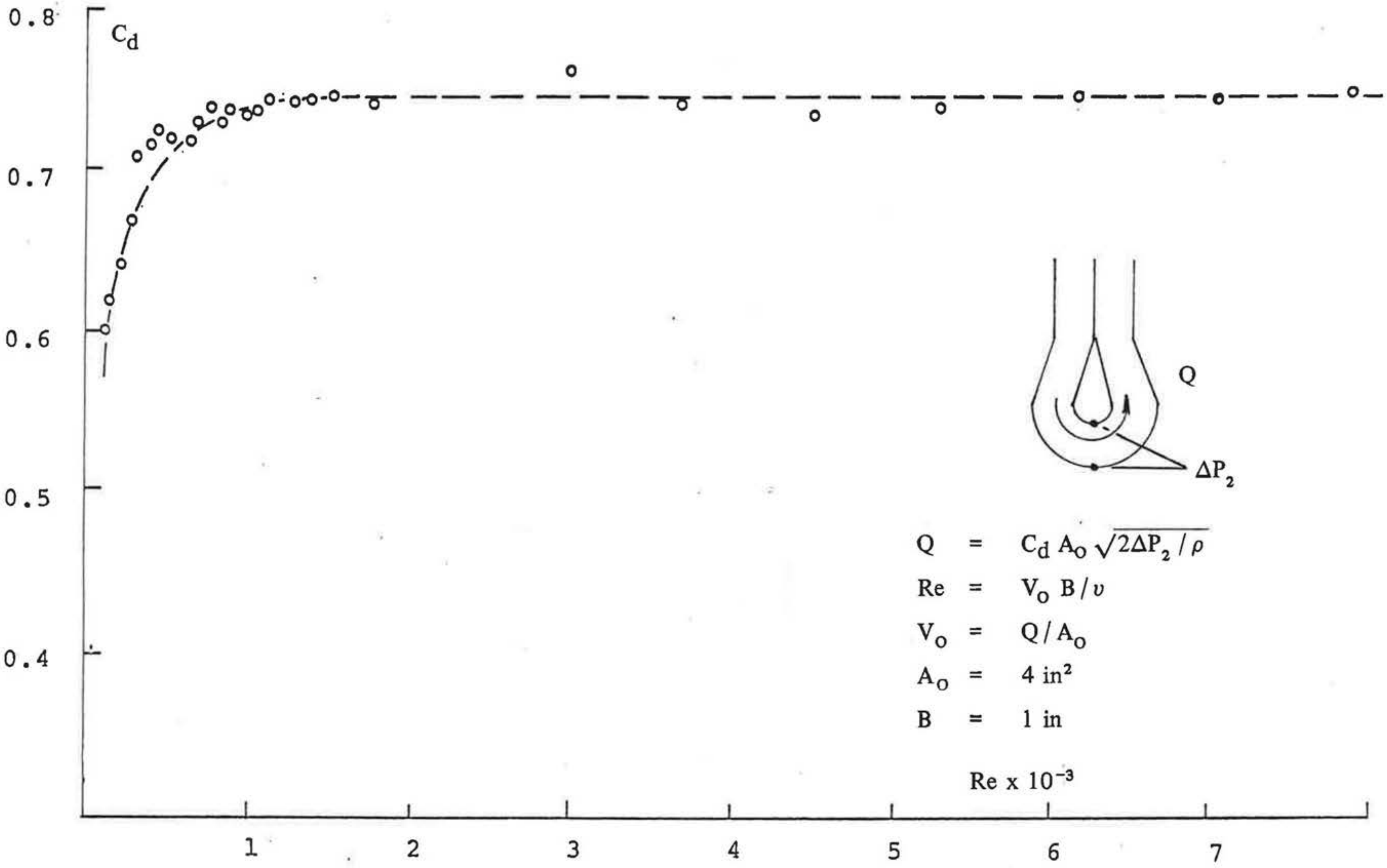

FIG. 2.10 DISCHARGE COEFFICIENT OF FLOWMETER AS A FUNCTION OF REYNOLDS NUMBER

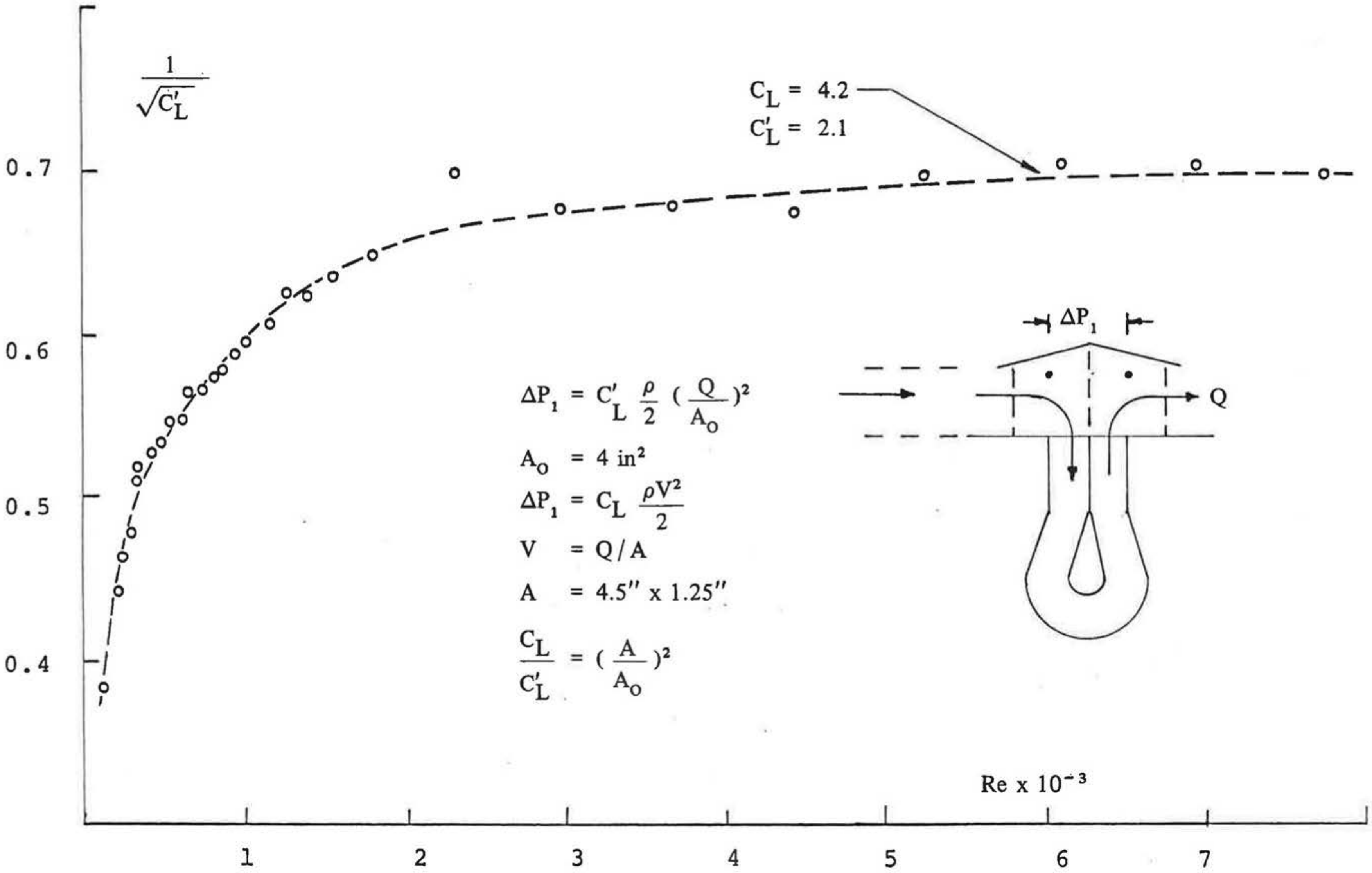

FIG. 2.11 INTERNAL LOSS COEFFICIENT AS A FUNCTION OF REYNOLDS NUMBER

FIG. 2.12 1:100 PRESSURE MODEL IN BOUNDARY LAYER WIND TUNNEL

FIG. 2.13 1:100 FLOW MODEL IN BOUNDARY LAYER WIND TUNNEL

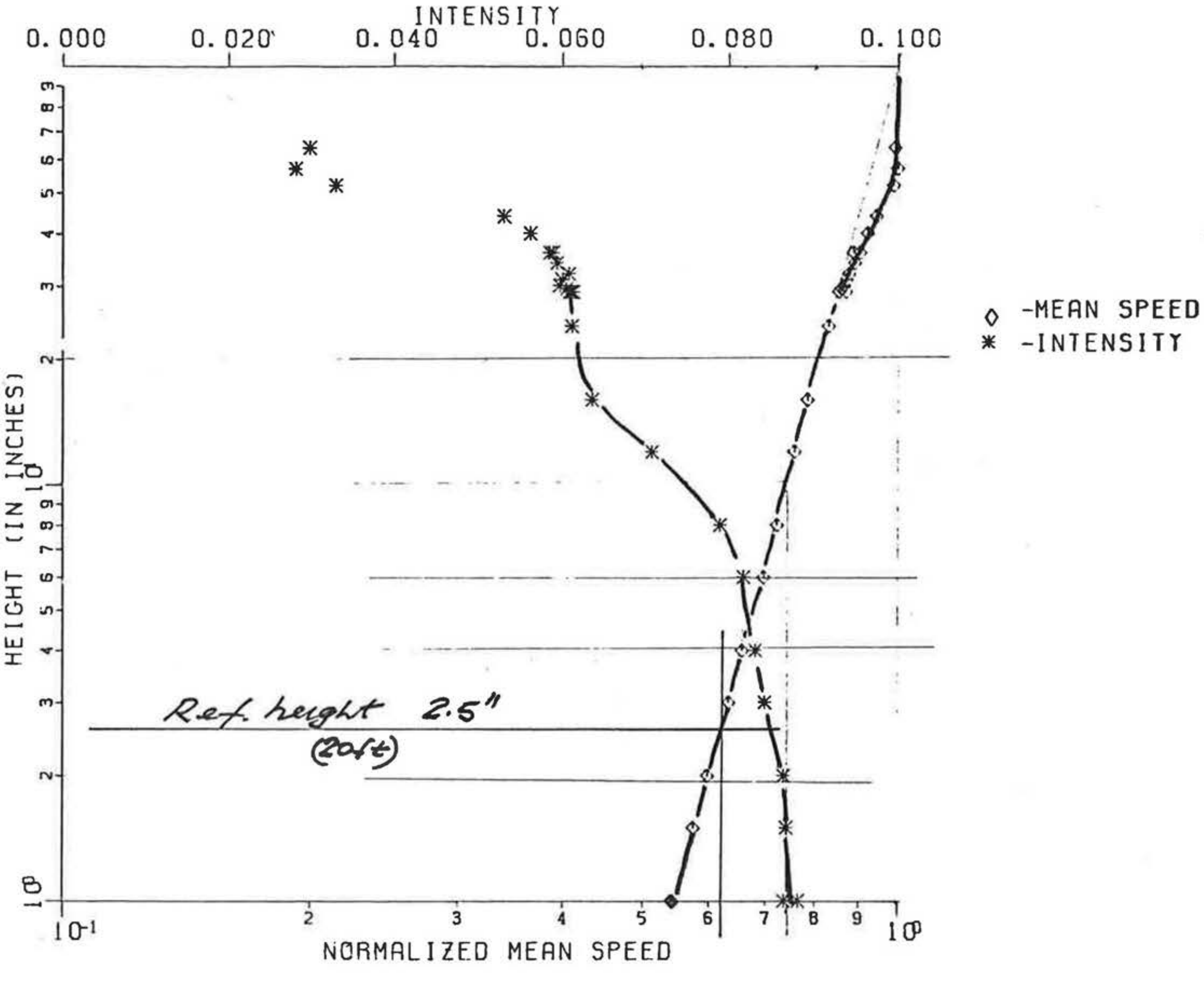

FIG. 2.14 VELOCITY PROFILE AND TURBULENCE LEVELS AT THE TEST POSITION

where, $\Delta p_{loss} = \Delta P_1$
$V = Q/A$
Q = total flow
A = frontal wall area (1.25" x 4.5")

Measurements of the pressure loss indicated a value of C_L of approximately 4. This loss coefficient would essentially be the same if the flow through the building is forced to pass through a sharp edged internal opening or openings of a total area equal to 50% of the total frontal wall area. Even if a dwelling contains no internal walls parallel to the windward wall the internal flow area (allowing for floor to ceiling height of about 80% of the external ground to eaves height and some loss in area due to the internal and external walls parallel to the sides) is unlikely to exceed 70% of the frontal wall area. The resistance offerred by the flow meter is thus comparable with the resistance that would be present in a home with a very open interior floor plan. The internal losses contribute less than one third of the total losses for wall porosities less than 47%.

The model employed in the flow measurements is shown in Figs. 2.5 and 2.6 (the model is fitted with walls containing 24 3/8" holes). The complete model with the flow meter, the removeable wing walls and the removeable roof elements is shown in Fig. 2.7. The perforated wall panels are shown in Fig. 2.8.

2.2 Model Calibration

The experimental arrangement employed for the calibration of the flow meter and the determination of the internal losses is shown in Fig. 2.9. The flow ducted into and out of the model was measured with two calibrated "Rotameters". The pressure drop through the model (Δp_1) and the pressure difference (Δp_2) across the bend of the flow meter were measured with an electronic micromanometer. The variation of the discharge coefficient of the flow meter (Equation 2.2) and the loss coefficient (Equation 2.3) were computed and plotted as a function of Reynolds Number (Equation 2.4).

$$Q = C_d A_o \sqrt{2\Delta p_2 / \rho} \quad (2.2)$$

$$\Delta p_1 = C_L' \rho V_o^2/2 = C_L \rho V^2/2 \quad (2.3)$$

$$R_e = V_o B / \nu \quad (2.4)$$

where;

Q = flow
C_d = discharge coefficient
Δp_2 = pressure difference across bend
ρ = air density

A_o	=	throat area of meter (4" x 1")
C_L'	=	loss coefficient
V_o	=	Q/A_o
Δp_1	=	pressure drop through model building
R_e	=	Reynolds Number
B	=	throat depth (1")
ν	=	kinematic viscosity of air.
V	=	Q/A
A	=	frontal wall area

The variation of C_d and C_L with R_e is shown in Fig. 2.10 and Fig. 2.11 respectively. The discharge coefficient is essentially constant and equal to 0.73 ± 0.01 for $R_e > 700$ while the loss coefficient is essentially constant and equal to $4 \pm .2$ for $R_e > 1200$. The average velocity through the meter can be expected to be of the order $C_c \cdot \gamma \cdot V$

where;

γ	=	wall porosity
V	=	external speed
C_c	=	contraction coefficient

All wind tunnel tests were conducted with V of the order of 30 fps and hence a Reynolds Number of 700 would be exceeded with a wall porosity in excess of about 7%. The discharge coefficient varies rapidly with R_e below about 400 and, as a result, it might be anticipated that accurate flow measurement at porosities less than 4% would be difficult. As is discussed in Section 2.5 this proved to be the case and it was not possible to achieve reliable measurements at a porosity of 3% and the results at 5% porosity exhibited considerable scatter.

2.3 Test Procedure

Both the external pressures and the internal flows were measured in turbulent shear flow generated in the 8 ft. wide x 100 ft. long Boundary Layer Wind Tunnel at the University of Western Ontario. The pressure model is shown in Fig. 2.12 and the flow metering model in Fig. 2.13. The models were mounted on the turntable (see Figs. 2.12 and 2.13) and the external pressures (or flows) were measured for wind approach angles of 0^o to 90^o in 10^o increments. The properties of the flow at the test section are shown in Fig. 2.14. The wind speed profile and turbulence is typical of that off water and was chosen to maximize the speeds near the surface and hence maintain as high a Reynolds Number as possible. Since the prime aim of the study was to compare measured and predicted flows the actual profile employed is of little consequence. Again to maximize the Reynolds Number, all tests were conducted at the maximum speed of the tunnel which, at the eaves height of the model, was about 30 fps.

The reference velocity in the Wind Tunnel was monitored by the use of a pitot tube located in the smooth flow above the boundary layer. The pressures and the flow rates were initially expressed in a dimensionless form as follows;

$$C_p = \frac{p - p_s}{\frac{1}{2}\rho V^2}$$

$$C_Q = \frac{Q}{A \cdot V}$$

where; V = reference velocity measured by pitot tube
A = frontal wall area of model
Q = measured internal flow
p = measured surface pressure on model
p_s = pressure from static taps of pitot.

The coefficients were later adjusted using a reference speed in the vicinity of the model as defined in Section 2.4.

2.4 External Pressures

The measured external pressure coefficients for wind angles 0^o to 90^o are presented in Tables 2.1 for the basic model and 2.2 for the model with wing walls added, the coefficients in these tables have been defined with respect to the mean speed at a height of 2.5 inches,

ie; $$C_p = \frac{p - p_s}{\frac{1}{2}\rho V_z^2}$$

V_z = mean speed @ $z = 2.5$ *inches*

which, accepting a model scale of 1:100, corresponds to a full-scale height above ground of 20 ft.

2.5 Internal Flow Rates

The measured internal flows, are presented in Appendix 1. The flows have been expressed in the form of flow coefficients, C_Q defined as;

$$C_Q = \frac{Q}{A\, V_z}$$

A = frontal area (1.25" x 4.50")
Q = internal flow
V_z = reference speed @ $z = 2.5$ ins.

NO WING-WALLS

	AZIMUTH 0	10	20	30	40	50	60	70	80	90
VELOCITY:	45.38	44.90	44.69	44.47	45.00	45.00	44.23	44.19	44.15	44.17
TAP 1:	0.026	-0.154	-0.103	-0.154	-0.154	-0.154	-0.103	-0.103	-0.077	-0.051
TAP 2:	-0.180	-0.154	-0.180	-0.231	-0.257	-0.282	-0.282	-0.231	-0.128	-0.077
TAP 3:	-0.180	-0.180	-0.385	-0.205	-0.205	-0.231	-0.231	-0.205	-0.128	-0.103
TAP 4:	-0.205	-0.154	-0.411	-0.180	-0.180	-0.180	-0.154	-0.128	-0.103	-0.051
TAP 5:	-0.180	-0.154	-0.411	-0.231	-0.257	-0.308	-0.282	-0.231	-0.154	-0.051
TAP 6:	-0.205	-0.154	-0.385	-0.205	-0.231	-0.257	-0.257	-0.231	-0.180	-0.077
TAP 7:	-0.180	-0.128	-0.385	-0.180	-0.231	-0.231	-0.205	-0.205	-0.154	-0.051
TAP 8:	-0.180	-0.128	-0.385	-0.231	-0.308	-0.308	-0.308	-0.282	-0.205	-0.077
TAP 9:	-0.180	-0.128	-0.360	-0.231	-0.257	-0.282	-0.257	-0.257	-0.231	-0.103
TAP 10:	-0.128	-0.103	-0.360	-0.231	-0.257	-0.257	-0.257	-0.282	-0.231	-0.103
TAP 11:	-0.154	-0.103	-0.334	-0.257	-0.308	-0.334	-0.308	-0.334	-0.257	-0.103
TAP 12:	-0.154	-0.103	-0.308	-0.231	-0.282	-0.282	-0.308	-0.308	-0.282	-0.154
TAP 13:	-0.128	-0.103	-0.334	-0.257	-0.282	-0.257	-0.308	-0.334	-0.308	-0.154
TAP 14:	-0.128	-0.128	-0.308	-0.282	-0.334	-0.334	-0.360	-0.385	-0.360	-0.180
TAP 15:	-0.128	-0.128	-0.282	-0.257	-0.308	-0.308	-0.334	-0.385	-0.360	-0.205
TAP 16:	-0.128	-0.128	-0.282	-0.257	-0.282	-0.308	-0.360	-0.411	-0.411	-0.257
TAP 17:	-0.154	-0.128	-0.282	-0.308	-0.334	-0.360	-0.385	-0.437	-0.437	-0.308
TAP 18:	-0.154	-0.128	-0.257	-0.282	-0.334	-0.334	-0.385	-0.411	-0.411	-0.308
TAP 19:	-0.154	-0.128	-0.257	-0.282	-0.334	-0.360	-0.385	-0.411	-0.437	-0.385
TAP 20:	-0.154	-0.128	-0.257	-0.334	-0.360	-0.360	-0.411	-0.437	-0.462	-0.437
TAP 21:	-0.154	-0.128	-0.231	-0.334	-0.360	-0.385	-0.385	-0.437	-0.437	-0.437
TAP 22:	-0.128	-0.128	-0.205	-0.308	-0.334	-0.334	-0.360	-0.385	-0.437	-0.488
TAP 23:	-0.128	-0.128	-0.205	-0.308	-0.360	-0.360	-0.360	-0.385	-0.437	-0.488
TAP 24:	-0.128	-0.128	-0.205	-0.334	-0.360	-0.360	-0.360	-0.385	-0.411	-0.462
TAP 25:	-0.488	-0.539	-0.591	-0.565	-0.462	-0.385	-0.334	-0.231	-0.128	-0.077
TAP 26:	-0.488	-0.539	-0.591	-0.591	-0.488	-0.411	-0.334	-0.231	-0.154	-0.077
TAP 27:	-0.488	-0.539	-0.616	-0.616	-0.565	-0.488	-0.385	-0.282	-0.128	-0.077
TAP 28:	-0.437	-0.565	-0.616	-0.642	-0.539	-0.488	-0.411	-0.282	-0.128	-0.077
TAP 29:	-0.411	-0.591	-0.642	-0.693	-0.668	-0.565	-0.462	-0.308	-0.128	-0.077
TAP 30:	-0.411	-0.591	-0.642	-0.693	-0.668	-0.591	-0.462	-0.334	-0.154	-0.077
TAP 31:	-0.385	-0.693	-0.719	-0.796	-0.745	-0.668	-0.488	-0.308	-0.154	-0.103
TAP 32:	-0.385	-0.693	-0.719	-0.770	-0.719	-0.642	-0.514	-0.360	-0.205	-0.103
TAP 33:	-0.385	-0.770	-0.796	-0.847	-0.796	-0.693	-0.539	-0.308	-0.231	-0.180
TAP 34:	-0.385	-0.770	-0.796	-0.822	-0.796	-0.745	-0.591	-0.411	-0.282	-0.180
TAP 35:	-0.411	-0.847	-0.873	-0.950	-0.899	-0.719	-0.462	-0.437	-0.411	-0.360
TAP 36:	-0.411	-0.668	-0.873	-0.924	-0.924	-0.770	-0.642	-0.514	-0.437	-0.360
TAP 37:	-0.462	-0.642	-0.976	-1.002	-0.770	-0.514	-0.668	-0.745	-0.693	-0.668
TAP 38:	-0.437	-0.668	-0.976	-1.027	-0.976	-0.873	-0.822	-0.796	-0.693	-0.693
TAP 39:	-0.488	-0.770	-0.847	-0.693	-0.899	-1.181	-1.053	-0.873	-0.822	-0.796
TAP 40:	-0.488	-0.822	-1.130	-1.181	-1.207	-1.335	-1.104	-0.899	-0.822	-0.796

NO WING-WALLS

	AZIMUTH 0	10	20	30	40	50	60	70	80	90
VELOCITY:	45.38	44.90	44.69	44.47	45.00	45.00	44.23	44.19	44.15	44.17
TAP 41:	0.334	0.051	0.077	0.026	-0.026	-0.051	-0.077	-0.026	-0.077	-0.077
TAP 42:	0.231	0.154	0.026	0.051	0.026	-0.026	-0.051	-0.051	-0.077	-0.077
TAP 43:	0.385	0.308	0.000	0.180	0.103	0.026	-0.051	-0.026	-0.077	-0.077
TAP 44:	0.308	0.257	-0.077	0.180	0.128	0.077	0.000	0.000	-0.051	-0.026
TAP 45:	0.334	0.282	-0.051	0.154	0.154	0.077	0.000	0.026	-0.077	-0.051
TAP 46:	0.488	0.437	0.077	0.308	0.205	0.128	0.000	0.026	-0.077	-0.077
TAP 47:	0.360	0.308	0.026	0.257	0.180	0.128	0.026	0.026	-0.077	-0.051
TAP 48:	0.360	0.334	0.026	0.231	0.180	0.154	0.026	0.026	-0.051	-0.077
TAP 49:	0.514	0.488	0.205	0.334	0.257	0.180	0.026	0.051	-0.077	-0.103
TAP 50:	0.385	0.360	0.128	0.308	0.231	0.180	0.051	0.026	-0.051	-0.103
TAP 51:	0.385	0.334	0.154	0.282	0.231	0.205	0.077	0.026	-0.077	-0.103
TAP 52:	0.539	0.462	0.257	0.385	0.282	0.205	0.077	0.051	-0.051	-0.128
TAP 53:	0.385	0.360	0.205	0.360	0.308	0.231	0.103	0.051	-0.077	-0.154
TAP 54:	0.385	0.385	0.231	0.360	0.308	0.205	0.103	0.051	-0.077	-0.205
TAP 55:	0.539	0.514	0.334	0.411	0.360	0.257	0.103	0.051	-0.077	-0.205
TAP 56:	0.385	0.411	0.360	0.360	0.360	0.257	0.128	0.026	-0.103	-0.282
TAP 57:	0.411	0.411	0.334	0.411	0.360	0.282	0.128	0.026	-0.128	-0.308
TAP 58:	0.539	0.514	0.437	0.462	0.385	0.257	0.128	0.026	-0.128	-0.334
TAP 59:	0.360	0.411	0.437	0.437	0.437	0.308	0.128	-0.026	-0.257	-0.385
TAP 60:	0.360	0.462	0.437	0.462	0.411	0.308	0.128	-0.051	-0.282	-0.437
TAP 61:	0.565	0.565	0.539	0.539	0.462	0.360	0.128	-0.026	-0.282	-0.437
TAP 62:	0.231	0.308	0.385	0.411	0.411	0.282	0.051	-0.180	-0.488	-0.462
TAP 63:	0.282	0.385	0.488	0.488	0.436	0.334	0.026	-0.282	-0.514	-0.462
TAP 64:	0.488	0.565	0.642	0.591	0.565	0.411	0.128	-0.257	-0.488	-0.462
TAP 65:	-0.231	-0.385	-0.334	-0.334	-0.257	-0.257	-0.231	-0.180	-0.128	-0.077
TAP 66:	-0.334	-0.437	-0.411	-0.411	-0.360	-0.308	-0.308	-0.180	-0.128	-0.103
TAP 67:	-0.257	-0.385	-0.360	-0.360	-0.334	-0.282	-0.231	-0.180	-0.103	-0.077
TAP 68:	-0.308	-0.488	-0.437	-0.462	-0.462	-0.360	-0.308	-0.205	-0.128	-0.077
TAP 69:	-0.231	-0.411	-0.360	-0.411	-0.360	-0.308	-0.257	-0.180	-0.103	-0.077
TAP 70:	-0.282	-0.514	-0.437	-0.488	-0.437	-0.385	-0.308	-0.205	-0.128	-0.103
TAP 71:	-0.205	-0.462	-0.385	-0.437	-0.385	-0.308	-0.282	-0.205	-0.128	-0.128
TAP 72:	-0.257	-0.565	-0.488	-0.514	-0.488	-0.385	-0.334	-0.231	-0.128	-0.128
TAP 73:	-0.205	-0.514	-0.385	-0.411	-0.385	-0.334	-0.308	-0.180	-0.154	-0.205
TAP 74:	-0.257	-0.591	-0.488	-0.514	-0.462	-0.411	-0.334	-0.231	-0.180	-0.205
TAP 75:	-0.205	-0.539	-0.411	-0.437	-0.411	-0.308	-0.257	-0.231	-0.334	-0.334
TAP 76:	-0.257	-0.411	-0.488	-0.514	-0.488	-0.385	-0.282	-0.282	-0.360	-0.385
TAP 77:	-0.205	-0.205	-0.385	-0.411	-0.360	-0.257	-0.308	-0.591	-0.693	-0.668
TAP 78:	-0.231	-0.308	-0.514	-0.539	-0.462	-0.360	-0.385	-0.642	-0.719	-0.668
TAP 79:	-0.205	-0.205	-0.334	-0.411	-0.616	-0.899	-1.079	-0.976	-0.924	-0.822
TAP 80:	-0.308	-0.385	-0.539	-0.565	-0.719	-0.976	-1.053	-0.950	-0.873	-0.822

TABLE 2.1: PRESSURE COEFFICIENTS FOR BASIC MODEL (FILE TAK2)

WING-WALLS ON - CARPET

	AZIMUTH									
	0	10	20	30	40	50	60	70	80	90
VELOCITY:	44.19	44.00	44.10	44.09	44.13	44.05	45.00	45.00	44.15	44.15
TAP 1:	-0.077	-0.077	-0.154	-0.205	-0.235	-0.180	-0.180	-0.154	-0.077	0.000
TAP 2:	-0.077	-0.103	-0.154	-0.205	-0.231	-0.257	-0.257	-0.231	-0.154	-0.051
TAP 3:	-0.077	-0.077	-0.154	-0.205	-0.231	-0.205	-0.231	-0.205	-0.154	-0.077
TAP 4:	-0.077	-0.077	-0.128	-0.180	-0.231	-0.257	-0.205	-0.180	-0.154	-0.103
TAP 5:	-0.077	-0.103	-0.154	-0.205	-0.257	-0.282	-0.282	-0.257	-0.205	-0.154
TAP 6:	-0.077	-0.077	-0.128	-0.205	-0.231	-0.257	-0.257	-0.231	-0.180	-0.128
TAP 7:	-0.077	-0.051	-0.103	-0.205	-0.257	-0.282	-0.257	-0.257	-0.231	-0.180
TAP 8:	-0.077	-0.077	-0.128	-0.205	-0.292	-0.308	-0.282	-0.282	-0.257	-0.205
TAP 9:	-0.077	-0.077	-0.128	-0.205	-0.257	-0.282	-0.282	-0.257	-0.231	-0.205
TAP 10:	-0.051	-0.051	-0.128	-0.205	-0.282	-0.308	-0.282	-0.308	-0.292	-0.257
TAP 11:	-0.077	-0.077	-0.128	-0.205	-0.282	-0.334	-0.308	-0.308	-0.308	-0.282
TAP 12:	-0.051	-0.051	-0.128	-0.205	-0.282	-0.308	-0.308	-0.282	-0.282	-0.257
TAP 13:	-0.051	-0.051	-0.128	-0.231	-0.282	-0.308	-0.308	-0.308	-0.308	-0.308
TAP 14:	-0.051	-0.051	-0.128	-0.205	-0.292	-0.334	-0.308	-0.308	-0.334	-0.308
TAP 15:	-0.051	-0.051	-0.128	-0.231	-0.292	-0.309	-0.308	-0.308	-0.308	-0.282
TAP 16:	-0.077	-0.051	-0.128	-0.231	-0.308	-0.308	-0.308	-0.334	-0.334	-0.308
TAP 17:	-0.077	-0.051	-0.128	-0.231	-0.308	-0.309	-0.308	-0.308	-0.334	-0.308
TAP 18:	-0.051	-0.051	-0.103	-0.205	-0.292	-0.308	-0.308	-0.308	-0.336	-0.308
TAP 19:	-0.051	-0.051	-0.103	-0.231	-0.282	-0.308	-0.308	-0.308	-0.334	-0.282
TAP 20:	-0.051	-0.051	-0.128	-0.231	-0.282	-0.303	-0.308	-0.308	-0.334	-0.282
TAP 21:	-0.077	-0.051	-0.103	-0.231	-0.282	-0.308	-0.308	-0.308	-0.308	-0.282
TAP 22:	-0.051	-0.051	-0.103	-0.231	-0.282	-0.308	-0.308	-0.309	-0.308	-0.282
TAP 23:	-0.051	-0.051	-0.103	-0.231	-0.282	-0.308	-0.308	-0.308	-0.308	-0.282
TAP 24:	-0.051	-0.051	-0.103	-0.205	-0.282	-0.308	-0.282	-0.282	-0.308	-0.257
TAP 25:	-0.565	-0.565	-0.616	-0.591	-0.488	-0.411	-0.334	-0.231	-0.154	-0.077
TAP 26:	-0.565	-0.591	-0.616	-0.591	-0.514	-0.437	-0.334	-0.231	-0.154	-0.103
TAP 27:	-0.539	-0.565	-0.616	-0.616	-0.565	-0.488	-0.385	-0.257	-0.154	-0.103
TAP 28:	-0.539	-0.539	-0.591	-0.591	-0.565	-0.514	-0.411	-0.282	-0.180	-0.103
TAP 29:	-0.488	-0.539	-0.642	-0.663	-0.642	-0.565	-0.462	-0.282	-0.180	-0.103
TAP 30:	-0.488	-0.539	-0.616	-0.668	-0.642	-0.591	-0.488	-0.334	-0.180	-0.128
TAP 31:	-0.462	-0.591	-0.668	-0.745	-0.745	-0.642	-0.488	-0.308	-0.205	-0.154
TAP 32:	-0.437	-0.565	-0.668	-0.770	-0.745	-0.642	-0.539	-0.360	-0.231	-0.154
TAP 33:	-0.462	-0.616	-0.745	-0.847	-0.822	-0.693	-0.488	-0.334	-0.282	-0.231
TAP 34:	-0.437	-0.616	-0.745	-0.822	-0.822	-0.719	-0.591	-0.411	-0.308	-0.257
TAP 35:	-0.514	-0.693	-0.847	-0.950	-0.873	-0.668	-0.437	-0.462	-0.462	-0.411
TAP 36:	-0.514	-0.693	-0.847	-0.899	-0.873	-0.796	-0.616	-0.539	-0.462	-0.411
TAP 37:	-0.565	-0.822	-0.976	-1.027	-0.770	-0.539	-0.693	-0.745	-0.693	-0.668
TAP 38:	-0.539	-0.796	-0.976	-1.053	-1.027	-0.847	-0.822	-0.770	-0.693	-0.668
TAP 39:	-0.616	-0.847	-0.873	-0.719	-0.976	-1.284	-1.027	-0.847	-0.796	-0.796
TAP 40:	-0.591	-0.873	-1.104	-1.181	-1.294	-1.412	-1.130	-0.899	-0.796	-0.770

WING-WALLS ON - CARPET

	AZIMUTH									
	0	10	20	30	40	50	60	70	80	90
VELOCITY:	44.19	44.00	44.10	44.09	44.13	44.05	45.00	45.00	44.15	44.15
TAP 41:	0.411	0.385	0.437	0.437	0.437	0.385	0.308	0.180	0.103	0.000
TAP 42:	0.437	0.411	0.437	0.437	0.462	0.411	0.308	0.180	0.077	-0.051
TAP 43:	0.462	0.462	0.437	0.462	0.462	0.385	0.308	0.205	0.051	-0.077
TAP 44:	0.411	0.360	0.385	0.411	0.411	0.308	0.231	0.077	-0.051	-0.128
TAP 45:	0.385	0.360	0.360	0.411	0.411	0.360	0.231	0.103	-0.026	-0.180
TAP 46:	0.395	0.385	0.360	0.411	0.437	0.360	0.257	0.077	-0.051	-0.154
TAP 47:	0.360	0.334	0.334	0.360	0.360	0.308	0.205	0.026	-0.128	-0.205
TAP 48:	0.360	0.334	0.308	0.360	0.360	0.334	0.205	0.051	-0.128	-0.231
TAP 49:	0.411	0.385	0.334	0.385	0.395	0.360	0.231	0.051	-0.128	-0.205
TAP 50:	0.360	0.360	0.360	0.385	0.360	0.308	0.154	-0.051	-0.180	-0.257
TAP 51:	0.395	0.334	0.334	0.360	0.360	0.308	0.180	0.000	-0.205	-0.282
TAP 52:	0.411	0.385	0.360	0.385	0.385	0.334	0.205	0.000	-0.180	-0.282
TAP 53:	0.360	0.360	0.395	0.411	0.385	0.282	0.103	-0.077	-0.231	-0.308
TAP 54:	0.335	0.360	0.360	0.385	0.395	0.308	0.103	-0.077	-0.231	-0.334
TAP 55:	0.437	0.385	0.411	0.411	0.437	0.334	0.128	-0.077	-0.231	-0.334
TAP 56:	0.360	0.411	0.437	0.437	0.395	0.257	0.026	-0.129	-0.231	-0.334
TAP 57:	0.385	0.385	0.462	0.462	0.411	0.231	0.026	-0.128	-0.231	-0.308
TAP 58:	0.411	0.411	0.488	0.488	0.462	0.292	0.077	-0.103	-0.205	-0.308
TAP 59:	0.385	0.462	0.462	0.411	0.334	0.180	0.000	-0.103	-0.205	-0.308
TAP 60:	0.385	0.462	0.514	0.462	0.360	0.180	0.000	-0.103	-0.205	-0.308
TAP 61:	0.411	0.514	0.565	0.514	0.360	0.205	0.026	-0.077	-0.205	-0.308
TAP 62:	0.437	0.462	0.411	0.385	0.308	0.180	0.000	-0.077	-0.205	-0.308
TAP 63:	0.437	0.514	0.411	0.385	0.308	0.180	0.000	-0.103	-0.205	-0.308
TAP 64:	0.437	0.539	0.437	0.385	0.308	0.180	0.026	-0.077	-0.180	-0.308
TAP 65:	-0.257	-0.282	-0.334	-0.334	-0.257	-0.257	-0.231	-0.154	-0.077	-0.103
TAP 66:	-0.385	-0.385	-0.411	-0.411	-0.360	-0.308	-0.308	-0.205	-0.129	-0.103
TAP 67:	-0.292	-0.308	-0.360	-0.385	-0.334	-0.257	-0.231	-0.180	-0.103	-0.103
TAP 68:	-0.335	-0.385	-0.462	-0.462	-0.411	-0.334	-0.308	-0.205	-0.103	-0.103
TAP 69:	-0.292	-0.308	-0.350	-0.385	-0.334	-0.282	-0.257	-0.180	-0.103	-0.129
TAP 70:	-0.334	-0.360	-0.437	-0.437	-0.411	-0.360	-0.334	-0.205	-0.154	-0.128
TAP 71:	-0.257	-0.309	-0.385	-0.385	-0.360	-0.308	-0.257	-0.180	-0.154	-0.154
TAP 72:	-0.308	-0.411	-0.462	-0.514	-0.488	-0.385	-0.360	-0.231	-0.154	-0.180
TAP 73:	-0.257	-0.334	-0.385	-0.411	-0.395	-0.308	-0.232	-0.180	-0.231	-0.231
TAP 74:	-0.292	-0.385	-0.462	-0.488	-0.462	-0.385	-0.334	-0.231	-0.231	-0.257
TAP 75:	-0.257	-0.360	-0.385	-0.411	-0.385	-0.334	-0.257	-0.257	-0.360	-0.411
TAP 76:	-0.308	-0.411	-0.488	-0.514	-0.488	-0.411	-0.308	-0.308	-0.385	-0.385
TAP 77:	-0.257	-0.360	-0.385	-0.437	-0.385	-0.309	-0.360	-0.616	-0.693	-0.668
TAP 78:	-0.308	-0.437	-0.488	-0.514	-0.488	-0.385	-0.462	-0.642	-0.642	-0.642
TAP 79:	-0.231	-0.282	-0.334	-0.462	-0.693	-0.976	-1.027	-0.924	-0.847	-0.770
TAP 80:	-0.334	-0.437	-0.514	-0.591	-0.796	-1.027	-1.053	-0.924	-0.822	-0.796

TABLE 2.2: PRESSURE COEFFICIENTS FOR MODEL WITH WING WALLS ADDED (FILE TAK1)

The results presented in Appendix 1 include the measured pressure difference across the bend of the flow meter, the discharge coefficient for the meter, the pitot reference speed and the reference speed, V_z. The flows measured with C_d < 0.6 or C_Q < .02 must be regarded as suspect since below 0.6 the variation of C_d with Reynolds Number is very strong and the coefficient is poorly defined. Values of C_Q < 0.02 were limited primarily to the models with 1/8" or 3/32" diameter holes of porosities less than 5%.

3.0 COMPARISON OF MEASURED AND COMPUTED FLOWS

3.1 Theoretical Estimates of Flow Rates

The basic assumptions in computing the flow rate from the external pressure distribution are as follows;

i) the internal flows do not disturb the external pressure field,

and ii) the flow rates through a given opening can be calculated from the relationship

$$Q = C_d A_o \sqrt{2 \Delta p/\rho}$$

where; A_o = area of opening
C_d = discharge coefficient
Δp = pressure difference across the opening

The method of computation involves further assumptions which are discussed after a description of the method. An idealisation of the flow path through the building is shown in Fig. 3.1. The equations defining the total flow Q follow the following definitions;

ΔQF_i = that part of the flow through the front wall which passes through the ith opening which has an area AF_i • *(+ ve in)*

ΔQR_i = that part of the flow through the rear wall which passes through the ith opening which has an area AR_i *(+ ve out)*

Q = total flow

PI_1 = pressure to the front of a grid representing the internal restrictions

PI_2 = pressure behind the grid representing the internal restrictions

PI'_1 = pressure just inside the front wall.

The equations defining the flow may then be written as;

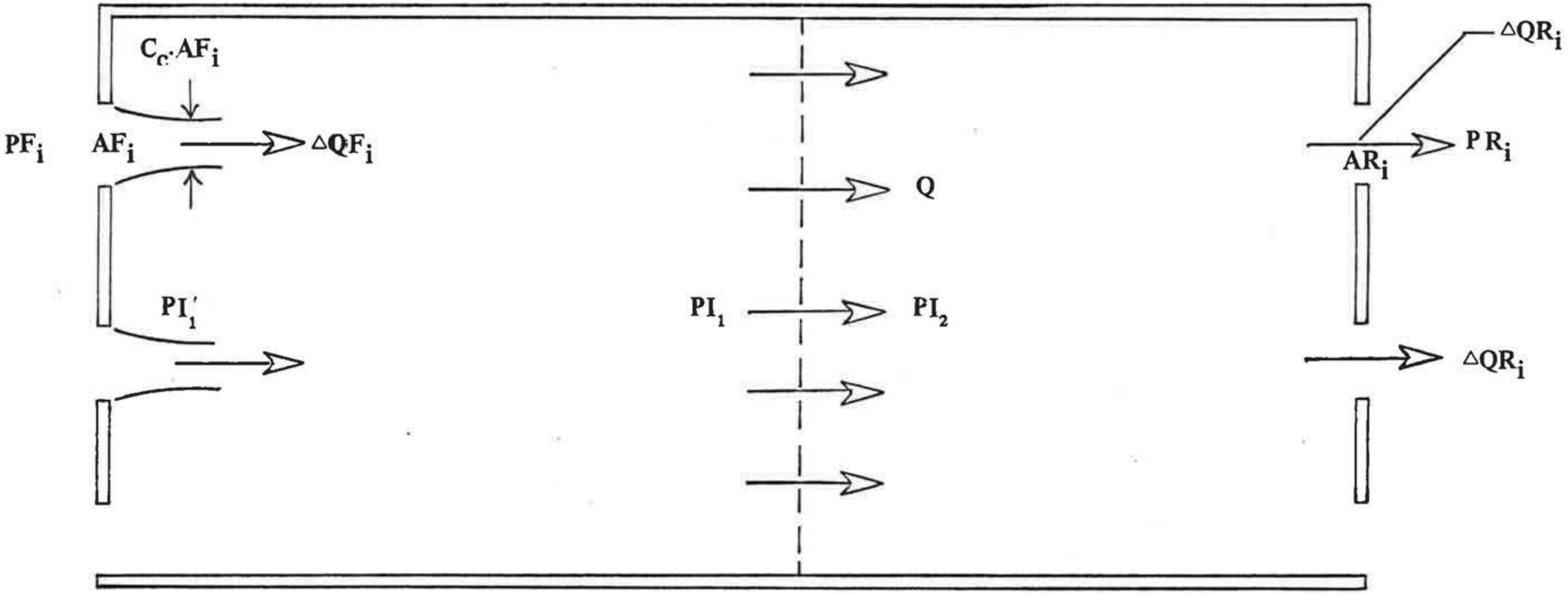

FIG. 3.1 IDEALIZED FLOW PATH THROUGH BUILDING

$$Q \quad = \quad Q_{in} = \sqrt{\frac{2}{\rho}} \sum_{i=1}^{N} C_{d_i} \, AF_i \, \frac{(PF_i - PI_1)}{\sqrt{|PF_i - PI_1|}} \tag{3.1}$$

$$\quad = \quad Q_{out} = \sqrt{\frac{2}{\rho}} \sum_{i=1}^{M} C_{d_i} \, AR_i \, \frac{PI_2 - PR_i}{\sqrt{|PI_2 - PR_i|}} \tag{3.2}$$

where; N = number of openings on front face
M = number of opening on rear face

and

$$PI_1 - PI_2 = C_L \frac{\rho V^2}{2} \tag{3.3}$$

where; V = Q/A
and A = frontal area

It is further assumed that the discharge coefficients for the inflow openings are those for the flow situation shown in Fig. 3.2 and that the discharge coefficients for the outflow openings are those for the flow situation shown in Fig. 3.3. Thus, it is assumed that the discharge coefficient for the front is that for a duct with an opening leading from a large volume and the ratio of the area of the opening to the duct area is equal to the ratio of the total open area to the total area of the frontal wall. Similarly, C_d for the rear openings is assumed to be that for a duct discharging into a large volume. Implicit in these idealisations is the assumption that flow across the face of a building does not influence the discharge through an opening in that face. This is not unreasonable for the rear face which will generally lie in a separated flow region with low mean speeds but is doubtful for the front face when this is inclined to the flow. The comparison of the measured and computed flows is as much a test of this approach as it is of the basic assumptions defined earlier.

Accepting the Equations 3.1 to 3.3 the flow Q can be computed from the external distribution. For the most part the number and position of the openings matched the number and position of the pressure taps and the values of PF_i and PR_i were readily defined. In the cases where large single openings were employed the procedure was modified slightly; in this case the flow was computed as if the total open area was equally distributed among "N" openings positioned at the pressure tap locations. In the case of wall openings $M = N = 24$ while for roof openings $M = 8$.

The unknowns in Equations 3.1 to 3.3 are Q_i, PI_1 and PI_2. The method of computation was as follows;

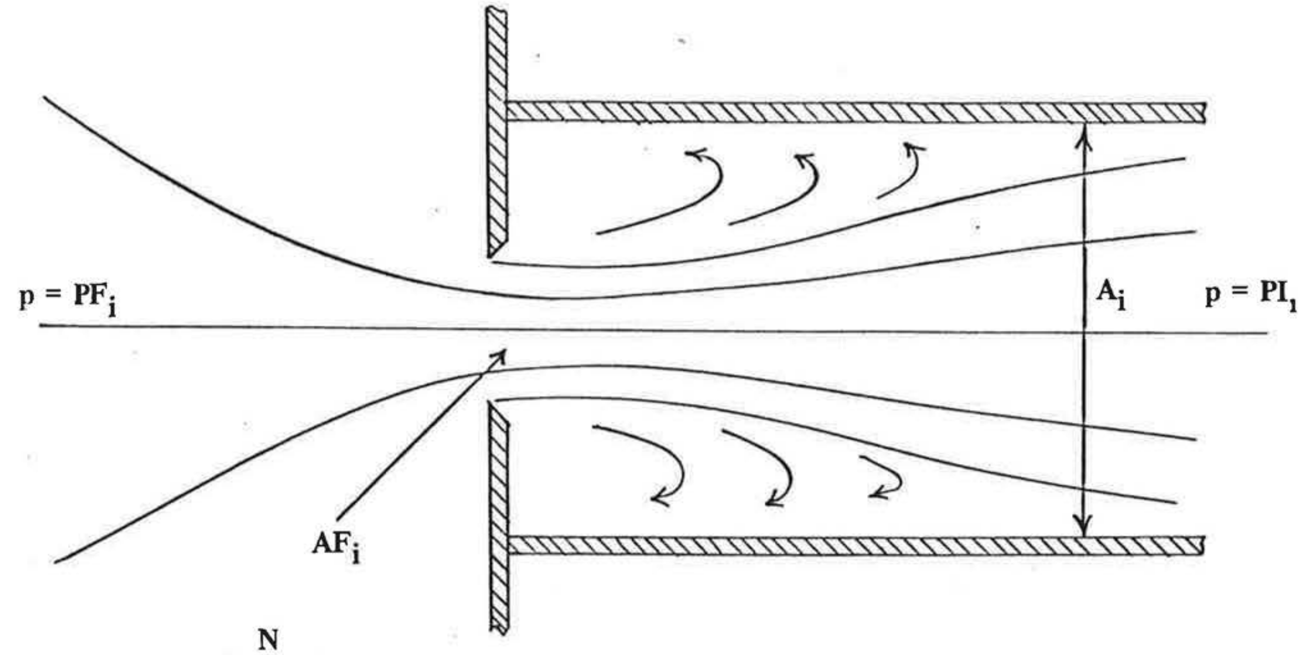

$$\frac{AF_i}{A_i} = \frac{\sum_{1}^{N} AF_i}{A}$$

FIG. 3.2 ASSUMED FLOW PATTERN FOR INFLOW

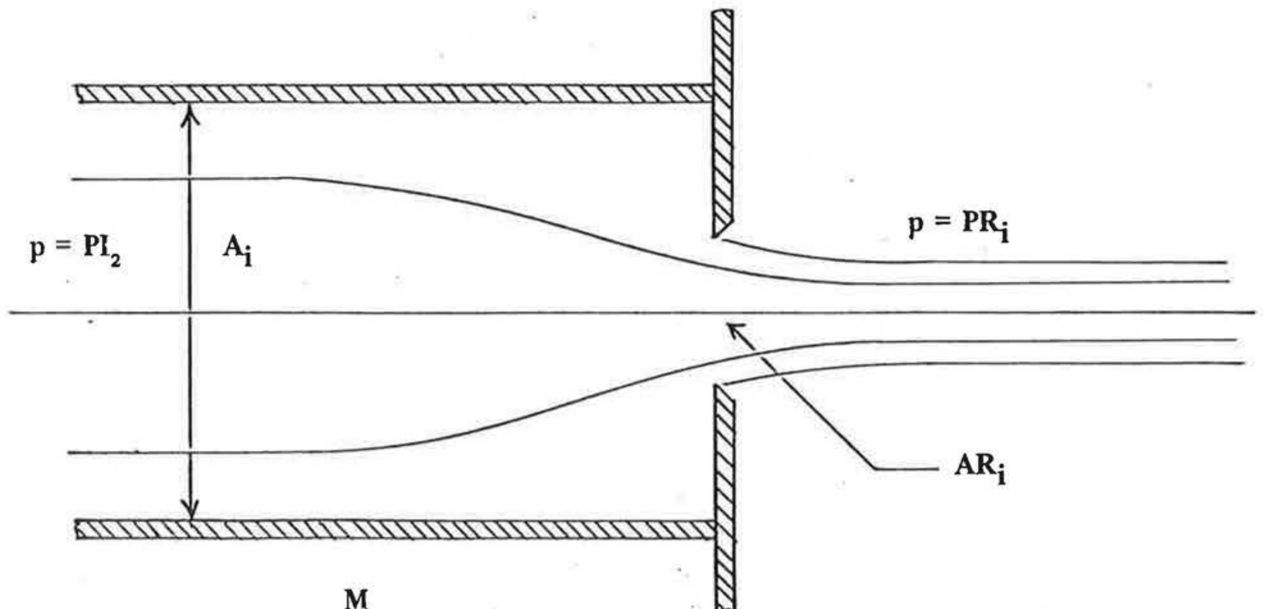

$$\frac{AR_i}{A_i} = \frac{\sum_{1}^{M} AR_i}{A}$$

FIG. 3.3 ASSUMED FLOW PATTERN FOR OUTFLOW

(1) Put $PI_1 = PI + \Delta P/2$

$PI_2 = PI - \Delta P/2$

where $\Delta P = C_L \, \rho V^2/2$

(2) Compute Initial PI, Δ P

$$(PI)_o = \tfrac{1}{2} \left\{ 1/N \sum PF_i + 1/M \sum PR_i \right\}$$

$$(\Delta P)_o = 0$$

(3) Compute (i) Q_{in} and $\partial Q_{in}/\partial P_I$

and (ii) Q_{out} and $\partial Q_{out}/\partial P_I$

(4) Compute $$\Delta P_I = \frac{Q_{out} - Q_{in}}{(\partial Q_{in}/\partial P_I - \partial Q_{out}/\partial P_I)}$$

(5) Compute $$\Delta P = C_L \, \rho \, \{(Q_{out} + Q_{in})/2A)\}^2/2$$

(6) Modify P_I, ΔP, C_L (and recompute Q_{in}, Q_{out})

(7) Test for convergence

If $Q_{in} - Q_{out}/Q_{out} < 0.1\%$; Stop
If $Q_{in} - Q_{out}/Q_{out} > 0.1\%$; Return to 3.

The procedure outlined above was designed for systems where the internal loss (ΔP) was small compared to the losses through the external walls. In such cases the computations converged rapidly but for large wall porosities (> 40%) it was necessary to modify the program.

The loss coefficient, C_L, for the interior flow path was taken as measured (see Section 2.2). The discharge coefficients were computed from existing data which are shown in Figs. 3.4 and 3.5. The range of practical interest is $0 < A_o/A < 0.5$ or thereabouts and within this range $0.6 < C_d < 0.8$. The results shown in Figs. 3.4 and 3.5 are for large values of R_e (VD/ν) and there is some dependency on R_e below values of about 10^4. The speeds through the openings of the model were typically, 15 to 20 fps and the Reynolds Number about 10^5 x hole diameter or $10^3 < R_e < 3 \times 10^3$. Data for plate orifices in pipes indicate an increase in C_d from $R_e = 10^4$ (C_d is approximately constant for $R_e > 10^4$) to $R_e = 10^3$ of between 5% and 10% for $A_o/A < 15\%$ and up to a 50% increase for $A_o/A > 50\%$.

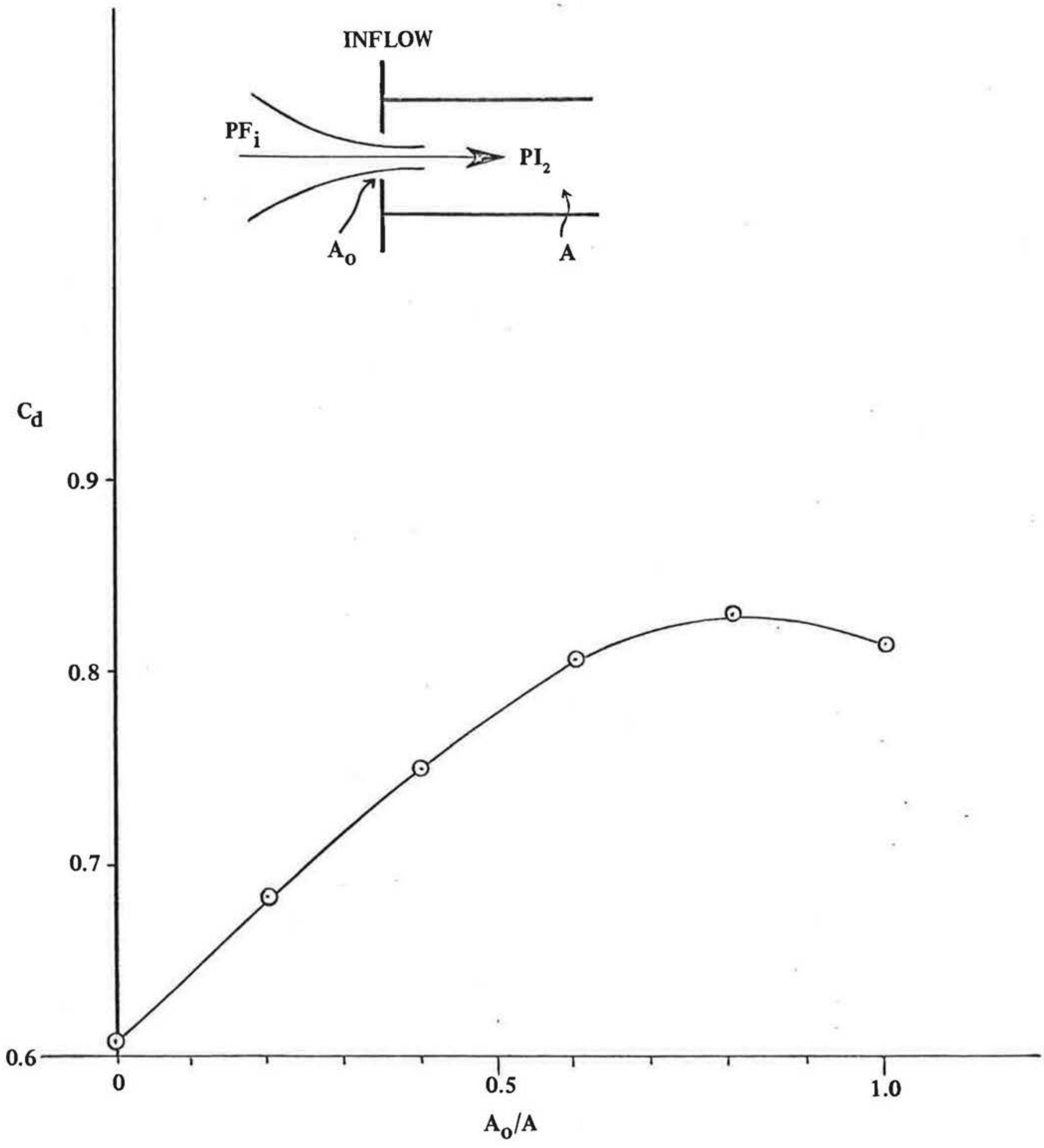

FIG 3.4 DISCHARGE COEFFICIENT FOR HIGH REYNOLDS NUMBER FLOWS AS SHOWN IN FIG. 3.2

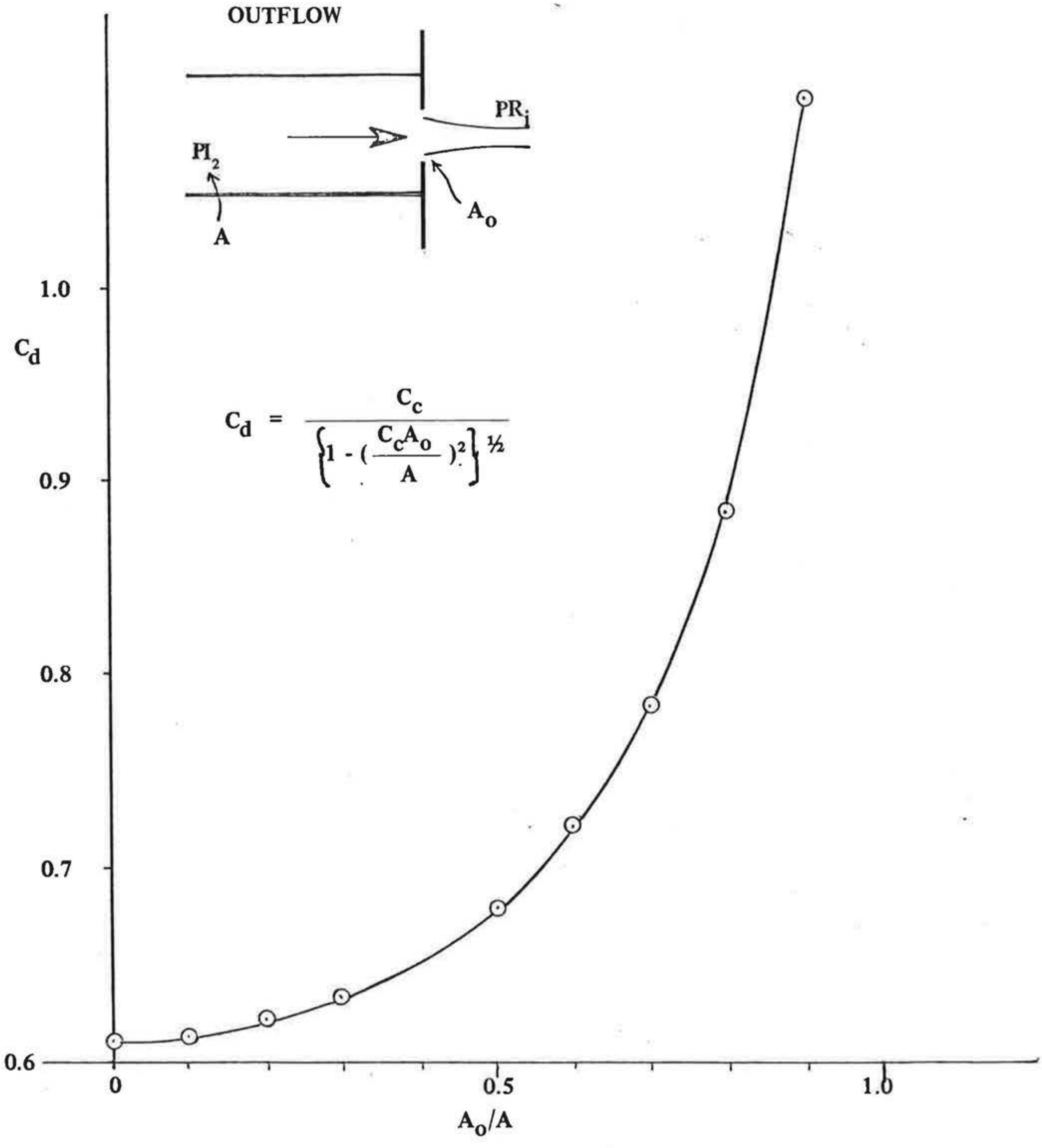

$$C_d = \frac{C_c}{\left\{1 - \left(\frac{C_c A_o}{A}\right)^2\right\}^{1/2}}$$

FIG. 3.5 DISCHARGE COEFFICIENTS FOR HIGH REYNOLDS NUMBER FLOWS AS SHOWN IN FIG. 3.3

In order to check the results shown in Fig. 3.4 and 3.5 and in particular, the sensitivity to Re, direct measurements were made of the discharge coefficient for the inflow situation shown in Fig. 3.4. The experimental arrangement is shown in Fig. 3.6 and the discharge coefficient for 3/8", 1/4" and 3/16" diameter perforations are shown in Figs. 3.7, 3.8 and 3.9. In the significant range of Re (that corresponding to the higher flow rates) the measured coefficients tend to be greater than those predicted (Fig. 3.4) although the Reynolds Number effects are not as strong as those reported by Johansen for plate orifice meters. All computed flows were based upon Figs. 3.4 and 3.5 with no corrections for Reynolds Number. The measured values of C_d suggest that the use of Fig. 3.4 and 3.5 might lead to slight underestimates (by perhaps 10%) of the theoretical flow rates.

3.2 Comparison of Measured and Predicted Internal Flow Rates

The measured internal flows and those computed using the methods and data detailed in Section 3.1 are presented graphically in Figs. 3.10 to 3.37. The conditions under which the flows were measured are as listed in Table 3. In all figures the measured flows are denoted by circles (O) and the computed flows by triangles (Δ).

For the tests with flow through walls only the trend of the results is similar for both models (with and without wing walls). At the larger openings the flows are consistently overestimated by the theoretical methods. The trend is shown in Fig. 3.38 in which Q_T/Q_E (the ratio of the theoretical to the measured flows) is plotted against C_Q, the theoretical flow coefficient. The results shown in Fig. 3.38 were derived from Figs. 3.10 to 3.37 with the values of C_Q, Q_T and Q_E evaluated as average values for azimuth angles from 0^o to 60^o.

The ratio Q_T/Q_E for flow out through ridge vents are shown in Fig. 3.39. These results indicate a highly significant overestimate of about 40% with a tendency for the error to increase with the flow coefficient although the scatter is considerable.

3.3 Discussion

Before considering the comparison of the measured and predicted flow rates some attention will be given to the expected form of the comparison. The external pressure distribution will be influenced by the "through-flow" which will itself reduce the pressure gradient across the model and hence lead to an overprediction of the flows calculated on the basis of "solid model" pressure distributions. If we consider the case of flow through a planar grid with a total area A and a porosity (A_{open}/A_{total}) α, then data are available which enable the drag coefficient $(C_D = F_D/\frac{1}{2}\rho V^2 A_T)$ to be expressed as a function of α. The data of Flachsbart, Georgiou and Vickery and others shows that;

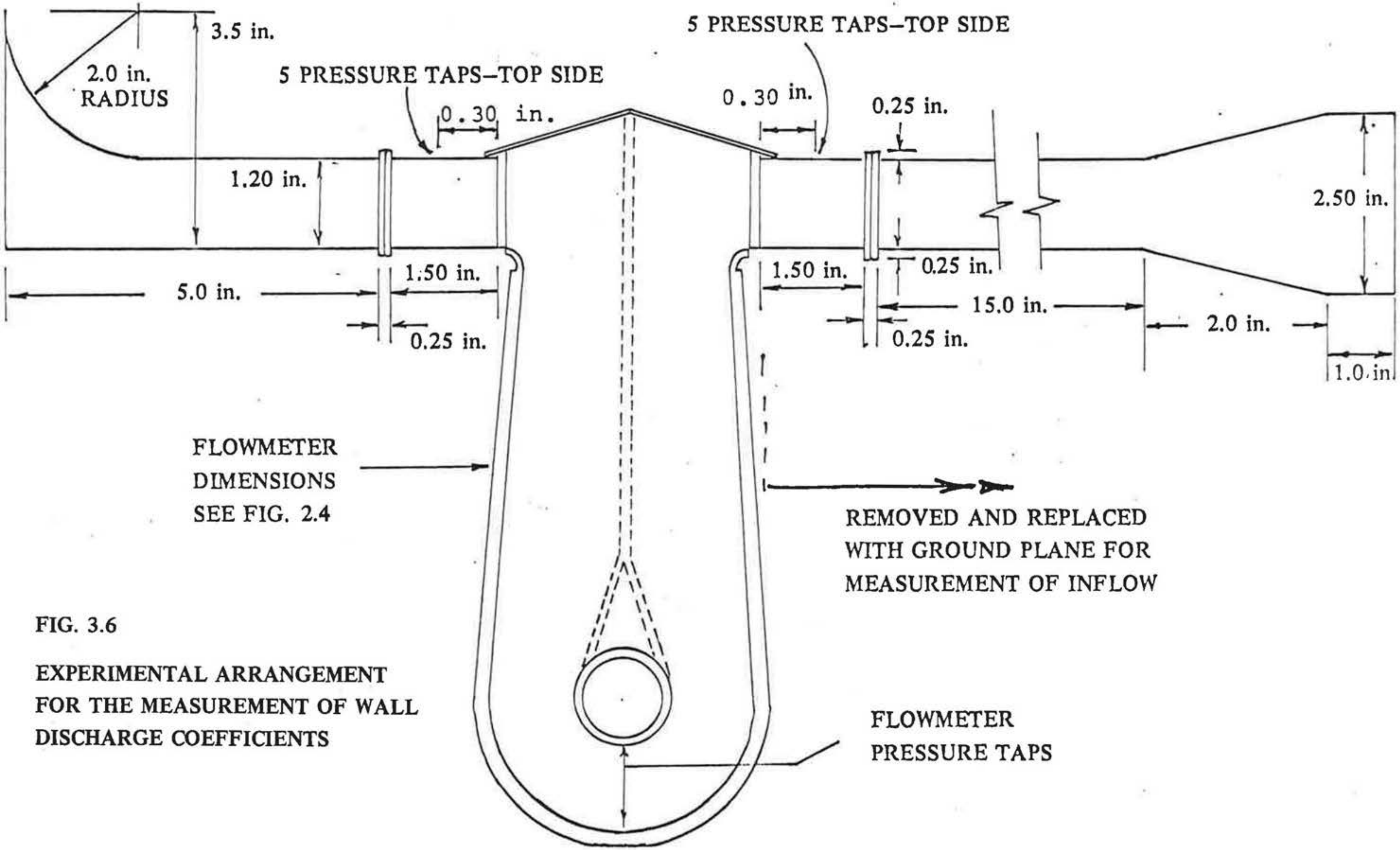

FIG. 3.6

EXPERIMENTAL ARRANGEMENT FOR THE MEASUREMENT OF WALL DISCHARGE COEFFICIENTS

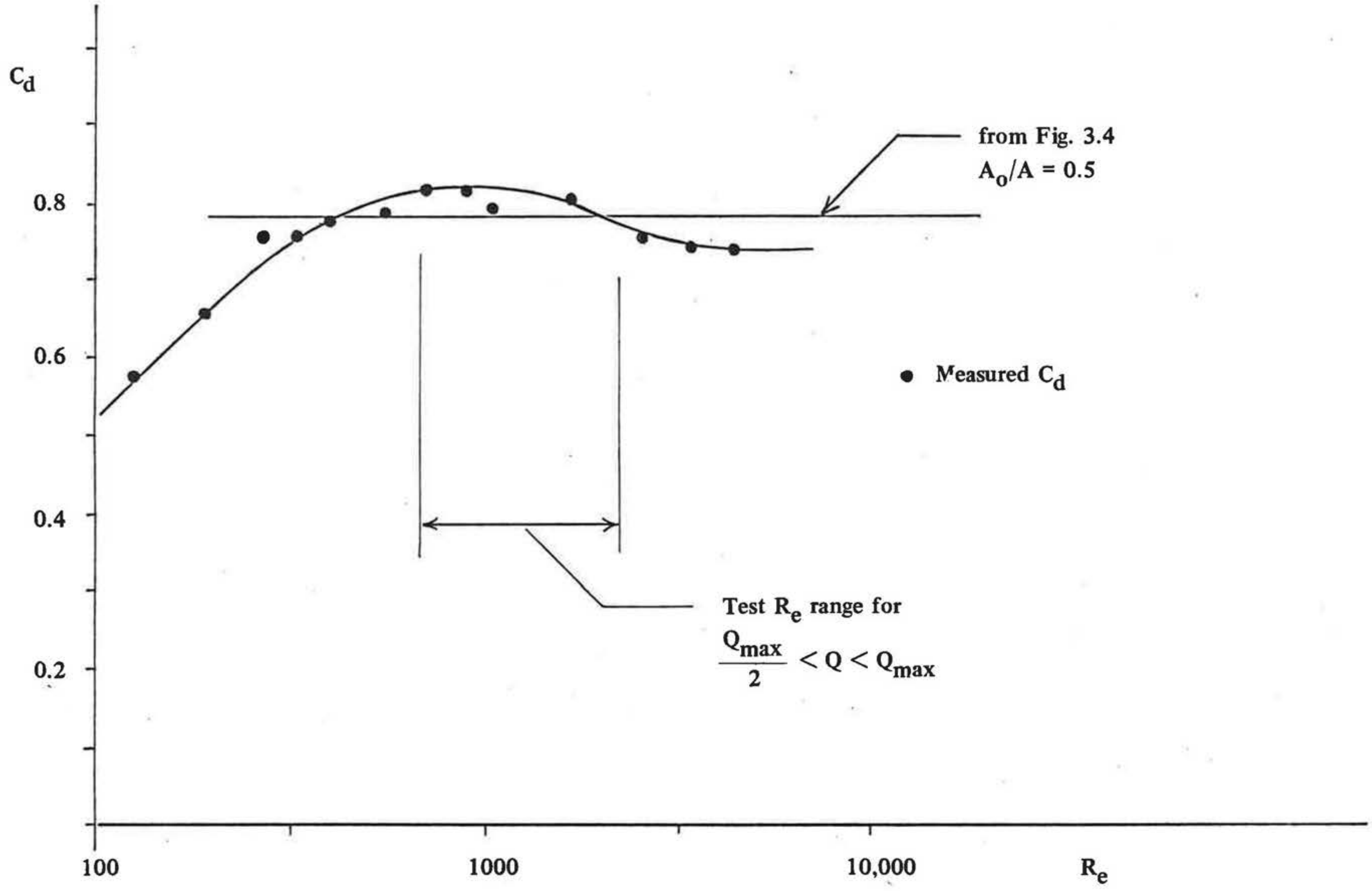

FIG. 3.7 MEASURED DISCHARGE COEFFICIENTS FOR FLOW INTO 3/8" PERFORATIONS

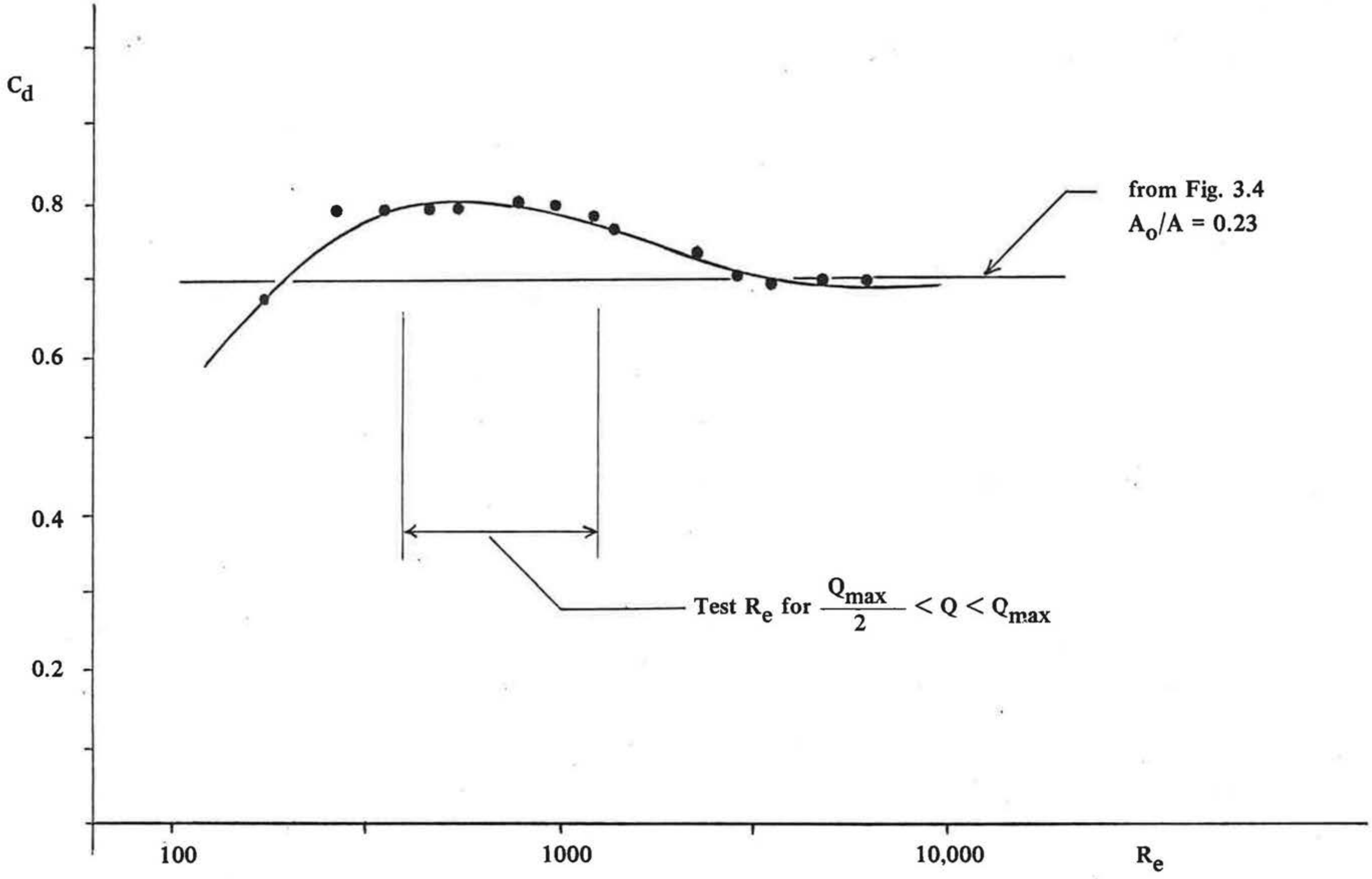

FIG. 3.8 MEASURED DISCHARGE COEFFICIENTS FOR FLOW INTO 1/4" DIAMETER PERFORATIONS

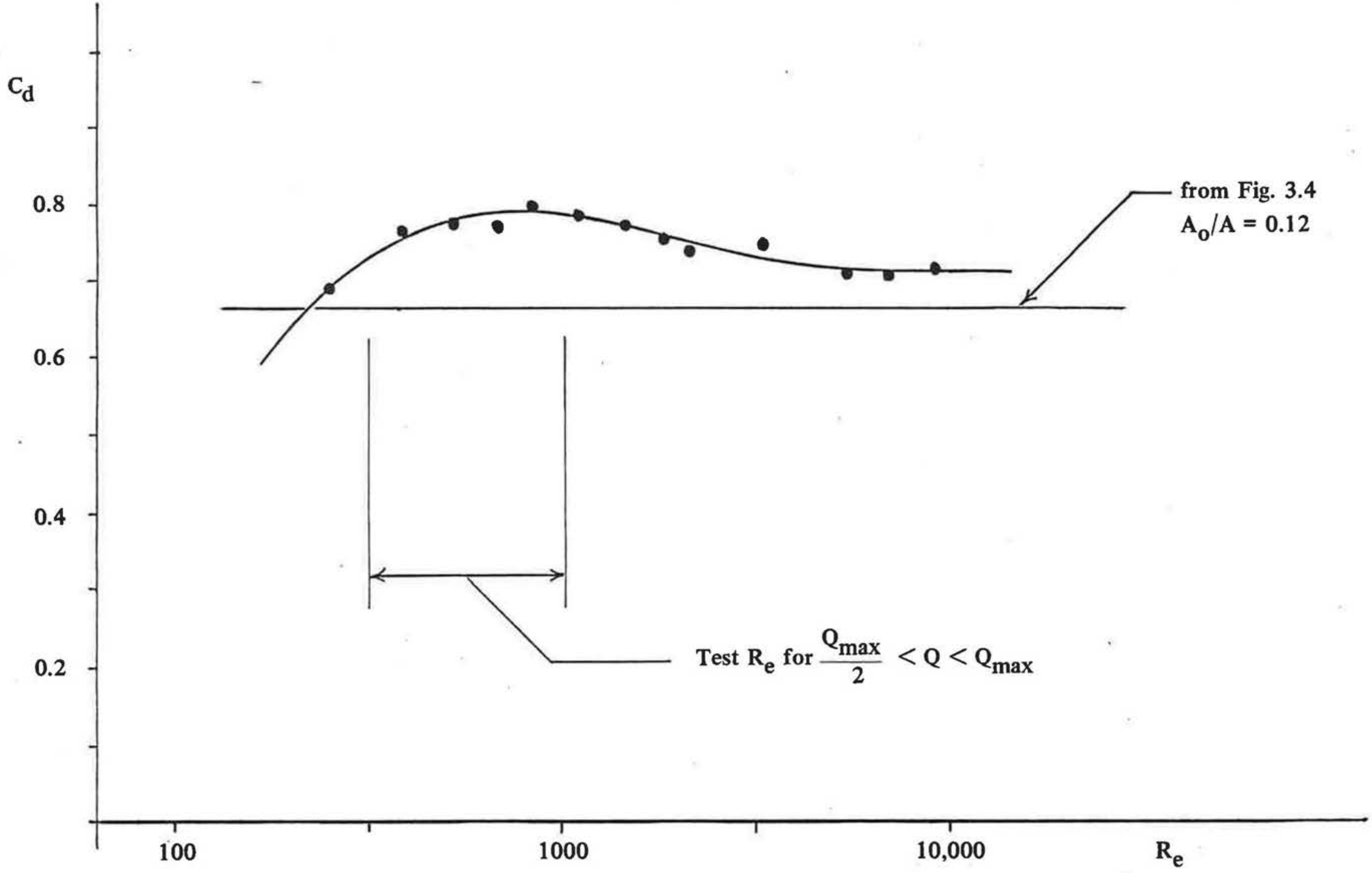

FIG. 3.9 MEASURED DISCHARGE COEFFICIENTS FOR FLOW INTO 3/16" DIAMETER PERFORATIONS

TABLE 3: TEST CONDITIONS FOR FIGS. 3.10 TO 3.37

FILE NAME AND FIG. NO.	DESCRIPTION						
	FRONT WALL OPENING	% OF FRONTAL WALL AREA	REAR WALL OPENING	% OF FRONTAL WALL AREA	RIDGE VENT.	% OF FRONTAL WALL AREA	
CAK22 - 3.10	Removed	100	Removed	100	NIL		BASIC MODEL
CAK24 - 3.11	4″ x 1″	71	4″ x 1″	71	″		
CAK25 - 3.12	3.2″ x 0.8″	46	3.2″ x 0.8″	46	″		
CAK26 - 3.13	24 @ 3/8″φ	47	24 @ 3/8″φ	47	″		
CAK27 - 3.14	24 @ 1/4″φ	21	24 @ 1/4″φ	21	″		
CAK28 - 3.15	24 @ 3/16″φ	12	24 @ 3/16″φ	12	″		
CAK29 - 3.16	24 @ 1/8″φ	5	24 @ 1/8″φ	5	″		
CAK30 - 3.17	24 @ 3/32″φ	3	24 @ 3/32″φ	3	″		
CAK31 - 3.18	24 @ 1/8″φ	5	NIL	0	1/8″ SLOT	9	
CAK32 - 3.19	24 @ 3/16″φ	12	″		1/8″ SLOT	9	
CAK33 - 3.20	24 @ 3/16″φ	12	″		1/4″ SLOT	18	
CAK34 - 3.21	24 @ 1/4″φ	21	″		1/4″ SLOT	18	
CAK35 - 3.22	24 @ 1/4″φ	21	″		1/2″ SLOT	36	
CAK36 - 3.23	24 @ 3/8″φ	47	″		1/2″ SLOT	36	
CAK37 - 3.24	Removed	100	Removed	100	NIL		WINGS ADDED
CAK38 - 3.25	4″ x 1″	71	4″ x 1″	71	″		
CAK39 - 3.26	3.2″ x 0.8″	46	3.2″ x 0.8″	46	″		
CAK40 - 3.27	24 @ 3/8″φ	47	24 @ 3/8″φ	47	″		
CAK41 - 3.28	24 @ 1/4″φ	21	24 @ 1/4″φ	21	″		
CAK42 - 3.29	24 @ 3/16″φ	12	24 @ 3/16″φ	12	″		
CAK43 - 3.30	24 @ 1/8″φ	5	24 @ 1/8″φ	5	″		
CAK44 - 3.31	24 @ 3/32″φ	3	24 @ 3/32″φ	3	″		
CAK45 - 3.32	24 @ 1/8″φ	5	NIL	0	1/8″ SLOT		
CAK46 - 3.33	24 @ 3/16″φ	12	″		1/8″ SLOT		
CAK47 - 3.34	24 @ 3/16″φ	12	″		1/4″ SLOT		
CAK48 - 3.35	24 @ 1/4″φ	21	″		1/4″ SLOT		
CAK49 - 3.36	24 @ 1/4″φ	21	″		1/2″ SLOT		
CAK50 - 3.37	24 @ 3/8″φ	47	″		1/2″ SLOT		

MEASURED VS CALCULATED CAK23

FIG. 3.10

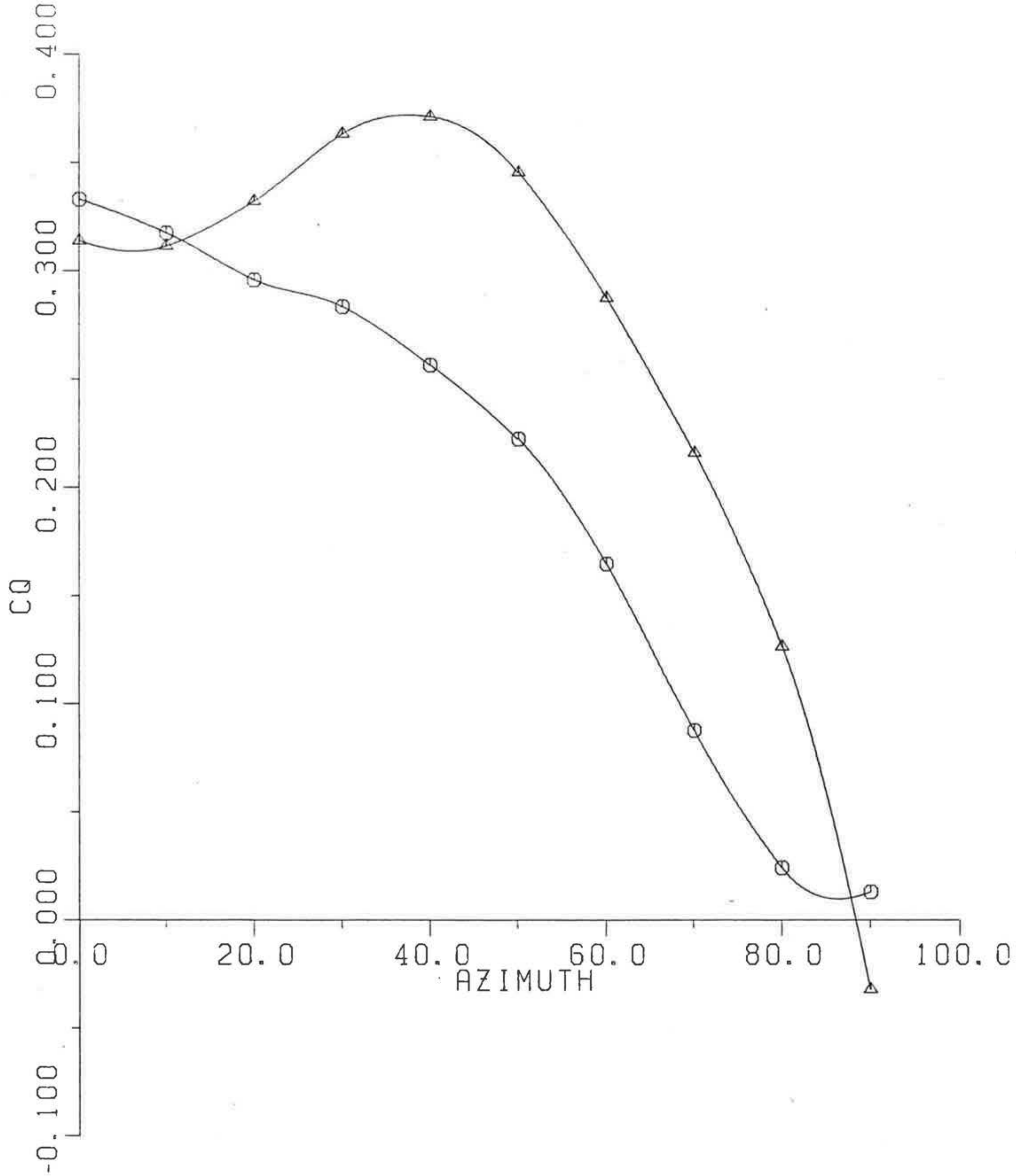

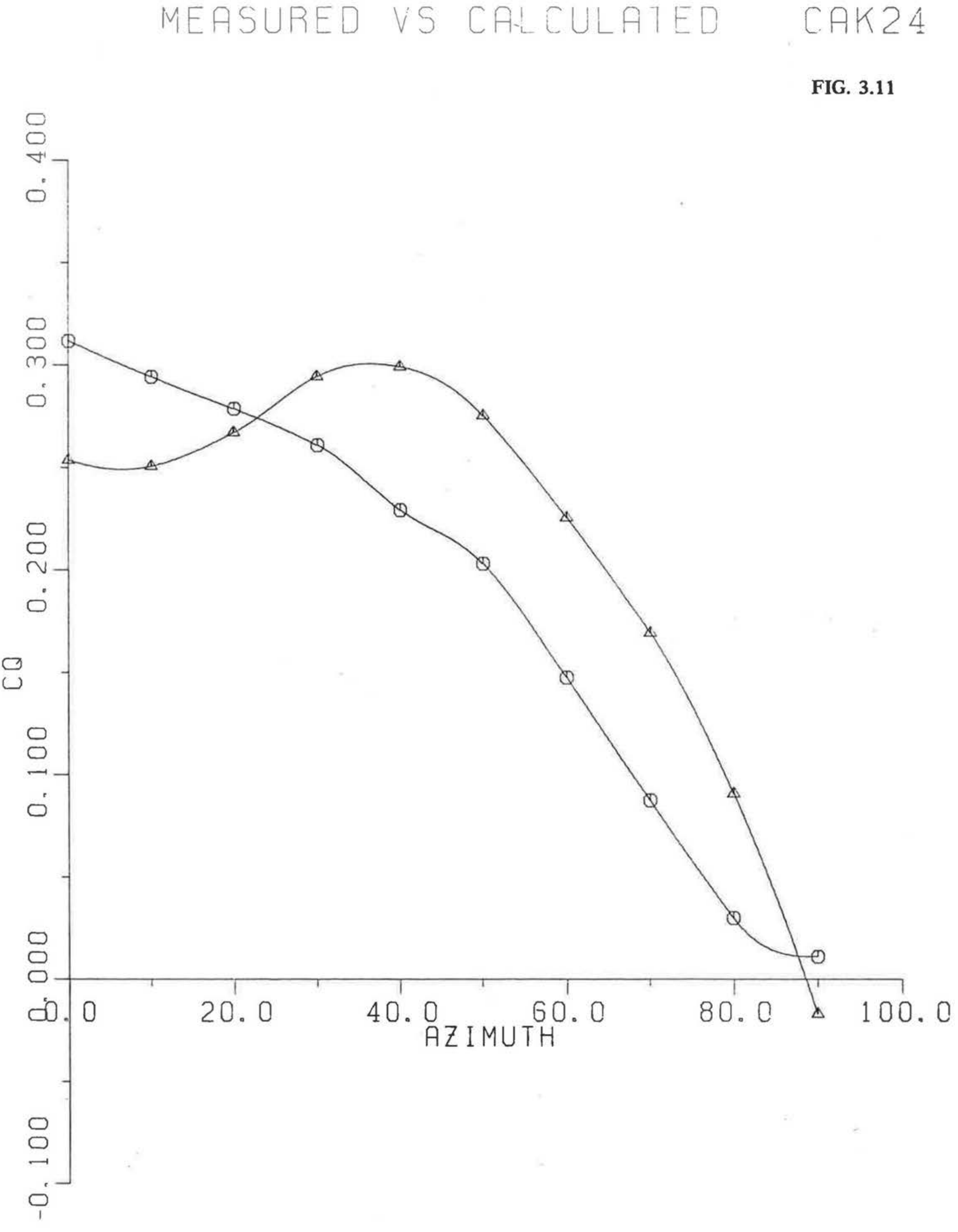
MEASURED VS CALCULATED CAK24
CQ
0.400
0.300
0.200
0.100
0.000
-0.100
0.0
20.0
40.0
60.0
80.0
100.0
AZIMUTH

FIG. 3.11

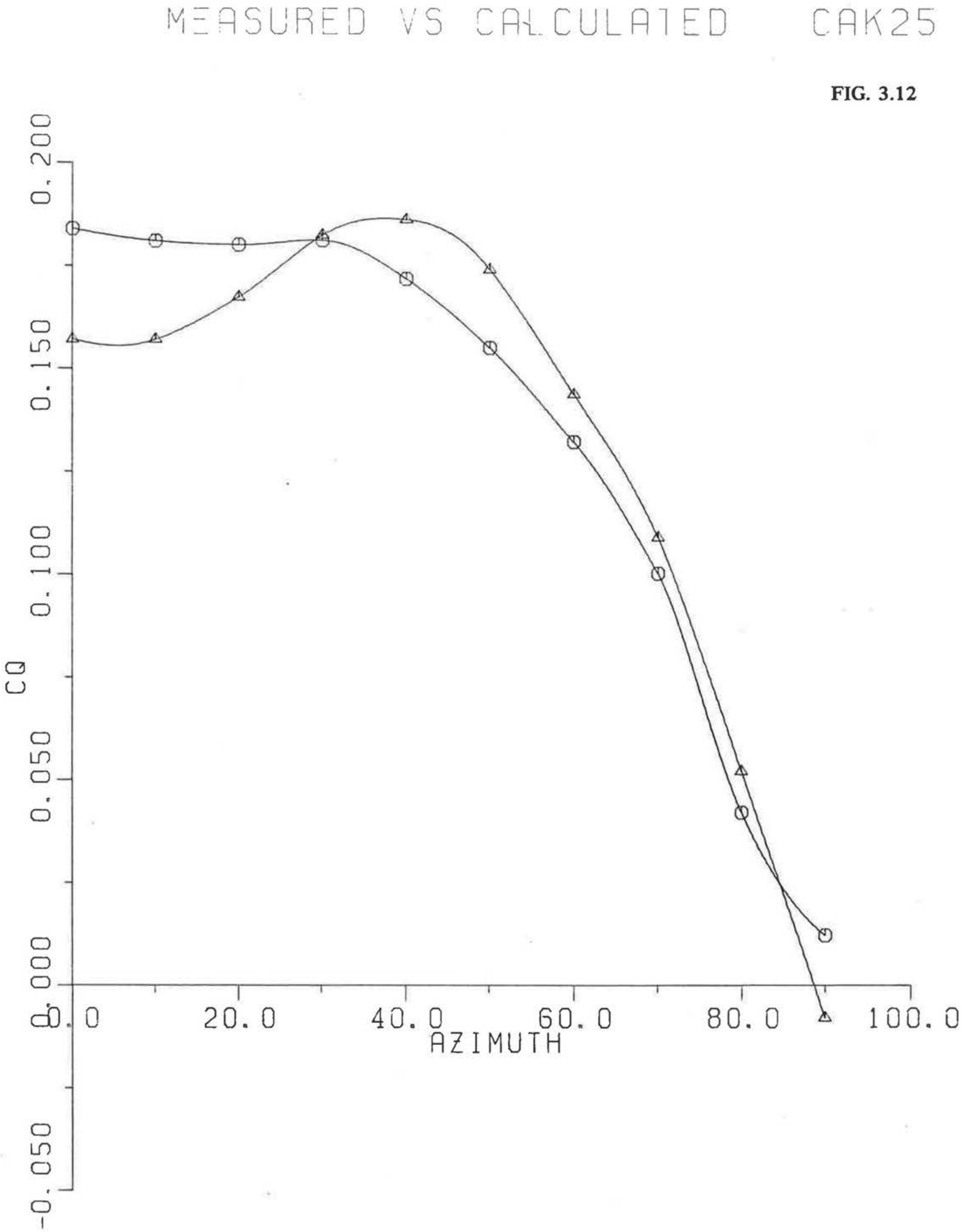
MEASURED VS CALCULATED CAK25
0.200
0.150
0.100
0.050
0.000
-0.050
CQ
0.0
20.0
40.0
60.0
80.0
100.0
AZIMUTH

FIG. 3.12

MEASURED VS CALCULATED CAK26

FIG. 3.13

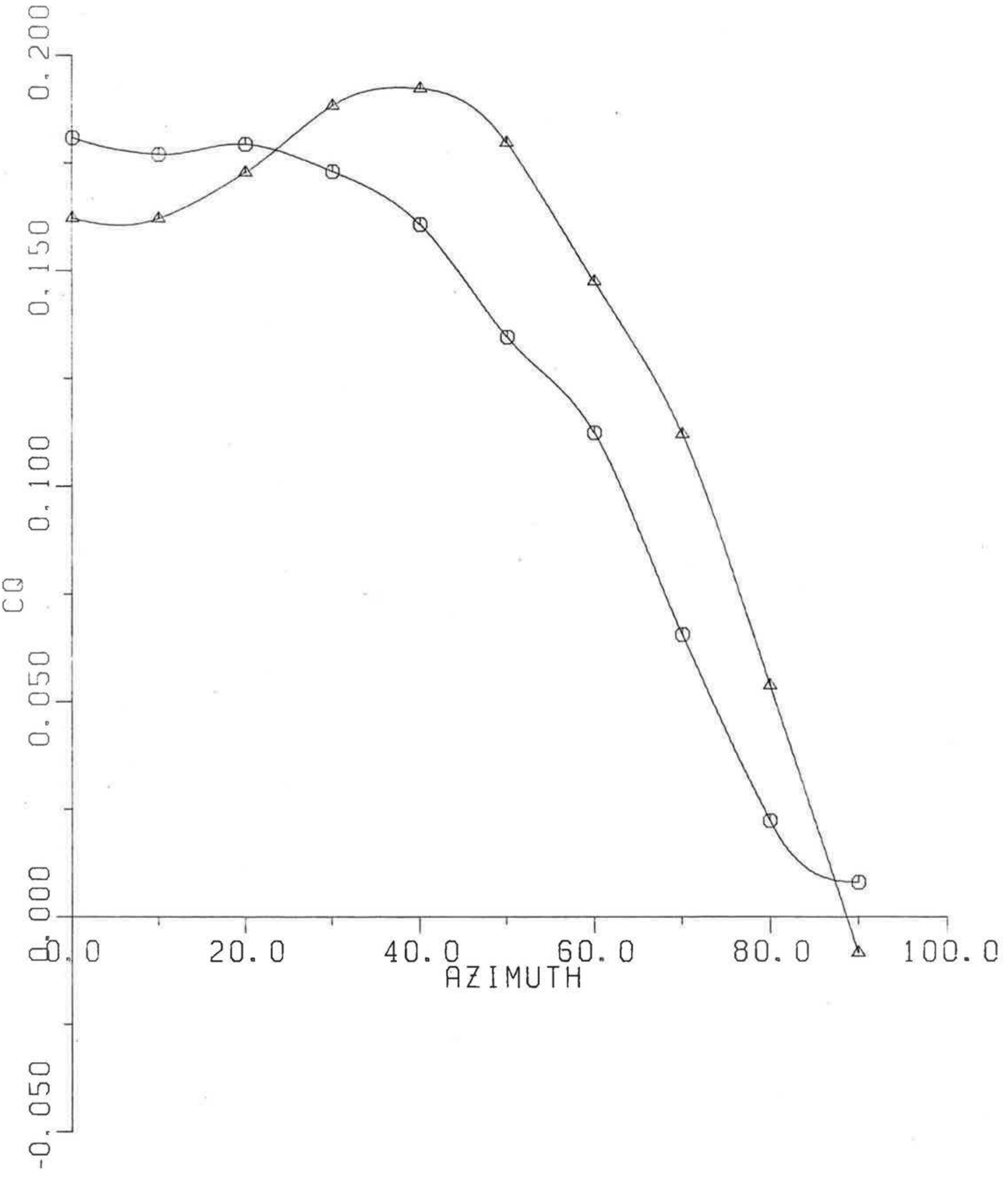

MEASURED VS CALCULATED CAK27

FIG. 3.14

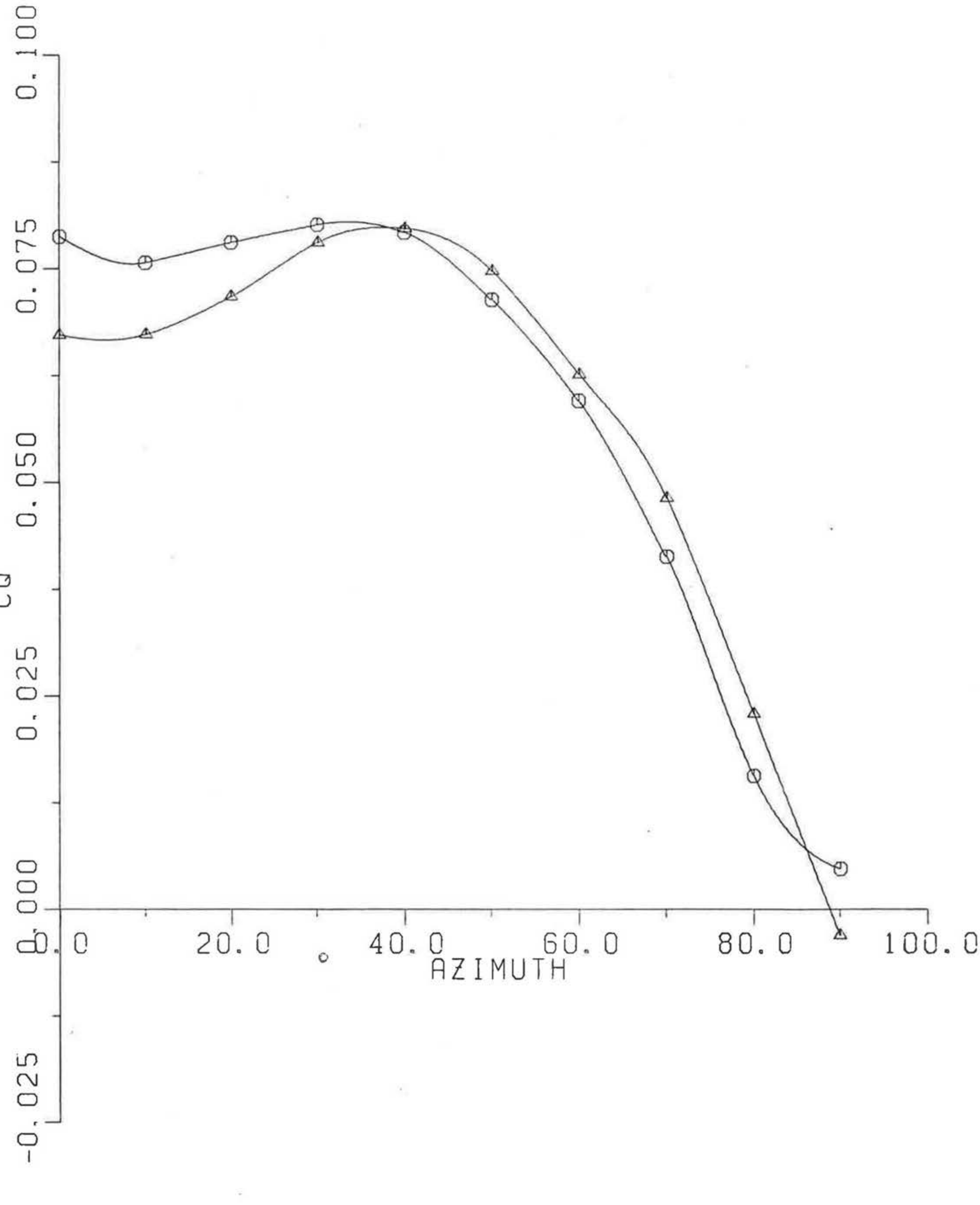

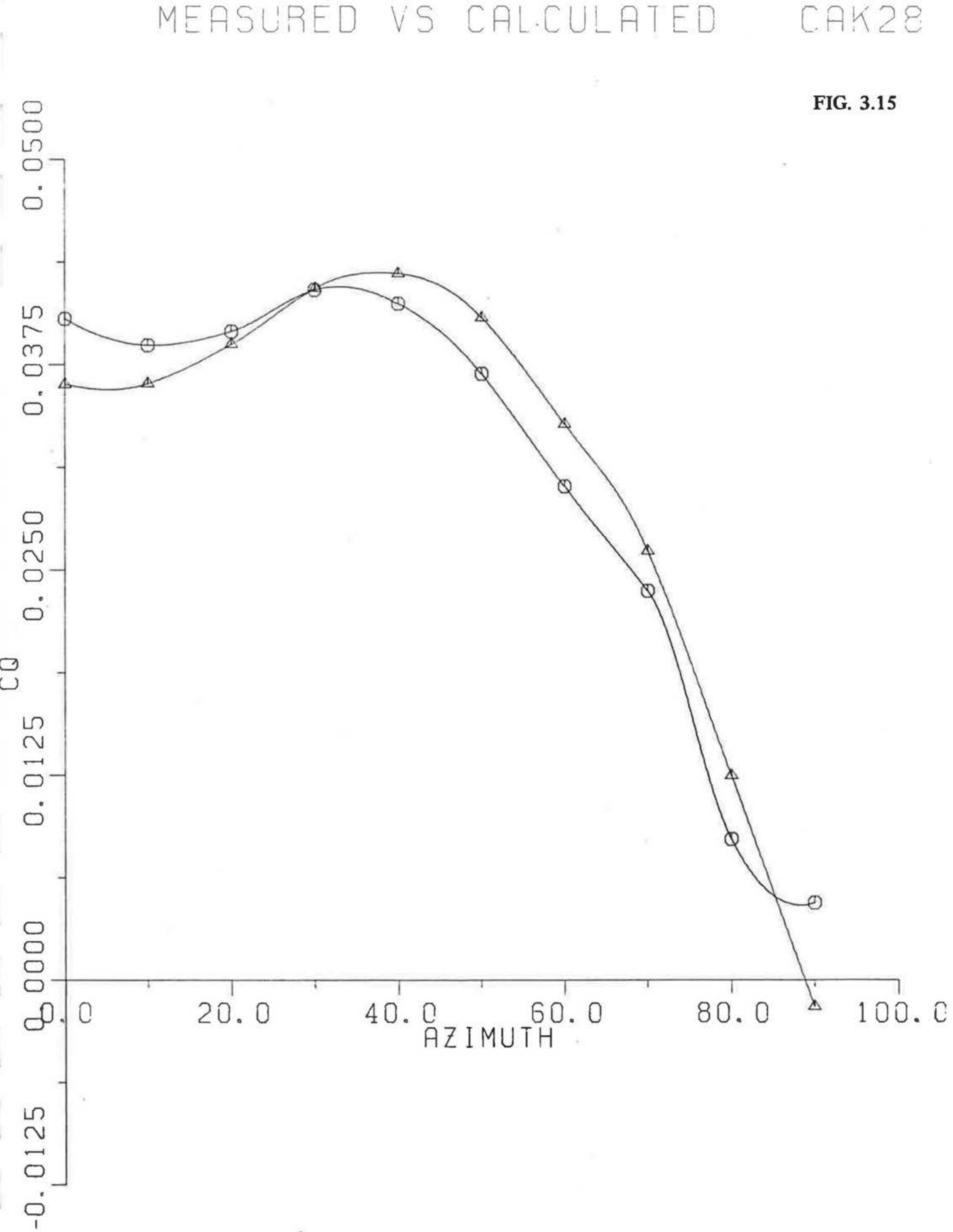
MEASURED VS CALCULATED CAK28
0.0500
0.0375
0.0250
0.0125
0.0000
-0.0125
CQ
0.0
20.0
40.0
60.0
80.0
100.0
AZIMUTH

FIG. 3.15

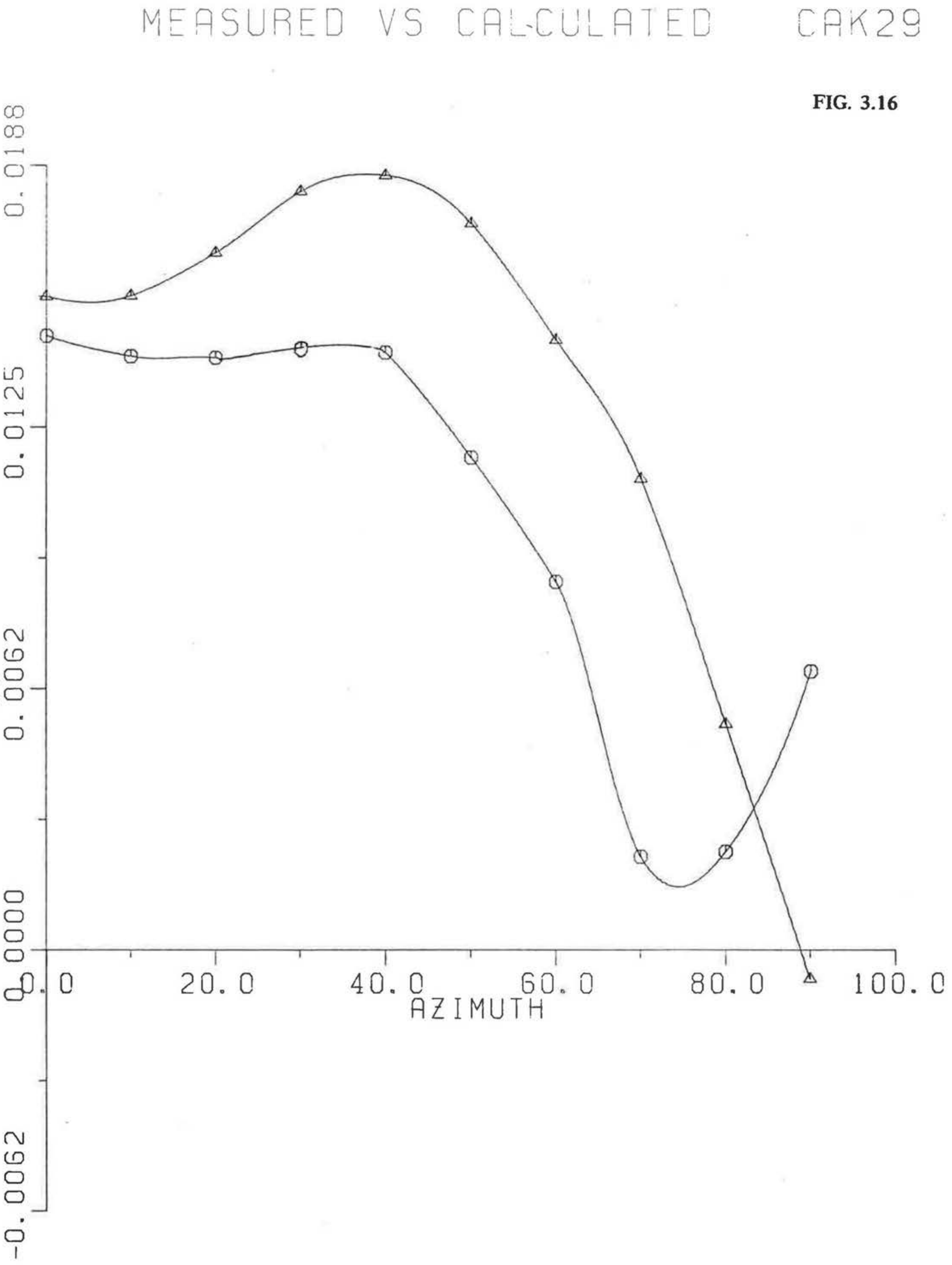
MEASURED VS CALCULATED CAK29
0.0188
0.0125
0.0062
0.0000
-0.0062
CQ
0.0
20.0
40.0
60.0
80.0
100.0
AZIMUTH

FIG. 3.16

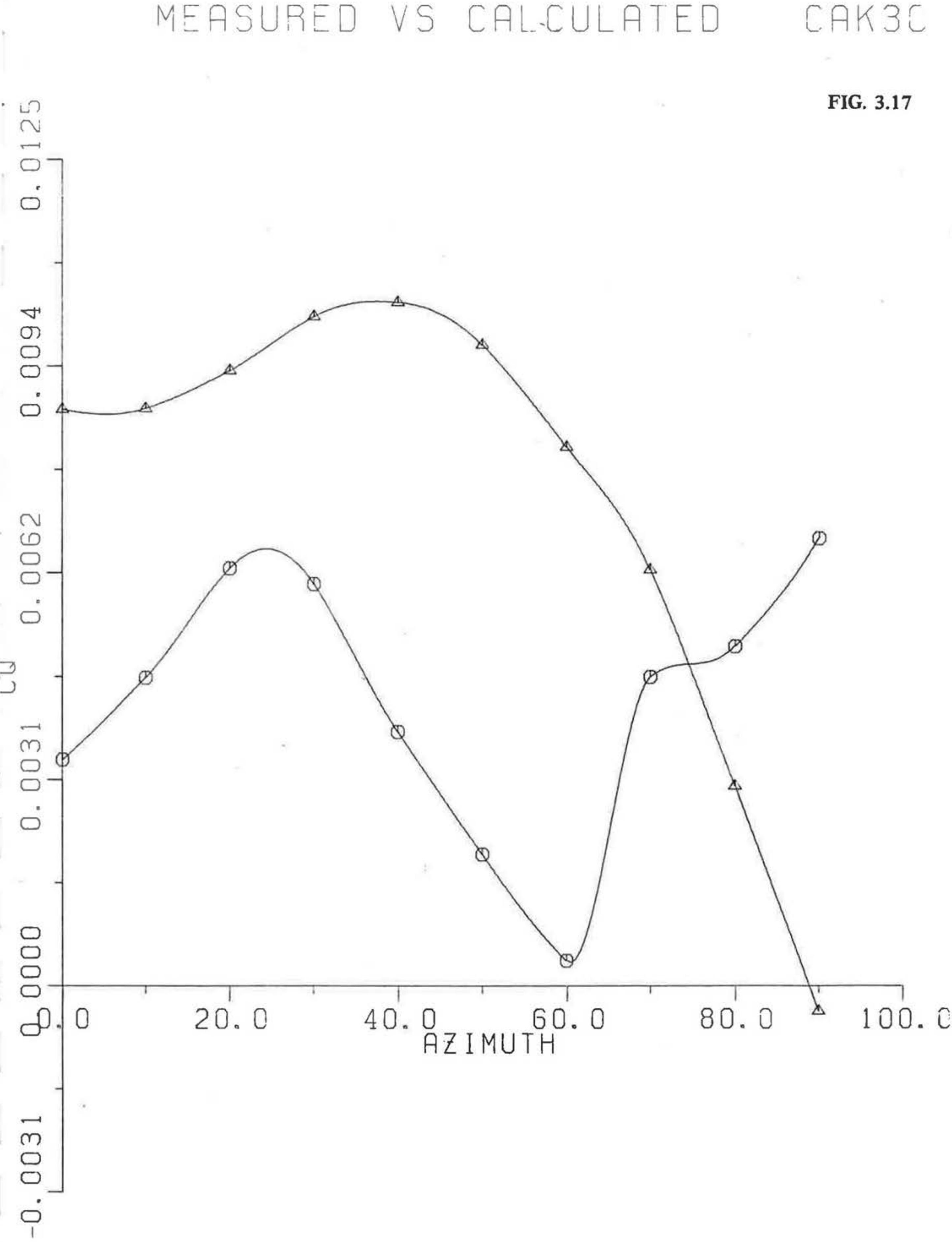
MEASURED VS CALCULATED CAK3C
0.0125
0.0094
0.0062
0.0031
0.0000
-0.0031
CQ
0.0
20.0
40.0
60.0
80.0
100.0
AZIMUTH

FIG. 3.17

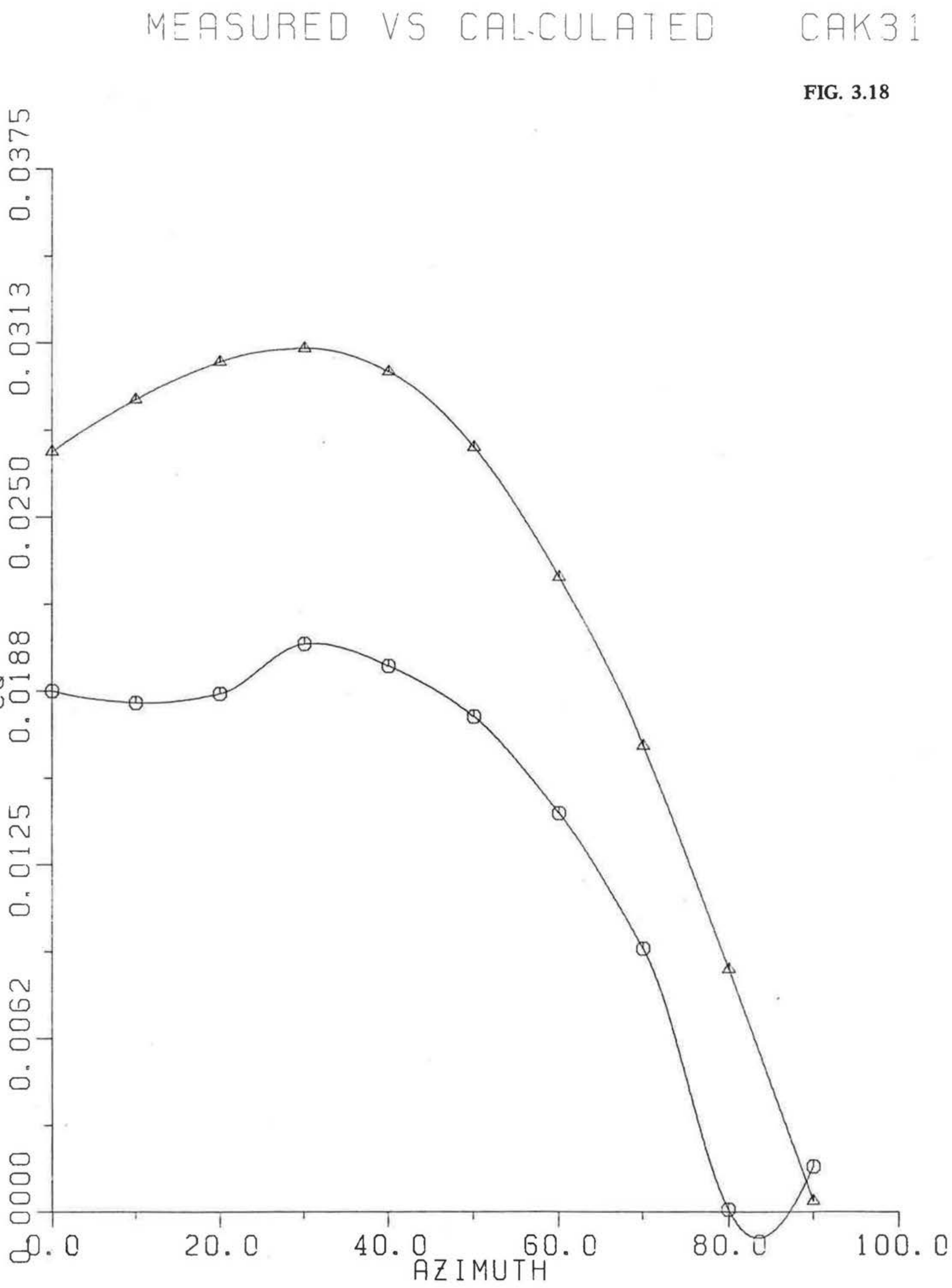
MEASURED VS CALCULATED CAK31
0.0375
0.0313
0.0250
0.0188
0.0125
0.0062
0.0000
CQ
0.0
20.0
40.0
60.0
80.0
100.0
AZIMUTH

FIG. 3.18

MEASURED VS CALCULATED CAK32

FIG. 3.19

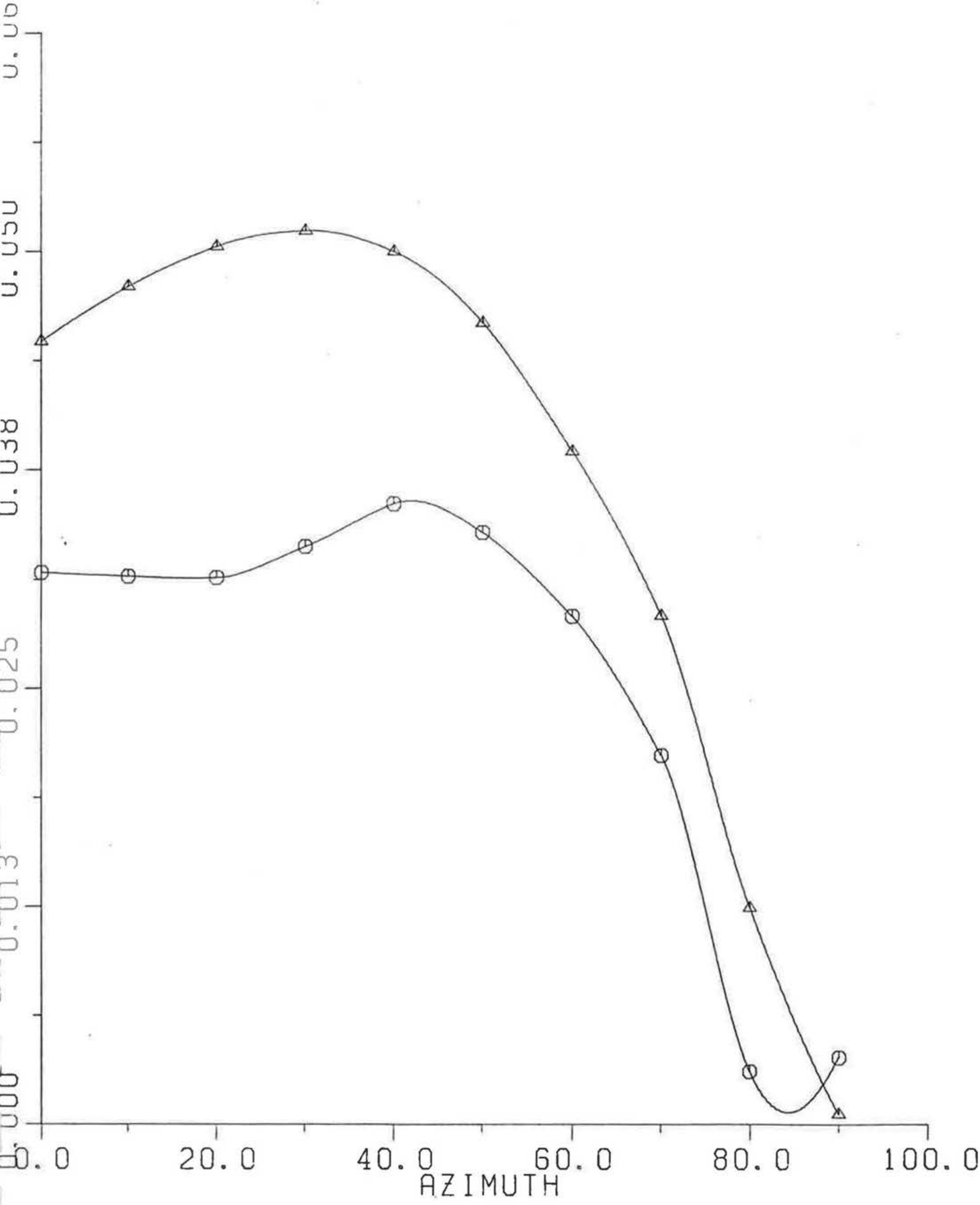

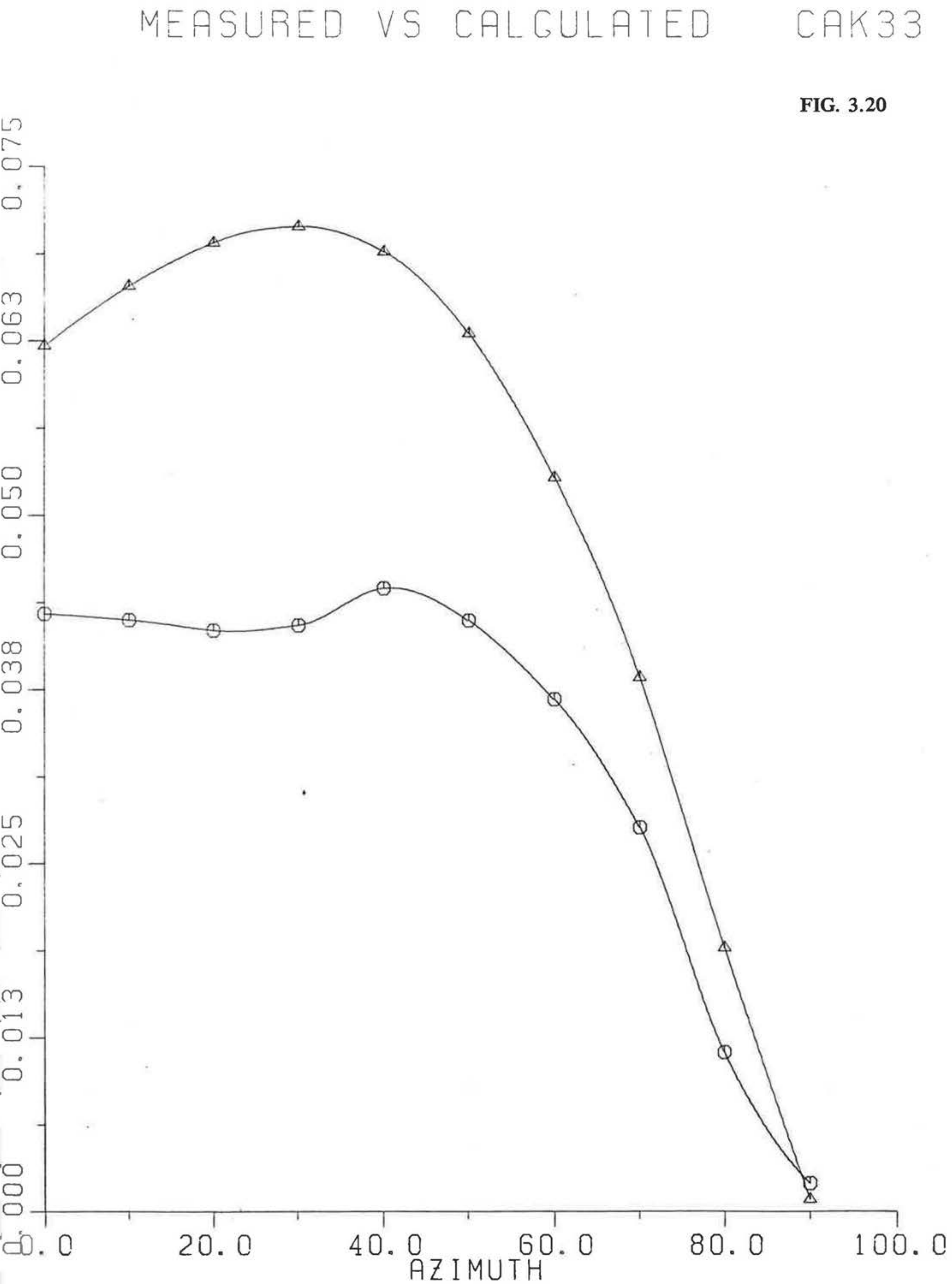
MEASURED VS CALCULATED CAK33
0.075
0.063
0.050
0.038
0.025
0.013
0.000
0.0
20.0
40.0
60.0
80.0
100.0
AZIMUTH

FIG. 3.20

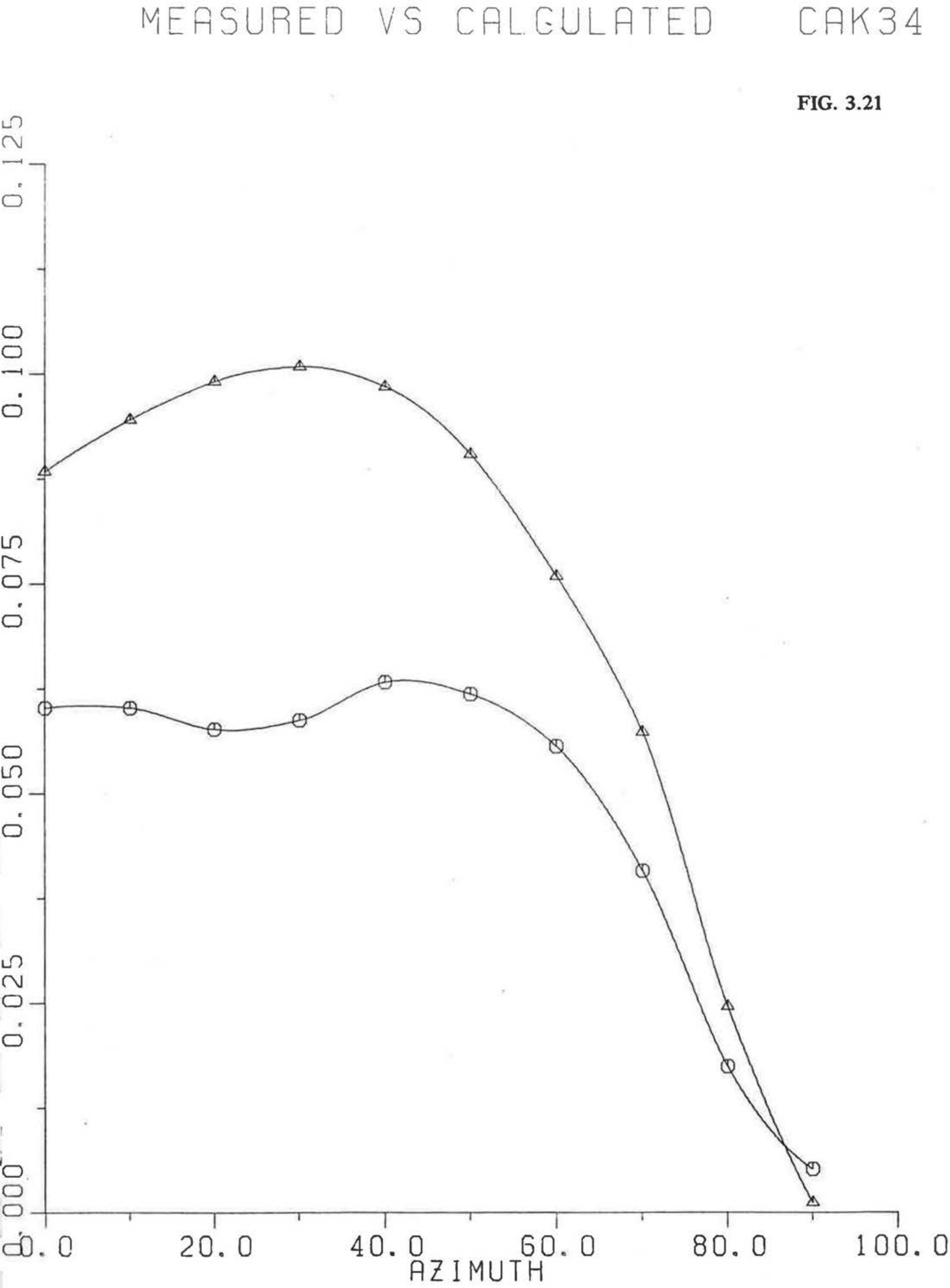
MEASURED VS CALCULATED CAK34
0.125
0.100
0.075
0.050
0.025
0.000
0.0
20.0
40.0
60.0
80.0
100.0
AZIMUTH

FIG. 3.21

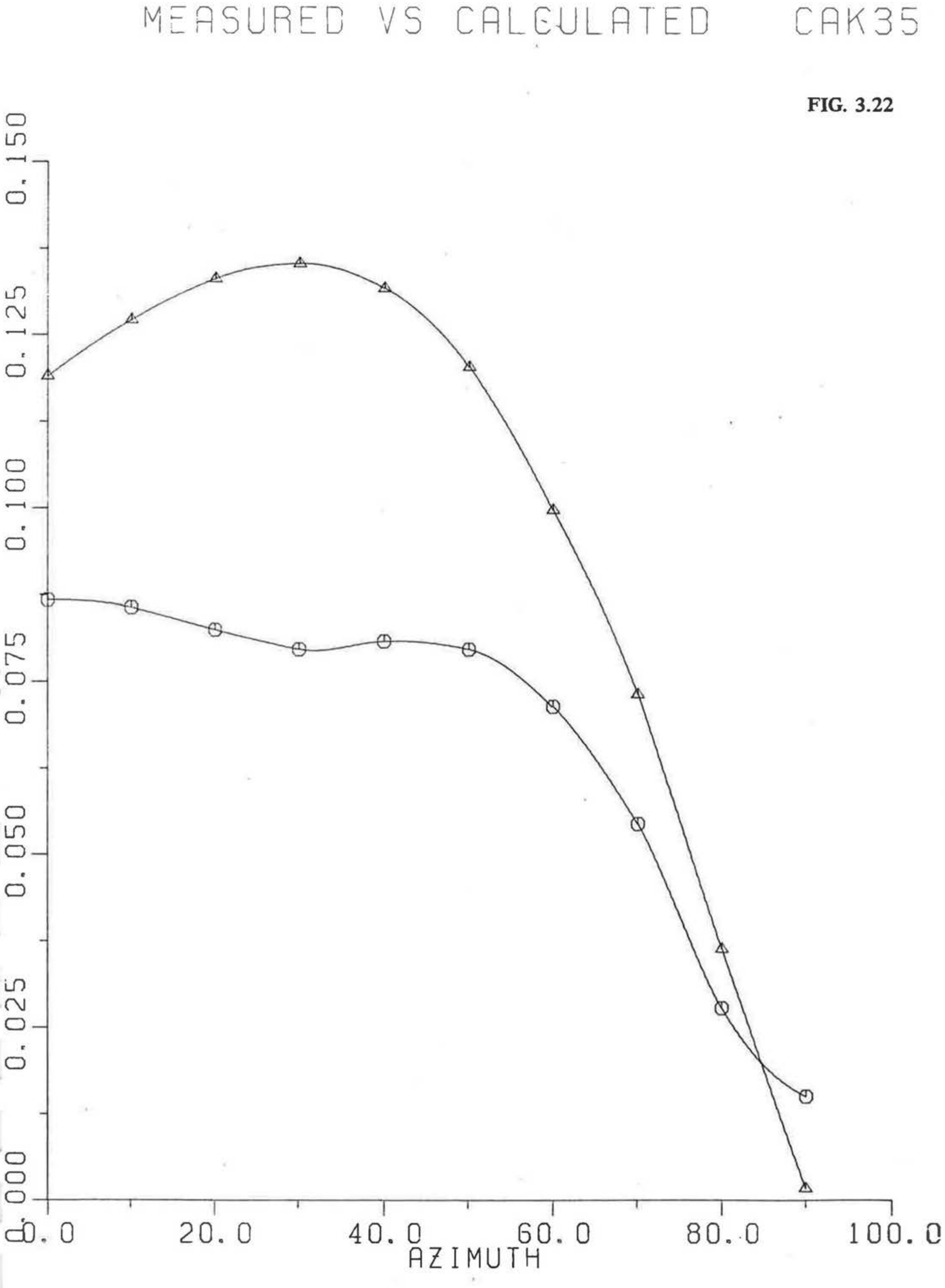
MEASURED VS CALCULATED CAK35
0.150
0.125
0.100
0.075
0.050
0.025
0.000
0.0
20.0
40.0
60.0
80.0
100.0
AZIMUTH

FIG. 3.22

MEASURED VS CALCULATED CAK36

FIG. 3.23

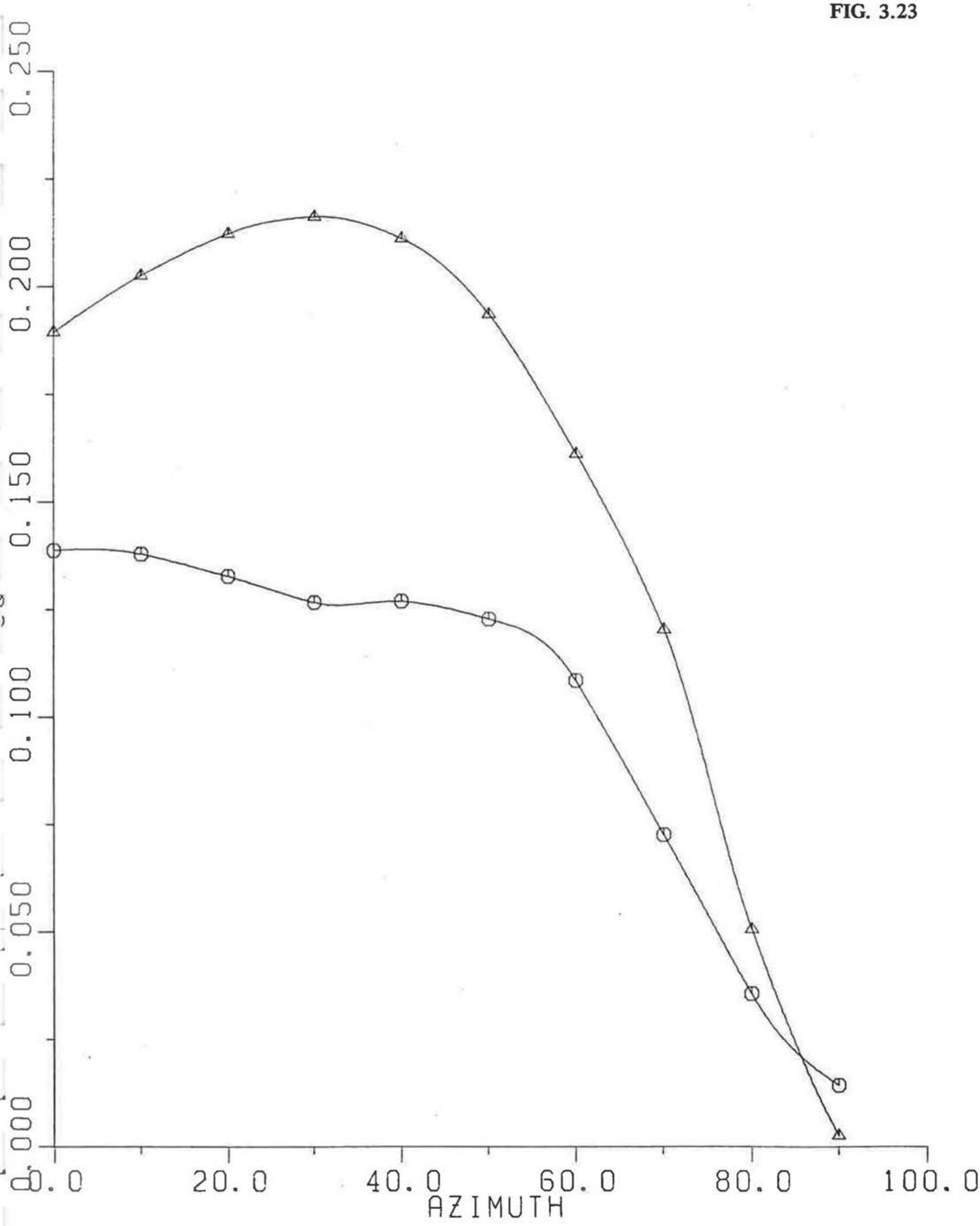

MEASURED VS CALCULATED CAK37

FIG. 3.24

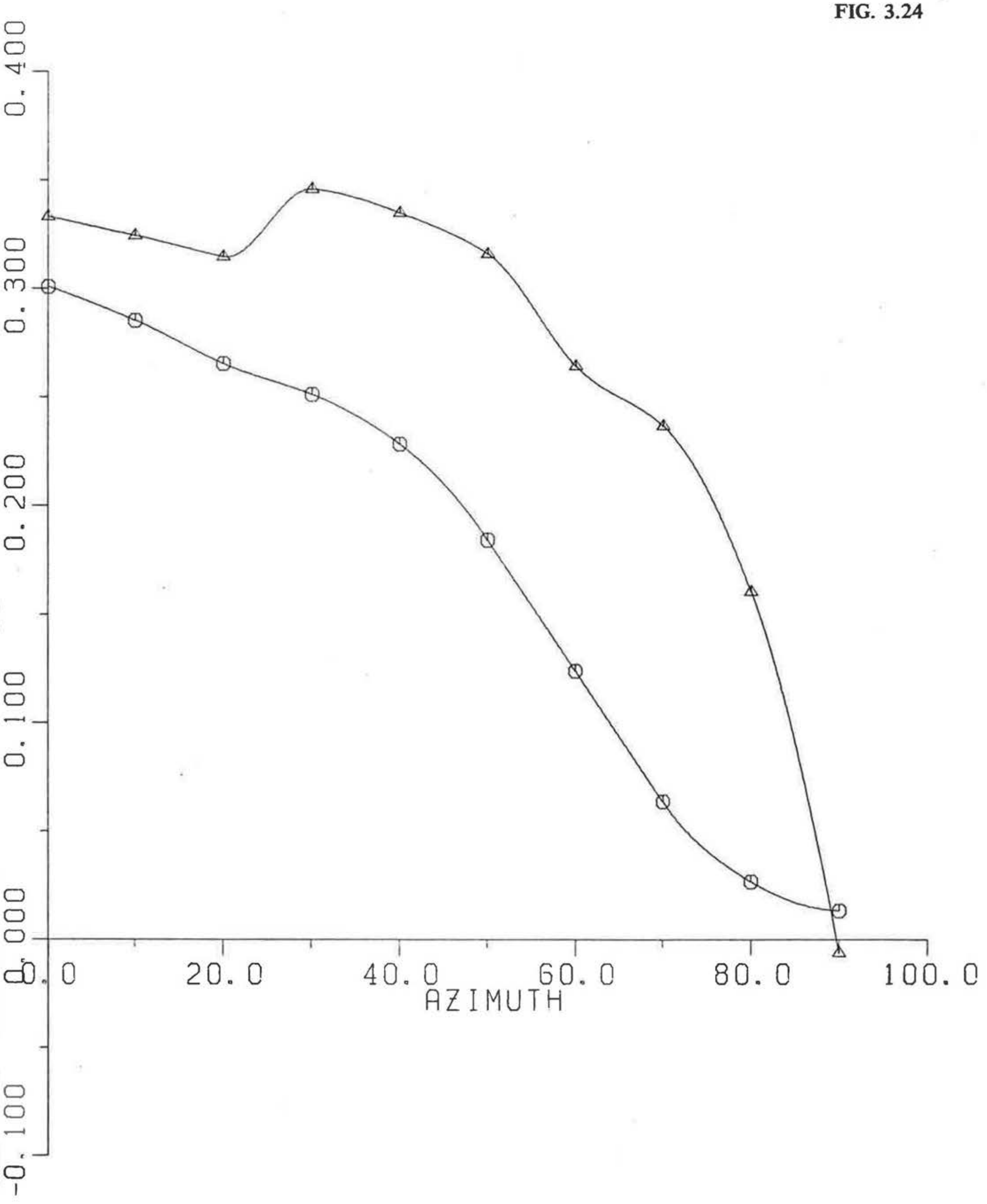

MEASURED VS CALCULATED CAK38

FIG. 3.25

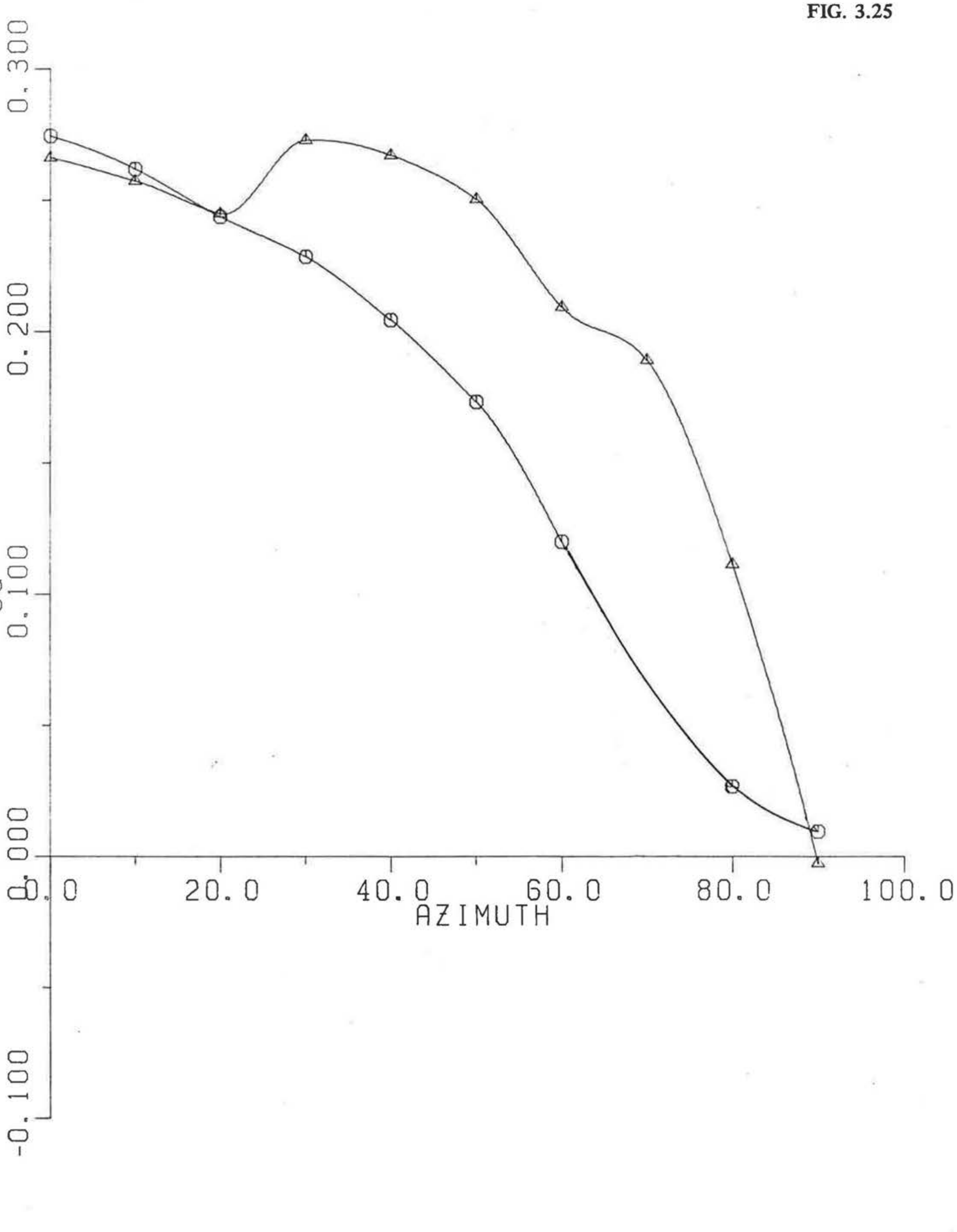

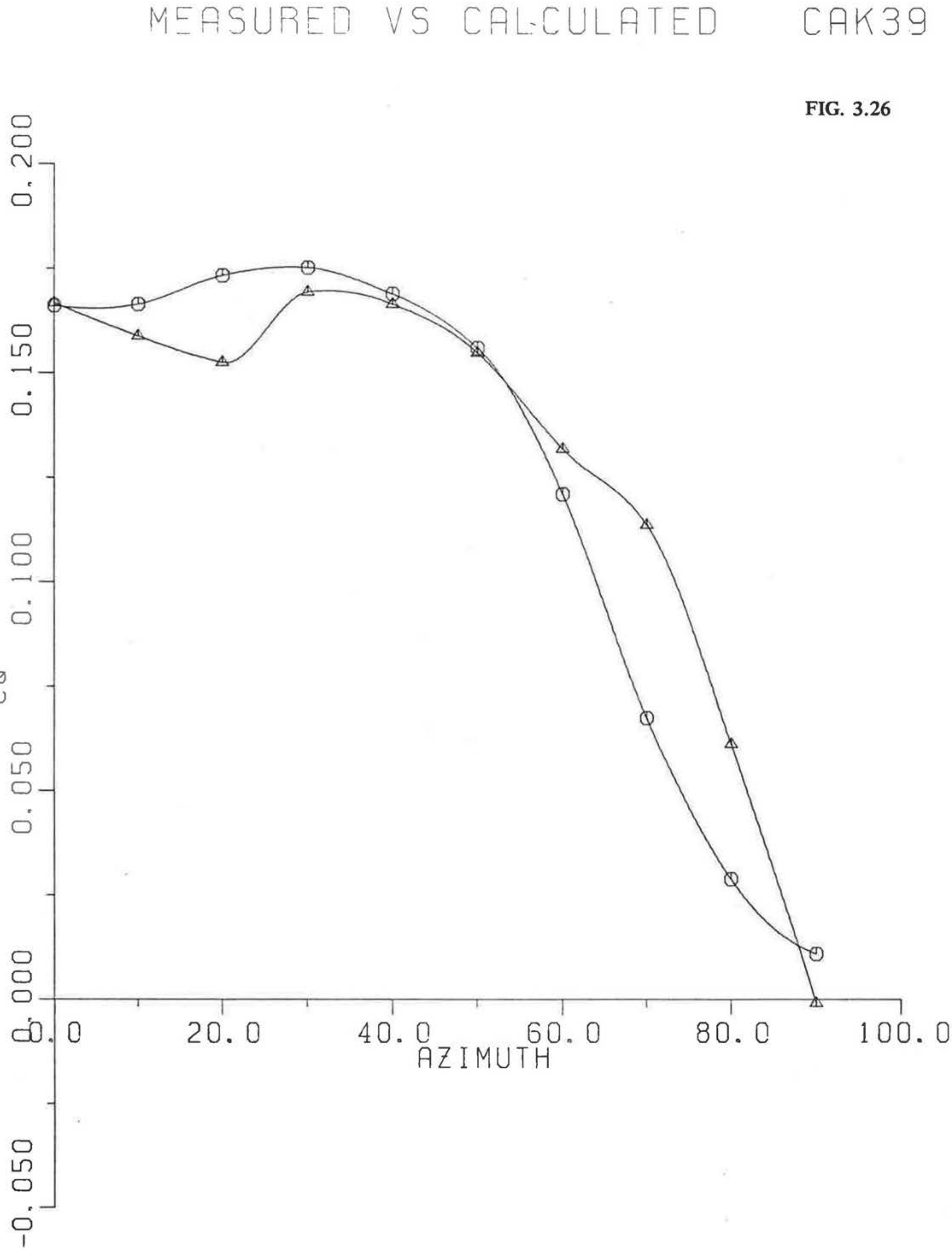
MEASURED VS CALCULATED CAK39
0.200
0.150
0.100
0.050
0.000
-0.050
CQ
0.0
20.0
40.0
60.0
80.0
100.0
AZIMUTH

FIG. 3.26

MEASURED VS CALCULATED CAK4C

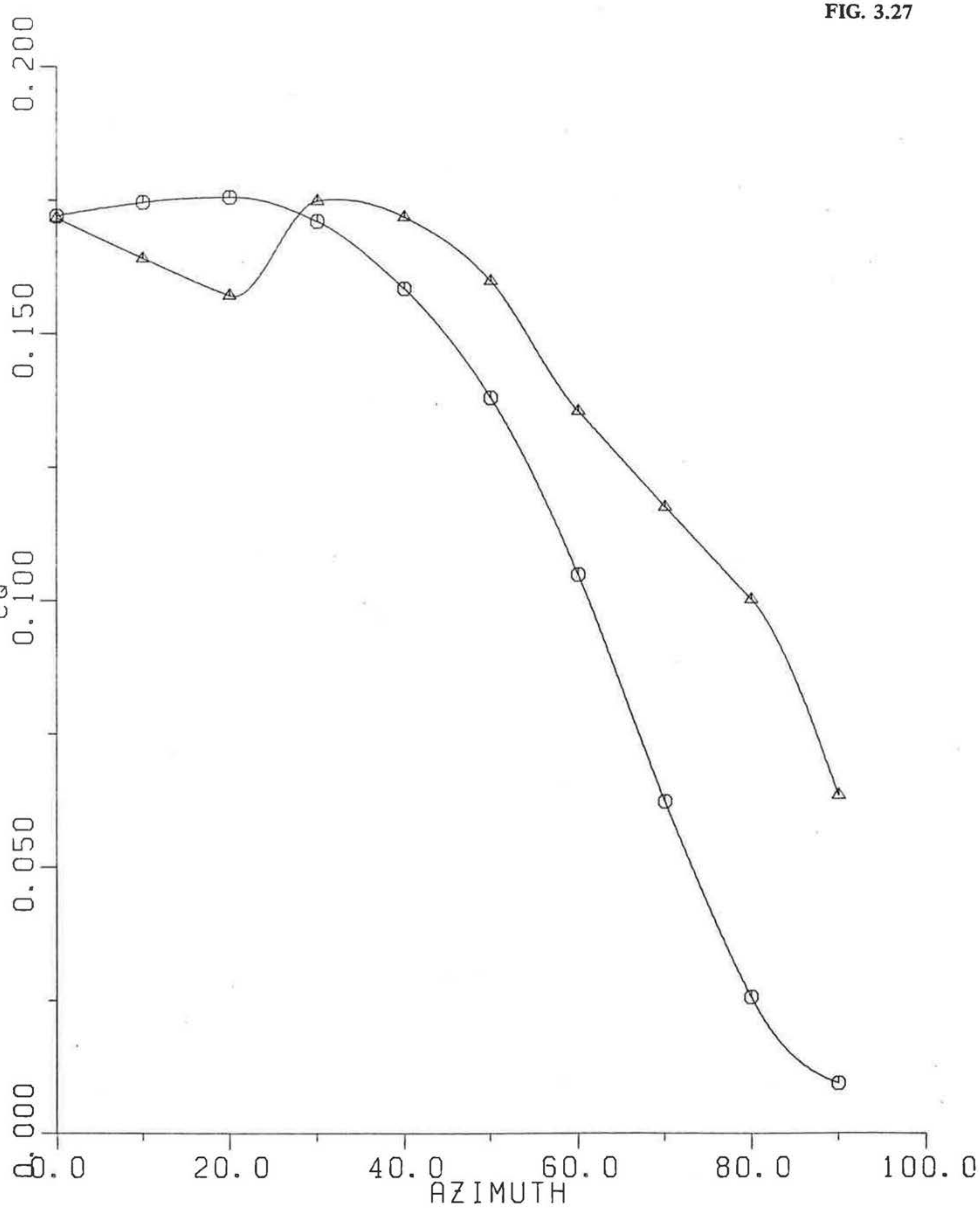

FIG. 3.27

MEASURED VS CALCULATED CAK41

FIG. 3.28

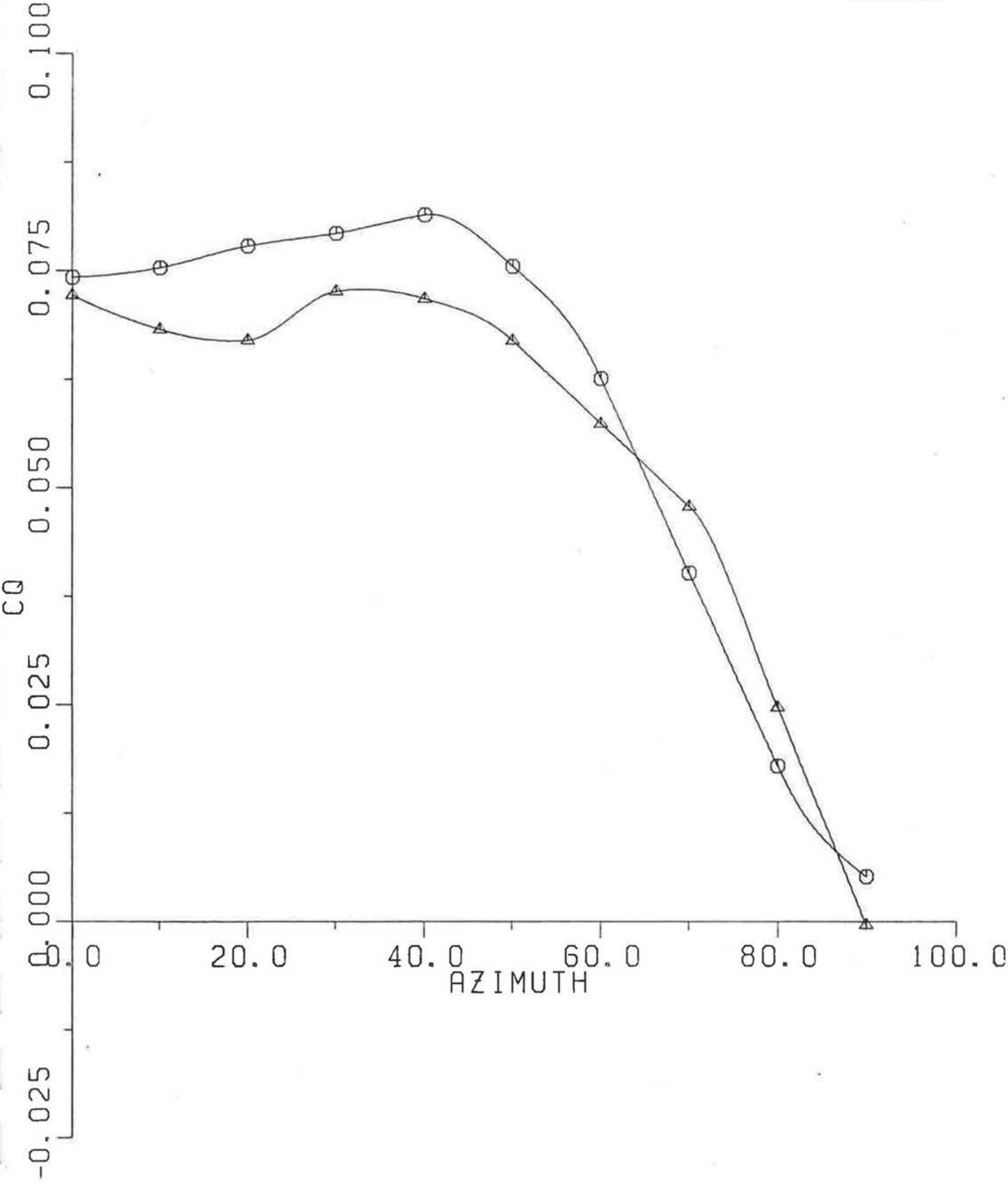

MEASURED VS CALCULATED CAK42

FIG. 3.29

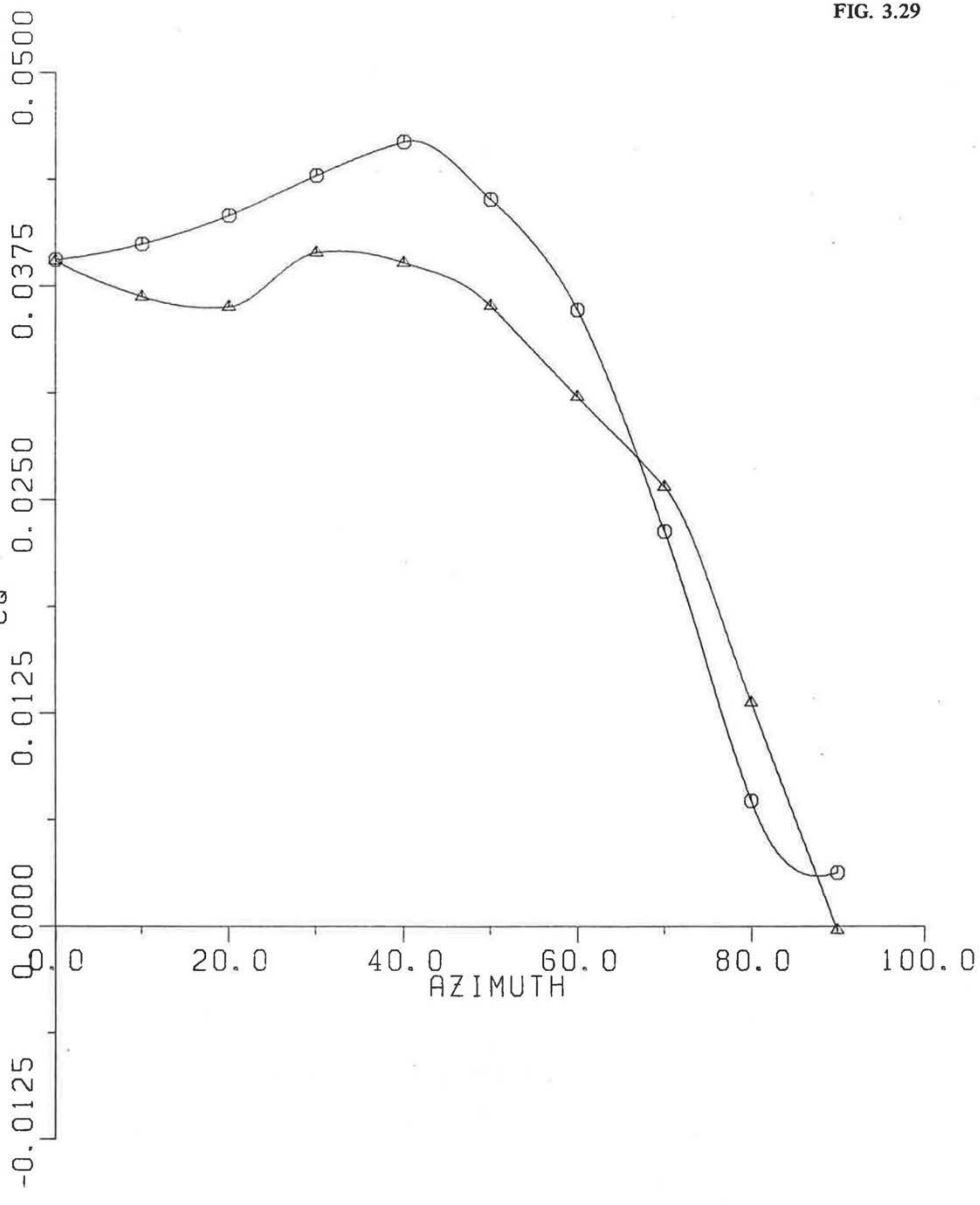

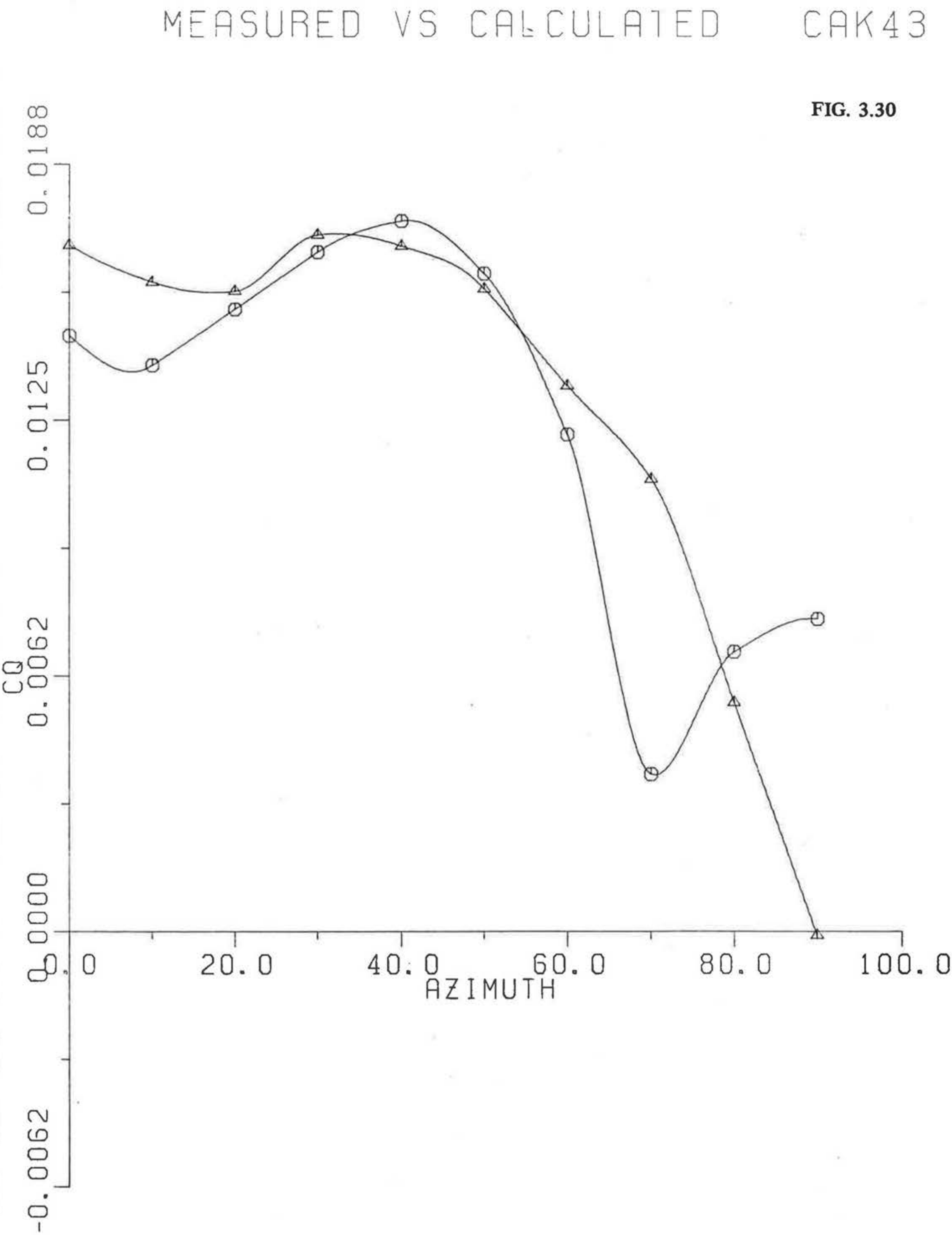
MEASURED VS CALCULATED CAK43
0.0188
0.0125
0.0062
CQ
0.0000
-0.0062
0.0
20.0
40.0
60.0
80.0
100.0
AZIMUTH

FIG. 3.30

MEASURED VS CALCULATED CAK44

FIG. 3.31

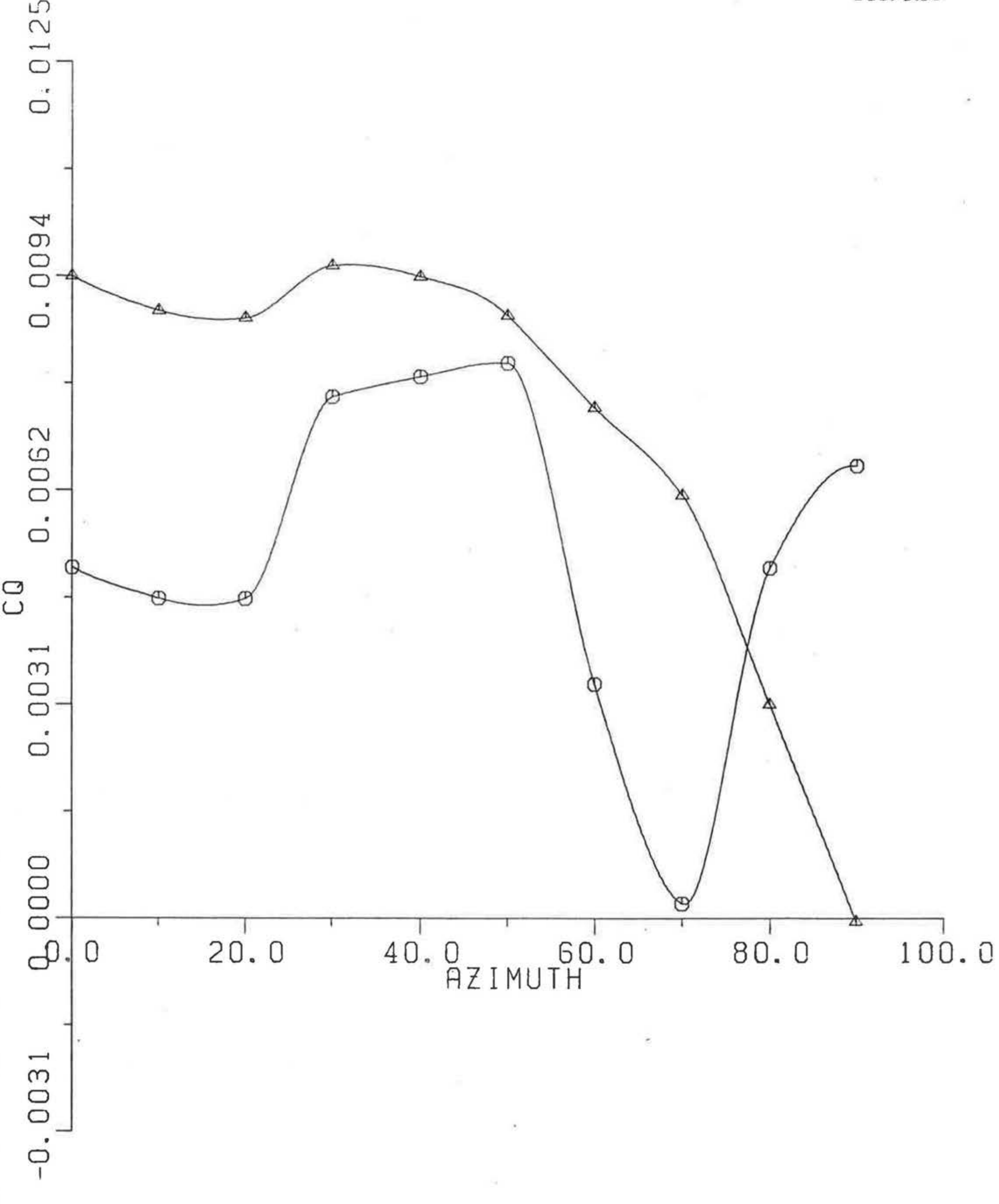

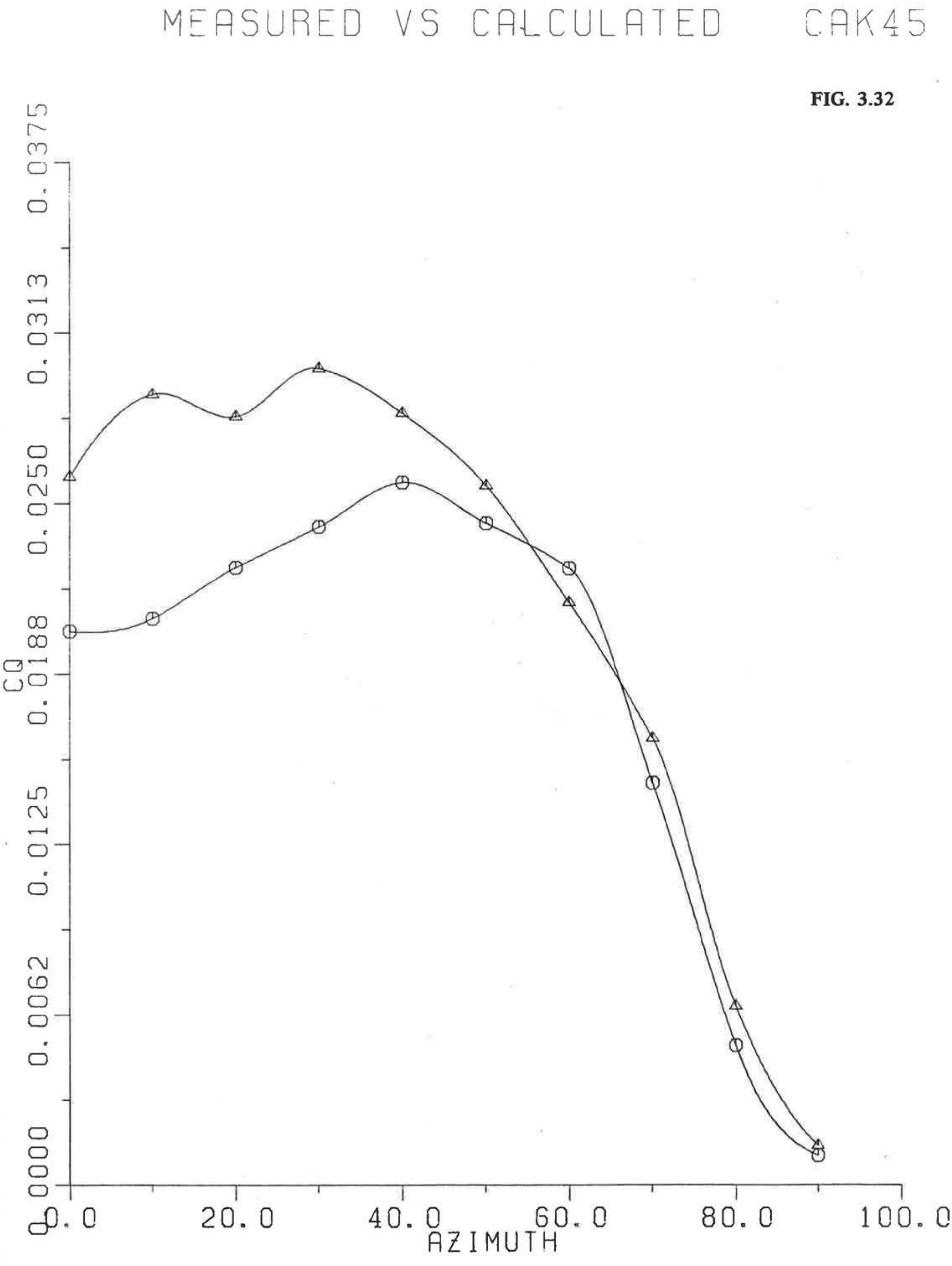
MEASURED VS CALCULATED CAK45
0.0000
0.0062
0.0125
0.0188
0.0250
0.0313
0.0375
CQ
0.0
20.0
40.0
60.0
80.0
100.0
AZIMUTH

FIG. 3.32

MEASURED VS CALCULATED CAK46

FIG. 3.33

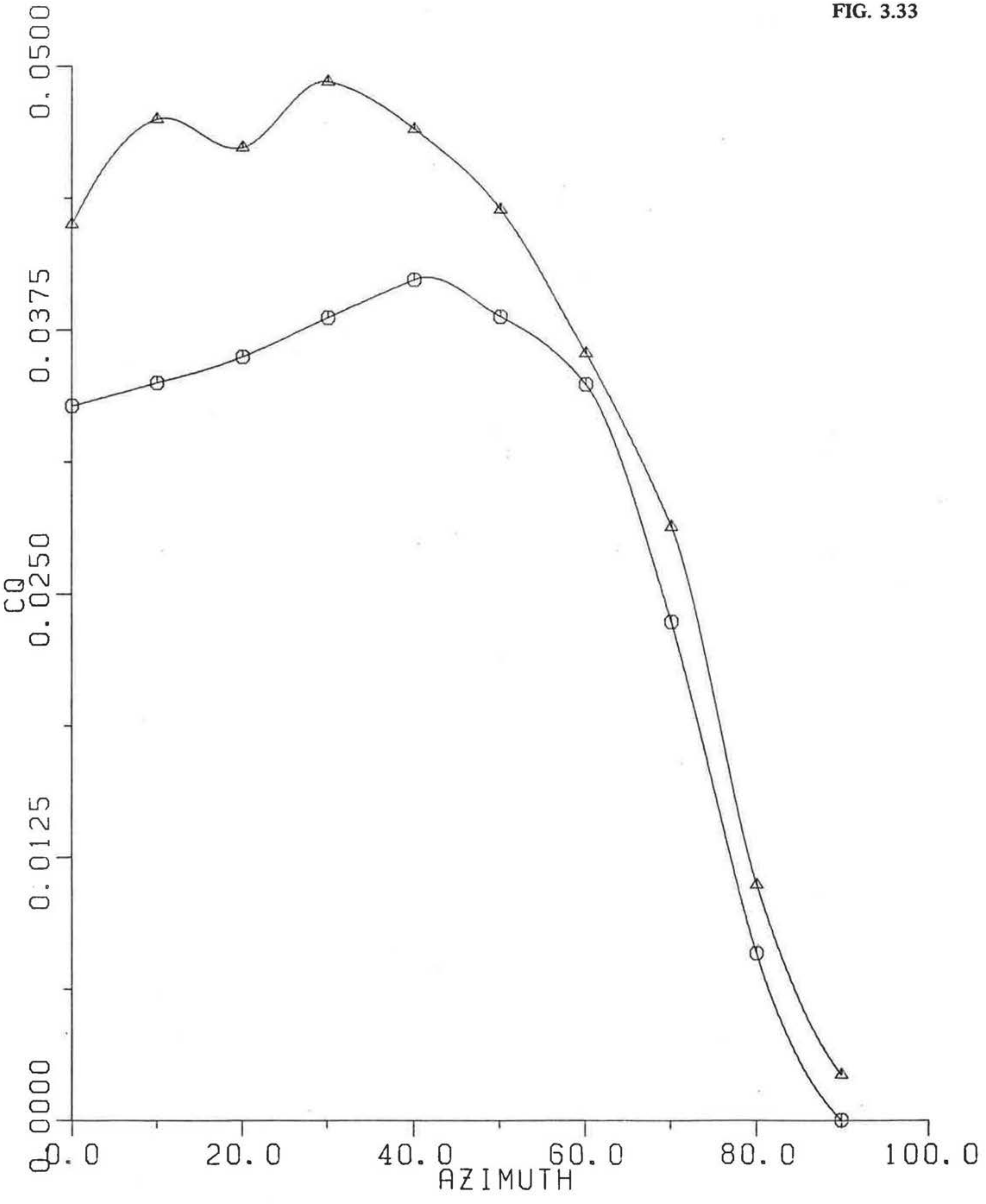

MEASURED VS CALCULATED   CAK47

FIG. 3.34

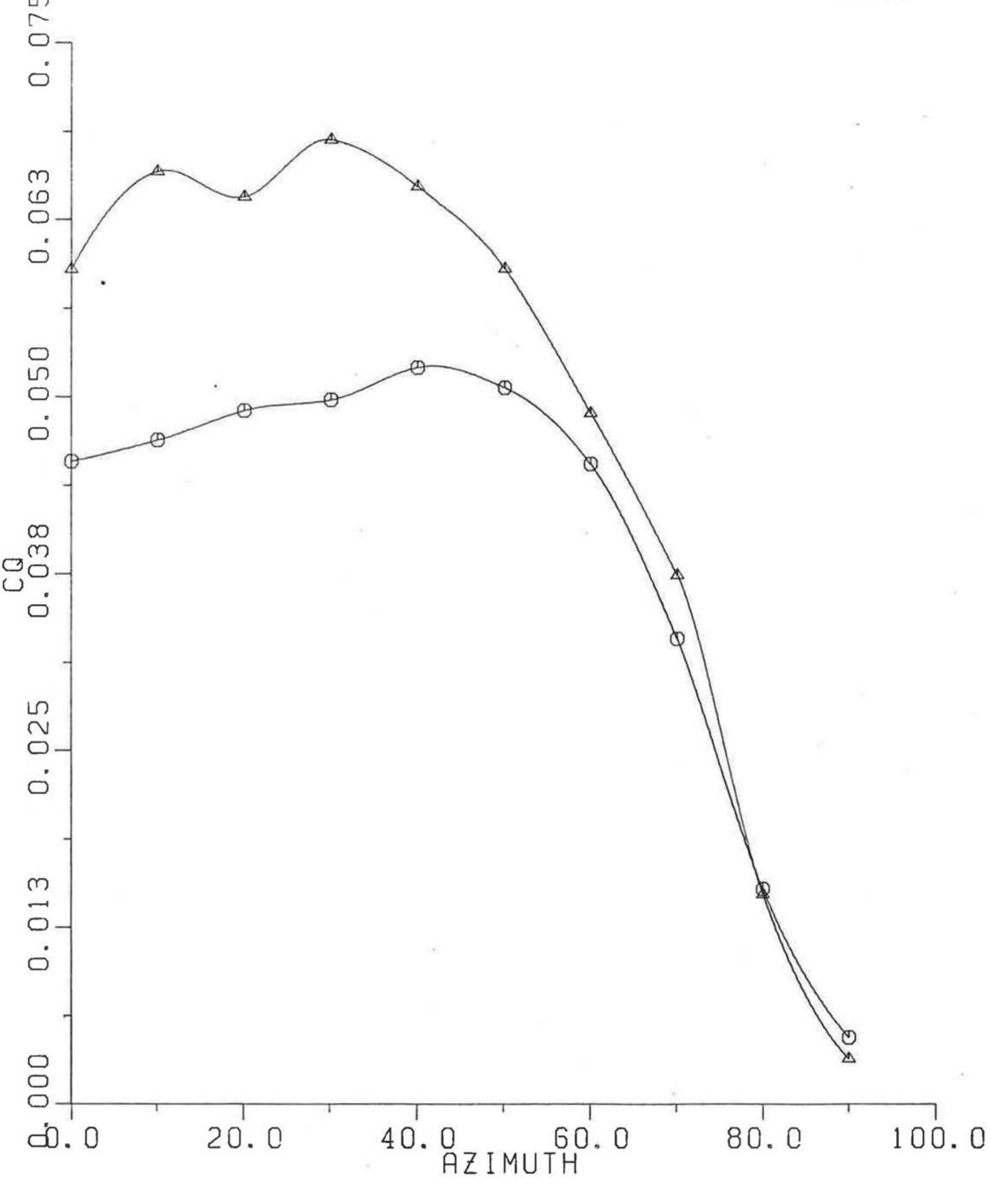

MEASURED VS CALCULATED CAK48

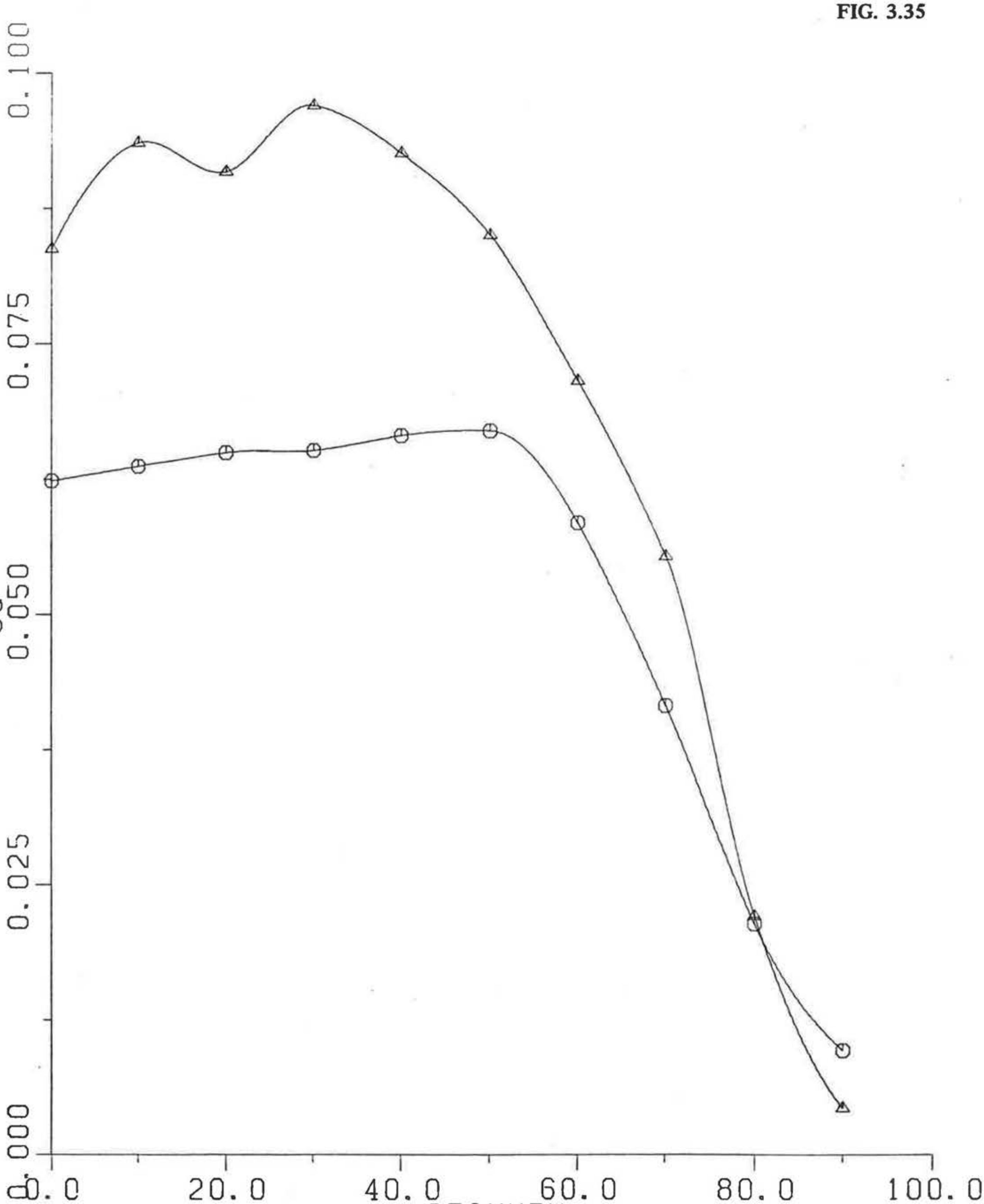

FIG. 3.35

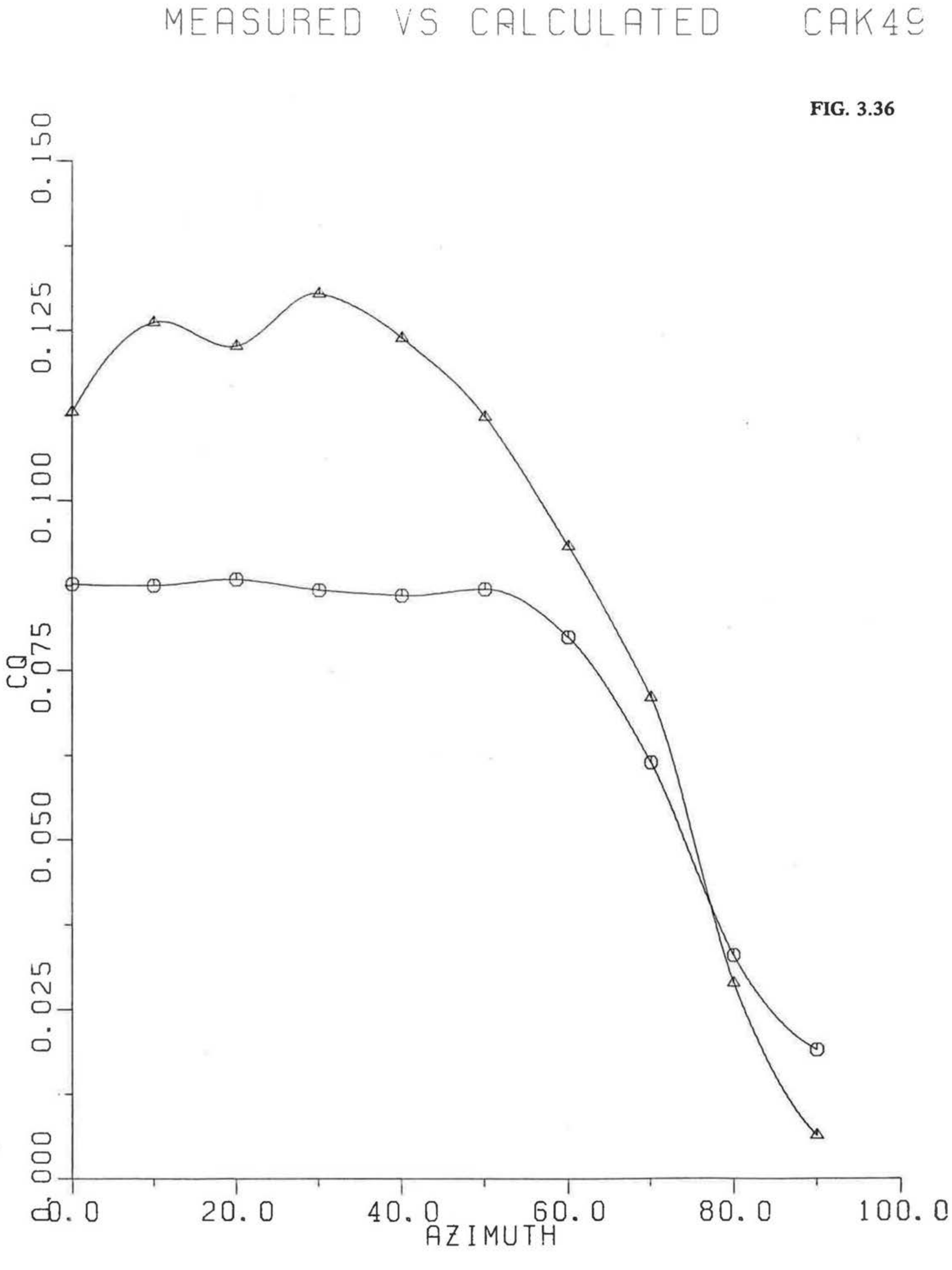
MEASURED VS CALCULATED CAK49
0.150
0.125
0.100
0.075
CQ
0.050
0.025
0.000
0.0
20.0
40.0
60.0
80.0
100.0
AZIMUTH

FIG. 3.36

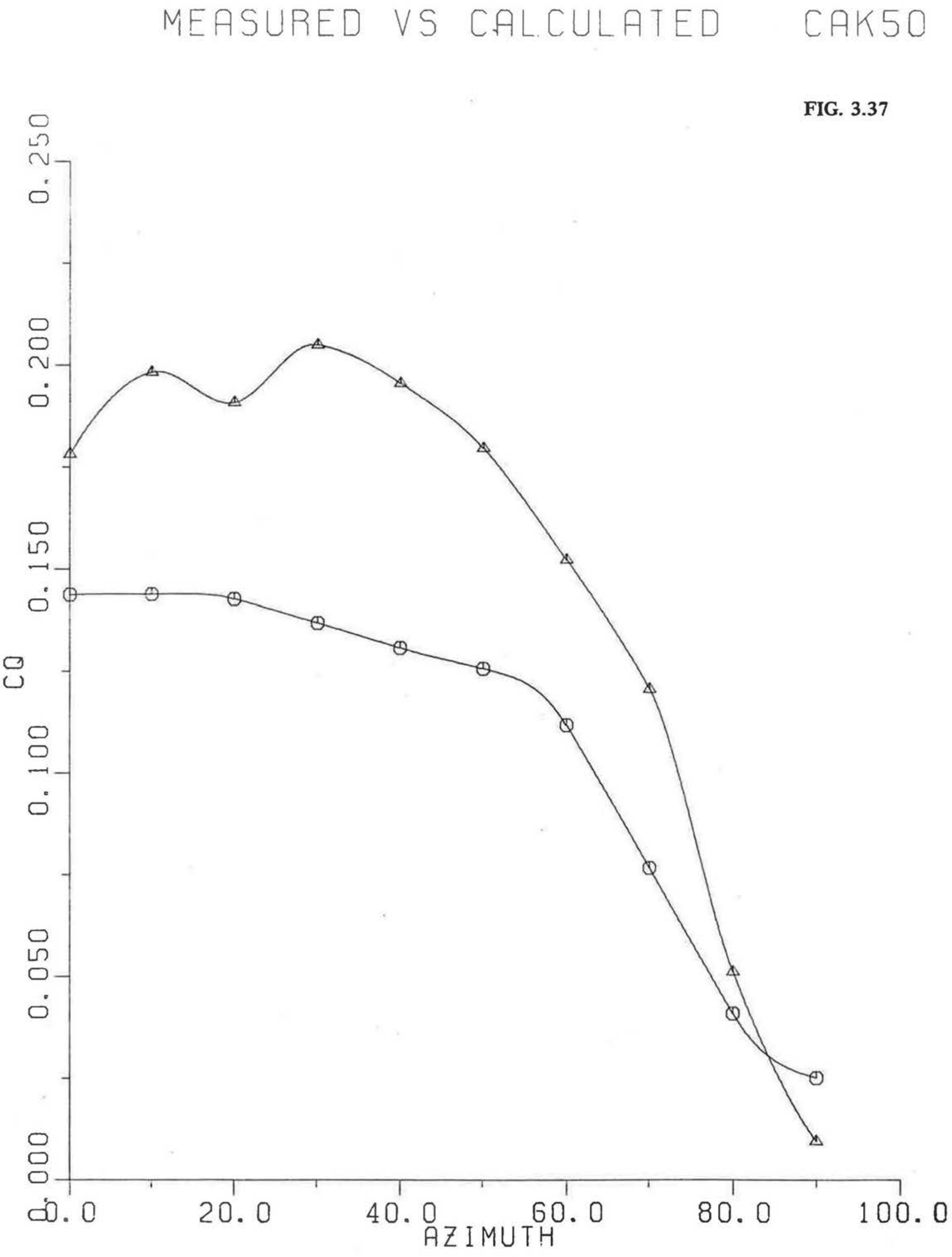
MEASURED VS CALCULATED CAK50
0.250
0.200
0.150
0.100
0.050
0.000
CQ
0.0
20.0
40.0
60.0
80.0
100.0
AZIMUTH

FIG. 3.37

$$\frac{C_D(\alpha)}{C_D(o)} \simeq (1 - \alpha)(1 + 0.3\,\alpha)$$

It can be argued that this ratio should depend on the resistance to flow through the grid rather than α itself. If the resistance is expressed in coefficient form as;

$$\Delta p = C_r \tfrac{1}{2} \rho V^2$$

where; Δp = pressure drop through the grid

when the average velocity through it is V ($V = Q/A_o$), then in the case of the grid;

$$C_r = \left(\frac{1}{C_d\,\alpha}\right)^2 \simeq \left(\frac{1.5}{\alpha}\right)^2$$

and hence;

$$\frac{C_D(\alpha)}{C_D(0)} \simeq \left(1 - \frac{1.5}{\sqrt{C_r}}\right)\left(1 + \frac{0.45}{\sqrt{C_r}}\right)$$

If it is assumed that this relationship is also applicable to porous buildings then, since the through-flow is proportional to $C_D^{-\frac{1}{2}}$, the ratio of the flow computed using the pressure distribution on a solid model to that computed with the distribution modified by the through-flow will be;

$$\frac{C_{Q_T}}{C_{Q_E}} = \frac{1}{((1 - 1.5/\sqrt{C_r})(1 + 0.45/\sqrt{C_r}))^{\frac{1}{2}}}$$

However;

$$C_r = \frac{\Delta p}{\tfrac{1}{2}\rho V^2} = \frac{C_D \cdot \tfrac{1}{2}\rho V^2_{ref}}{\tfrac{1}{2}\rho C^2_{Q_T} V^2_{ref}} = \frac{C_D}{C^2_{Q_T}}$$

and hence;

$$\frac{(C_Q)_T}{(C_Q)_E} \simeq \frac{1}{((1 - 1.5\, C_Q/\sqrt{C_D})\,(1 + 0.45\, C_Q/\sqrt{C_D})^{\frac{1}{2}}}$$

which, for small C_Q, and for a wind angle less than 60° is approximately given by;

$$\frac{(C_Q)_T}{(C_Q)_E} \simeq 1 + 0.65\ C_Q + 1.2\, C_Q^{\ 2} \qquad (3.4)$$

Equation 3.4 is plotted together with the experimental observations for flow through the rear wall in Fig. 3.38. The general trend of C_Q *(predicted)/* C_Q *(observed)* with C_Q given by Equation 3.4 is apparent but the experimental values are consistently low. This is probably due to an underestimate of the discharge coefficient as discussed earlier (Section 3.2). The results of Fig. 3.38 are replotted in Fig. 3.40 with the theoretical estimates increased by 8% to allow for the probable underestimate of the discharge coefficient. The relationship of Equation 3.4 then follows the observations with a root-mean-square deviation of 0.08 or about 6% on average.

It can be concluded that given the external pressure distribution and the discharge characteristics of building openings the internal flows can be predicted for openings in the walls. If the pressure distribution is determined from an unvented structure then the internal flows will be overestimated with C_Q *(predicted)/*C_Q *(true)* being roughly equal to $1 + C_Q$ *(predicted)*. The results obtained suggest that internal flow predicted from the empirical relationship;

$$C_Q = \frac{C_{Q_o}}{1 + C_{Q_o}}$$

where C_{Q_o} is the flow coefficient predicted using the pressure distribution on an unvented or solid model will have an accuracy of better than 10% (coefficient of variation).

In the case of flows vented through the ridge (Fig. 3.39) the predictions are substantially in error even at very small flow rates. There are significant differences between the basic model and that with wings but in both cases a very significant over prediction is apparent. At values of C_Q above 0.05 the measured internal flow was roughly 65% of that predicted for the basic model and 75% for the winged model. It would appear that injecting flow into the wake at the ridge line has a substantial influence on the pressure field. The mechanism by which the pressure field is modified was not studied but it may well be associated with the close proximity of the vent to the point of flow separation. This suggestion is supported by the observation that for large wind azimuth angles (above 50°) the predicted and observed flows are in fair agreement. At these angles the flow would separate from the gable end and the ridge would lie in the separated flow region (as was the case for the rear wall).

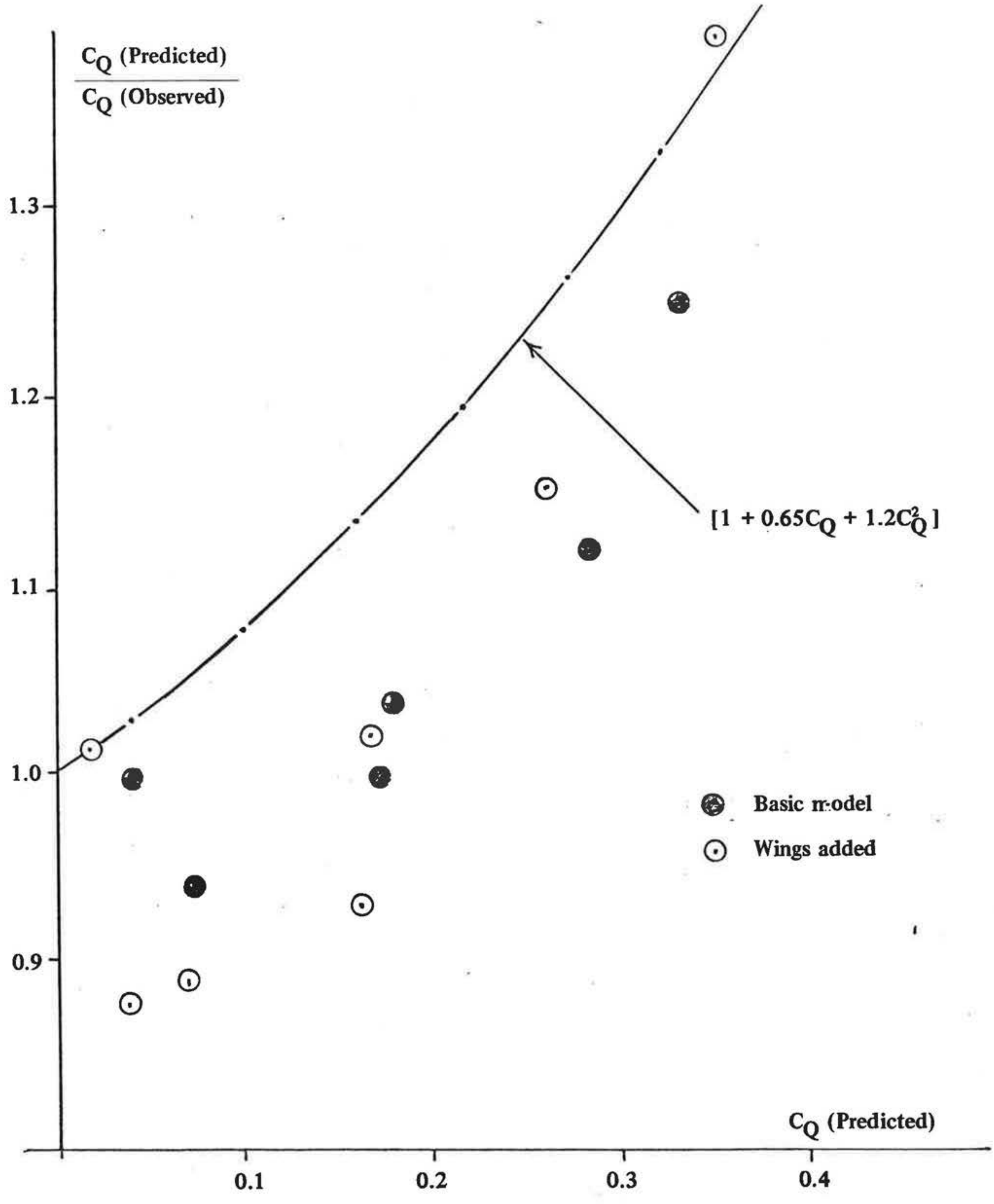

FIG. 3.38 COMPARISON OF PREDICTED AND OBSERVED FLOW RATES GENERATED BY OPENINGS IN THE FRONT AND REAR WALLS

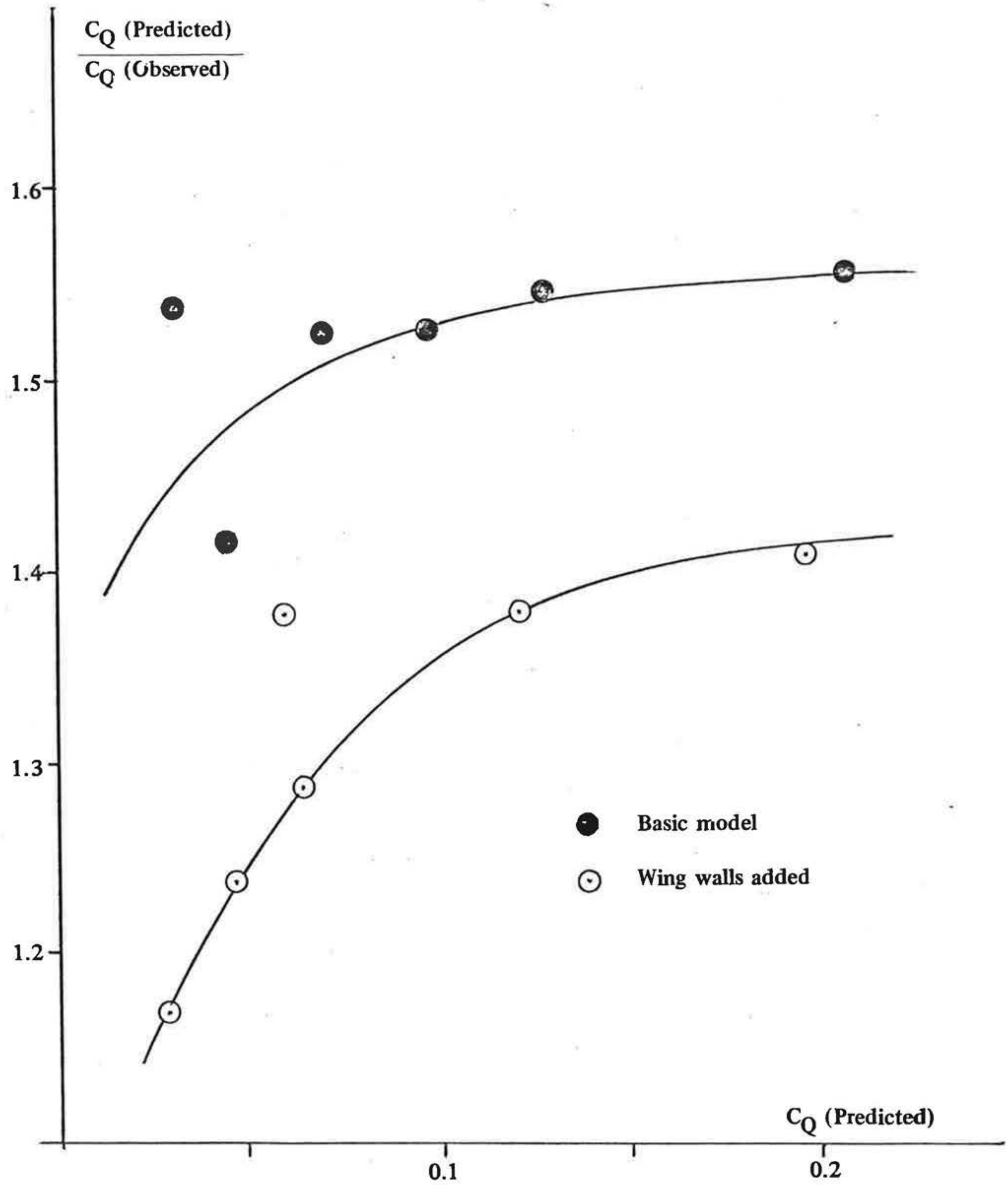

FIG. 3.39 C_Q (Predicted)/C_Q (Observed) VS C_Q FOR FLOW OUT THROUGH RIDGE

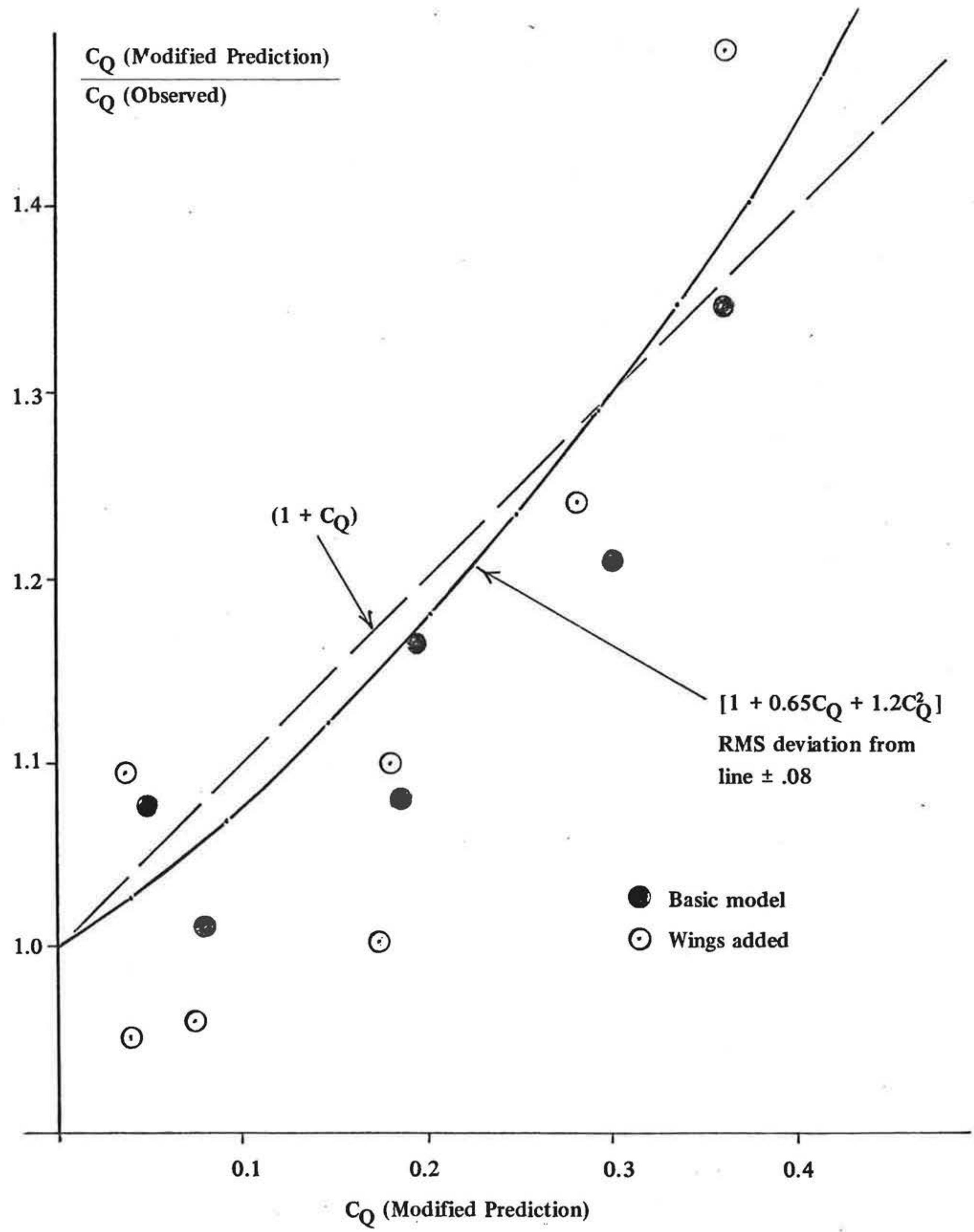

FIG. 3.40 COMPARISON OF MEASURED AND MODIFIED PREDICTED FLOWS DUE TO WALL OPENINGS

While there is insufficient evidence to draw general conclusions the results strongly suggest that vents placed near points of separation may have a marked influence on the pressure field and lead to erroneous predictions of the internal flows. This is a problem which deserves further investigation but is beyond the scope of the present study.

4.0 EXTERNAL PRESSURE DISTRIBUTIONS ON LOW-RISE INDUSTRIAL BUILDINGS

4.1 Data Base

The data base used to derive the mean pressure distribution on low-rise industrial buildings was obtained in a study of wind loads by Davenport, Surry and Stathopoulos. A report of this study "Wind Loads on Low-Rise Buildings: Final Report of Phases I and II" is attached as Appendix 2. Sections of the report dealing with member loads have been omitted.

Tests were conducted at three model scales (1:100, 1:250, 1:500) but the extensive test program was conducted at a scale of 1:250 and this scale only was extracted for the present study. Tests included three building heights, two terrain roughnesses and three roof slopes as specified in Section 4.0 (p 17-18) of Appendix 2.

4.2 Reformulation of Data for Computation of Flow Rates

The major task in dealing with the body of data gathered was to extract the mean pressure coefficients, adjust these coefficients to a reference stagnation pressure at eaves height and to compute the average pressures in a regular array of zones over the building surface.

The zoning pattern adopted is as shown in Fig. 4.1. The front and rear faces were divided into eighteen equal zones (six across by three high), the side or end faces into nine equal zones (three wide by three high) and a further six zones were defined along each side of the ridge line on the roof.

The mean pressure coefficient for each zone was computed and, for each set conditions, printed in a "picture" format as shown in Fig. 4.2. The complete set of results arranged as shown in Table 4.1 are presented in Appendix 3. The data in the Appendix may be used directly to evaluate flows given a distribution of openings and corresponding discharge coefficients. A method of computing the flows for a building in which the internal losses are negligble is outlined below.

C_{p_i} = the pressure coefficient for the i^{th} region as defined in the data base of Appendix 3.

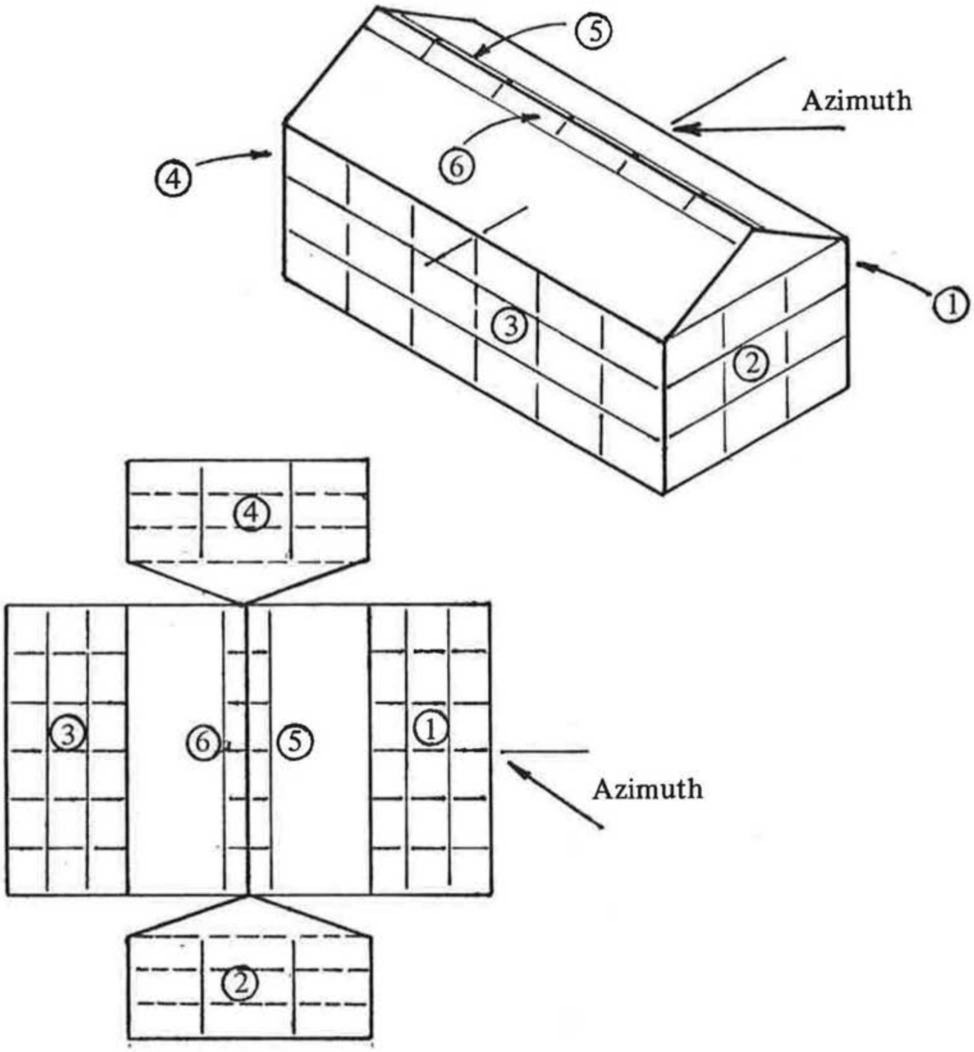

FIG. 4.1 ZONING PATTERN

```
ZIMUTH:    0

                                          (4)
                               -0.037  -0.169  -0.318
                               -0.051  -0.149  -0.331
                               -0.064  -0.176  -0.341
 -0.101   -0.101   -0.101         -0.260  -0.980          0.574    0.574    0.574
  0.000    0.000    0.000         -0.311  -1.048          0.608    0.608    0.608
  0.000 (3)0.000    0.000         -0.311  -1.115  (5)     0.574    0.574    0.574
 -0.010   -0.010   -0.010    (6)  -0.311  -1.115          0.605 (1)0.574    0.544
 -0.061   -0.061   -0.061         -0.304  -0.254          0.576    0.547    0.517
 -0.047   -0.014   -0.047         -0.304  -0.169          0.591    0.564    0.365
                               -0.034  -0.068  -0.338
                               -0.034  -0.068  -0.338
                               -0.034  -0.068  -0.338
                                          (2)
```

FIG. 4.2 LAYOUT OF "PICTURE" FILES

TABLE 4.1: PRESSURE DATA CONTAINED IN APPENDIX 3

FILE	SPAN	LENGTH	EAVES HEIGHT	ROOF SLOPE	TERRAIN	WIND DIRECTIONS	TABLE NO.
MBTZN	80 ft.	100 ft.	16 ft.	1:12	OPEN	$0\text{-}90^{\circ}$ x 10°	3.1.1-10
LLTZN	"	125 ft.	"	1:12	"	0°, 45°, 90°	3.2.1-3
LMTZN	"	"	"	4:12	"	"	3.3.1-3
LHTZN	"	"	"	12:12	"	"	3.4.1-3
LLRZN	"	"	"	1:12	SUBURBAN	"	3.5.1-3
LMRZN	"	"	"	4:12	"	"	3.6.1-3
LHRZN	"	"	"	12:12	"	"	3.7.1-3
MLTZN	"	"	24 ft.	1:12	OPEN	"	3.8.1-3
MMTZN	"	"	"	4:12	"	"	3.9.1-3
MHTZN	"	"	"	12:12	"	"	3.10.1-3
MLRZN	"	"	"	1:12	SUBURBAN	"	3.11.1-3
MMRZN	"	"	"	4:12	"	"	3.12.1-3
MHRZN	"	"	"	12:12	"	"	3.13.1-3
HLTZN	"	"	32 ft.	1:12	OPEN	"	3.14.1-3
HMTZN	"	"	"	4:12	"	"	3.15.1-3
HHTZN	"	"	"	12:12	"	"	3.16.1-3
HLRZN	"	"	"	1:12	SUBURBAN	"	3.17.1-3
HMRZN	"	"	"	4:12	"	"	3.18.1-3
HHRZN	"	"	"	12:12	"	"	3.19.1-3

A_i = the size of the opening in the i^{th} region.

C_{d_i} = the discharge coefficient for the i^{th} opening.

V = the mean speed at eaves height

ΔQ_i = the INFLOW through the i^{th} region

ΔC_{Q_i} = the INFLOW coefficient for the i^{th} region

= $\Delta Q_i / A \cdot V$

A = a reference area which may be the area of the windward face of the building

P_I = the internal pressure

C_{P_I} = the internal pressure coefficient

= $P_I / \frac{1}{2} \rho V^2$

The inflow coefficient, ΔC_{Q_i}, is given by;

$$\Delta C_{Q_i} = C_{d_i} \cdot \frac{A_i}{A} \cdot \frac{C_{p_i} - C_{P_I}}{| C_{p_i} - C_{P_I} |^{\frac{1}{2}}}$$

and C_{P_I} is given by the solution of;

$$\Sigma = \Sigma \Delta C_{Q_i} = 0 = \Sigma C_{d_i} \cdot \frac{A_i}{A} \cdot \frac{C_{p_i} - C_{P_I}}{| C_{p_i} - C_{P_I} |^{\frac{1}{2}}}$$

An iterative solution can be obtained as follows;

(i) Define two starting values of C_{P_I} as;

$$(C_{P_I})_1 = 1/N \, \Sigma \, C_{p_i}$$

$$(C_{P_I})_2 = (C_{P_I})_1 + 0.01$$

and compute the corresponding values of the net inflow, Σ_1 and Σ_2

(ii) Compute a new estimate $(Cp_I)_N$ from the relationship;

$$(Cp_I)_N = (Cp_I)_{N-1} + \frac{\Sigma_{N-1}}{\Sigma_{N-2} - \Sigma_{N-1}} \left((Cp_I)_{N-1} - (Cp_I)_{N-2}\right)$$

(iii) Compute the corresponding value of the net inflow, Σ_N, and test $|\Sigma_N| < 10^{-4}$

YES; put $Cp_I = (Cp_I)_N$ and compute the elemental flow coefficients ΔC_{Q_i}

NO; return to (ii).

The flow into the building can then be evaluated by summing ΔC_{Q_i} over all positive values while the flow through a given surface can be obtained by an algebraic sum over the regions comprising that surface. The computations are of course best accomplished with a simple computer code but for the purposes of illustration a simple case is presented below.

4.2.1 Sample computations

The building shown in Fig. 4.2 has four openings each of 20 ft^2 located at the centre of each face. The overall dimensions of the building is 100 ft long by 80 ft wide and 16 ft to eaves. Compute the internal flows when the wind speed is 10 mph at an azimuth of 10°.

From Table 3.1.2 of Appendix 3 the presure coefficients at the central regions of faces 1, 2, 3 and 4 are;

$$C_{p_1} = +0.576$$
$$C_{p_2} = -0.000$$
$$C_{p_3} = -0.101$$
$$C_{p_4} = -0.267$$

From (i) above;

$$(Cp_I)_1 = \tfrac{1}{4}(+0.576 - 0.000 - 0.101 - 0.267)$$
$$= +0.052$$
$$(Cp_I)_2 = +0.062$$

for an assumed discharge coefficient of 0.60,

$$\Sigma_1 = 0.60 \times \frac{20}{16 \times 100} \left\{ \frac{.576 - .052}{\sqrt{.524}} + \frac{0 - 0.052}{\sqrt{.052}} + \frac{-0.101 - .052}{\sqrt{.153}} + \frac{-0.267 - 0.052}{\sqrt{.319}} \right\}$$

$$= 0.60 \times \frac{20}{16 \times 100} \{.724 - 0.228 - 0.391 - 0.565\}$$

$$= -3.45 \times 10^{-3}$$

and,

$$\Sigma_2 = -3.82 \times 10^{-3}$$

From (ii) above the next estimate of the internal pressure coefficient is;

$$(Cp_I)_3 = 0.062 + \frac{-3.82}{-3.45 + 3.82} \{.062 - .052\}$$

$$= -0.041$$

and $\Sigma_3 = +2.0 \times 10^{-3}$

Successive applications of step (ii) yield;

$$(Cp_I)_4 = -0.006$$

$$\Sigma_4 = +0.16 \times 10^{-3}$$

$$(Cp_I)_5 = -0.003$$

$$\Sigma_5 = -0.08 \times 10^{-3}$$

$$= < 10^{-4}$$

Accept $Cp_I = -0.003$

and hence;

$$\Delta C_{Q1} = +0.0057$$

$$\Delta C_{Q2} = +0.004$$

$$\Delta C_{Q3} = -0.0023$$

$$\Delta C_{Q4} = -0.0038$$

The flow into the building is thus defined by;

$$C_{Q_{INFLOW}} = 0.0061$$

and the actual flow is given by;

$$\begin{aligned} Q_{IN} &= 0.0061 \times A \times V \\ &= 0.0061 \times 100 \times 16 \times (10 \times 44/30) \\ &= 143\ ft^3/sec. \end{aligned}$$

4.3 Potential Use of Pressure Data

The potential for the pressure data lies more in their use to develop simplified design aids, for evaluating the accuracy of simplified methods and for examining the sensitivity of the flow rates to variations in geometry and terrain roughness. This work represents the final phase of the study and it was not expected that this would be fully completed. The application of the data to this end has been attempted and the following section outlines the development of a simplified approach to flow rate prediction for the case when openings are restricted to the front and rear walls.

5.0 A SIMPLIFIED APPROACH TO FLOW RATE PREDICTION

The pressure data for the 16 ft. building in open country were employed to compute the flow rates with equal openings in front and rear walls. The flow coefficients were computed for a total fictitious opening in both front and back walls ($\sum A_o$) such that;

$$\frac{\sum C_d A_o}{A} = 1.0$$

where; A = frontal wall area
C_d = discharge coefficient

The flow coefficient, C_Q, for this situation is defined by,

Q	=	$C_Q \cdot A \cdot V$
V	=	wind speed at eaves level

Two values of Q were computed as follows;

Q_{in}	=	$C_{QI} \cdot A \cdot V$
	=	total INFLOW into the building
	=	$\sum \Delta Q$, where the summation is over <u>all</u> openings for which the flow in inward.
Q_c	=	$C_{Qc} \cdot A \cdot V$
	=	the cross-flow in the building
	=	$\sum \Delta Q$, where the summation is the algebraic sum of the flows on the front face;

ie. Q_c = net flow into the building from the front face
= net flow out of the building from the rear face.

The computed values of C_{QI} and C_{QA} are shown in Figs. 5.1 and 5.2. C_{QI} and C_{QA} were computed for seven different distributions of the open area as shown in Table 5.1.

TABLE 5.1

Pattern of Openings for Flow Calculations

1	2	3	4	5	6
7	8	9	10	11	12
13	14	15	16	17	18

Face Viewed From Up-Wind

Case 1:	$C_d A_o = 1/18$	for all 18 regions
Case 2:	$C_d A_o = 1/6$	for regions 1,2,3,4,5 & 6 and zero elsewhere
Case 3:	$C_d A_o = 1/6$	for regions 7,8,9,10,11 & 12 and zero elsewhere
Case 4:	$C_d A_o = 1/6$	for regions 13,14,15,16,17 & 18 and zero elsewhere

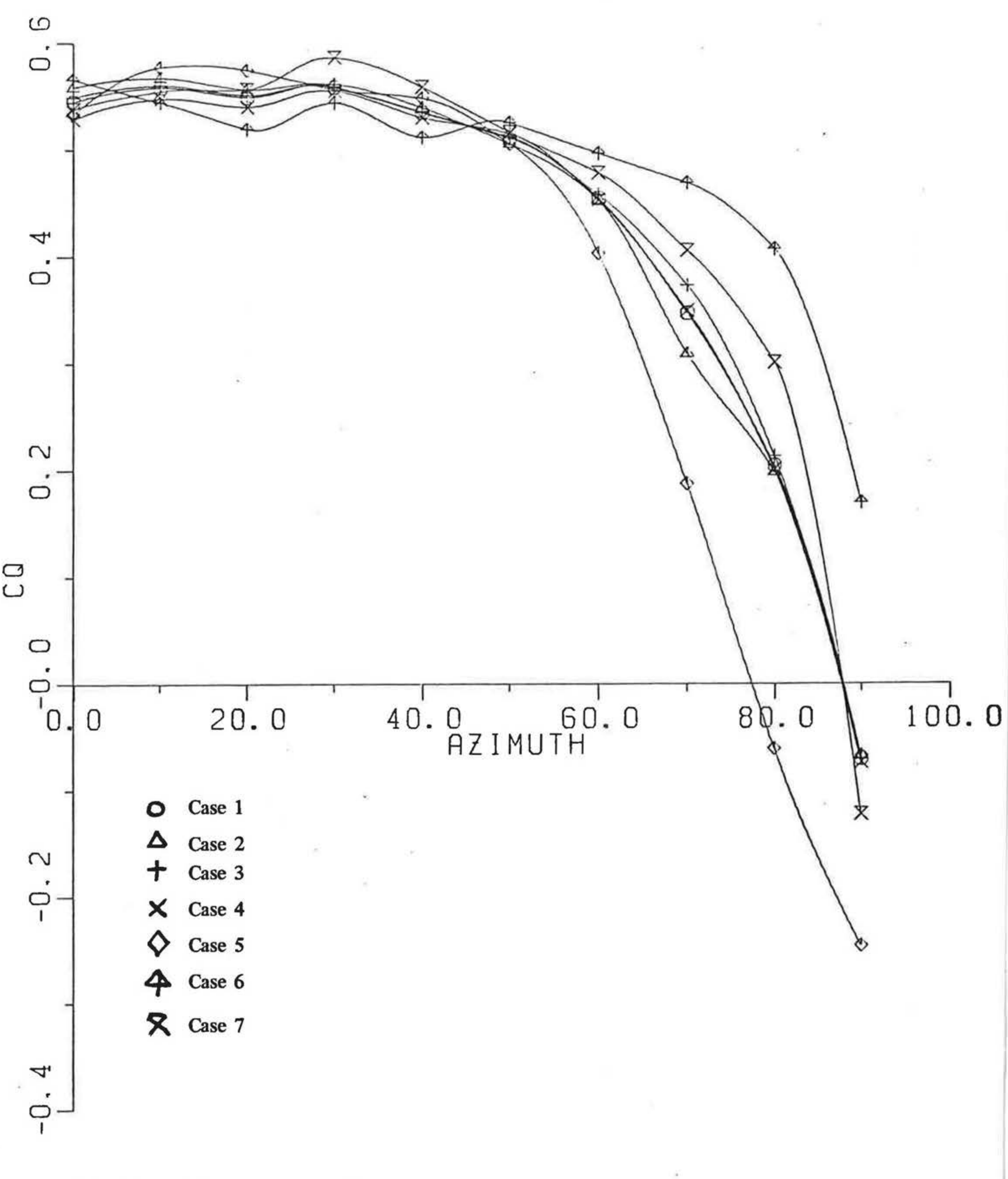

FIG. 5.1 COMPUTED CROSS–FLOW COEFFICIENTS

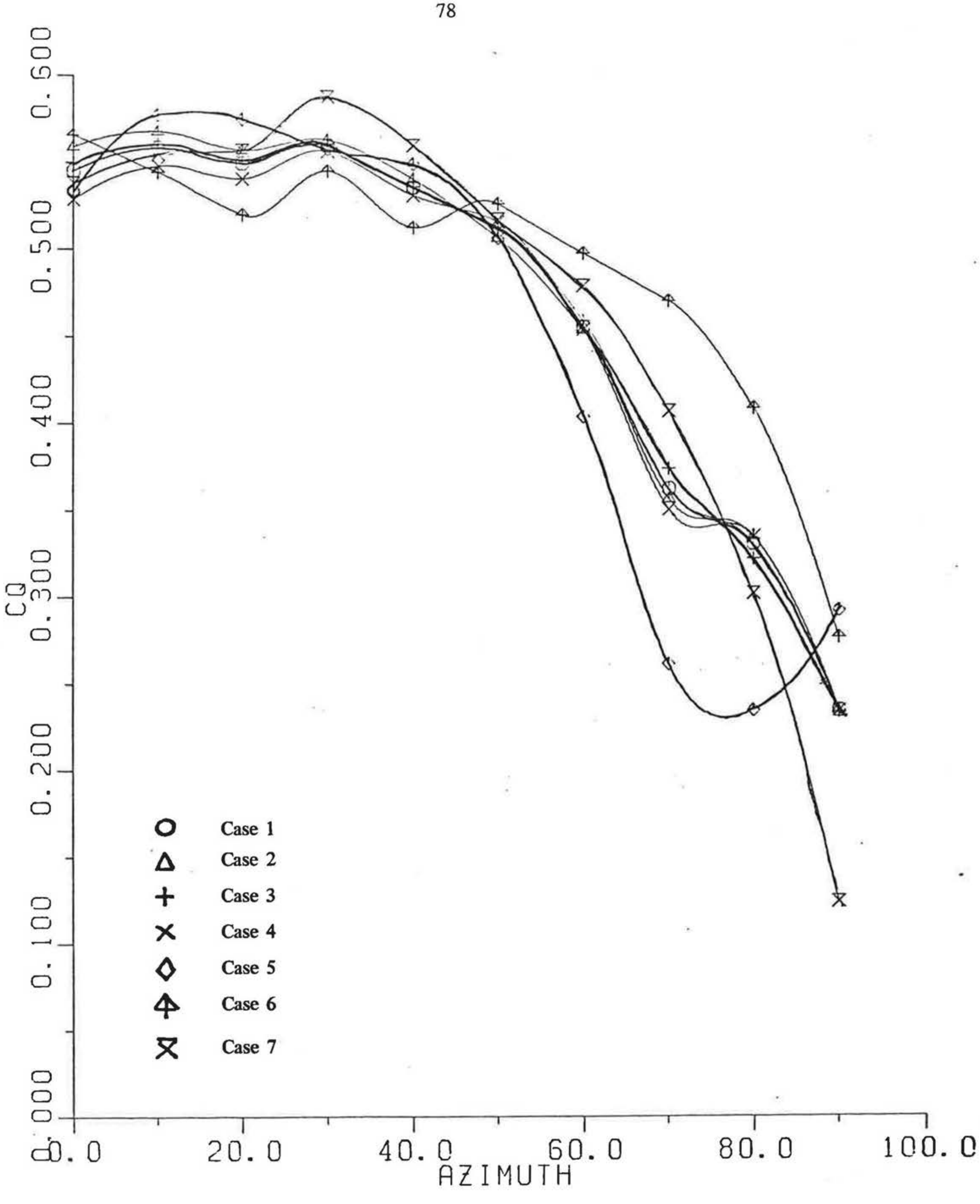

FIG. 5.2 COMPUTED IN–FLOW COEFFICIENTS

Case 5:	$C_d A_o = 1/6$	for regions 1,2,7,8,13 & 14 and zero elsewhere
Case 6:	$C_d A_o = 1/6$	for regions 3,4,9,10,15 & 16 and zero elsewhere
Case 7:	$C_d A_o = 1/6$	for regions 5,6,11,12,17 & 18 and zero elsewhere

From Figs. 5.1 and 5.2 it can be observed that for wind directions from 0-60°;

(i) the value of C_Q varies only slightly with the positioning of the openings; the typical variation is roughly ±5%.

and

(ii) the values of C_{QI} and C_{Qc} are virtually identical which indicates very little if any outflow on the front wall.

For wind angles from 60° to 90° the cross-flow (C_{Qc}) drops rapidly to zero and there are very substantial variations with the positioning of the openings. While C_{QI} also reduces markedly it reaches a minimum value at 90° which is roughly half the maximum value near 0°. This indicates that a large proportion of the inflow exits via the same wall, ie, the internal flows are generated by pressure gradients on a given face as well as by pressure differences between faces.

The average variation of C_{QI} and C_{Qc} with the wind angle is well represented by the simple algebraic expressions;

$$C_{Qc} = 0.56\,(1 - (\theta/90)^4) \qquad (5.1)$$

$$C_{QI} = 0.23 + 0.33\,(1 - (\theta/90)^3) \qquad (5.2)$$

The actual flow through a building with equal areas on the front and rear walls can be estimated as follows;

$$Q_c = A \cdot V \cdot \frac{(\sum C_d A_o)/A \cdot C_{Qc}}{1 + (\sum C_d A_o/A) \cdot C_{Qc}}$$

$$C_{Qc} = 0.56\,(1 - (\theta/90)^4)$$

<u>**Example 1:**</u>

A building with a frontal area of 16' x 80' has openings in the front and rear faces which total 500 ft ^{2} and have a discharge coefficient of 0.65. If the mean speed at eaves level is 15 mph the cross-flow with the wind at 45° to the front face is as follows;

$$C_{Qc} = 0.56\,(1 - (45/90)^4) = 0.525$$

$$\sum C_d\, A_o/A = 325/16 \times 80$$

$$= 0.254$$

$$V = 15 \text{ mph} = 22 \text{ fps}$$

$$Q = 16 \times 80 \times 22 \; \frac{0.525 \times 0.254}{1 + 0.525 \times 0.254}$$

$$= 3314 \text{ ft}^3/\text{sec}$$

and the average speed within the building

$$V_{interior} = \frac{3314}{16 \times 80}$$

$$= 2.6 \text{ fps}$$

If the openings in the two faces are not equal the cross-flow can be approximated by computing an effective area per wall $(\sum C_d\, A_o)_e$ given by;

$$(\sum C_d\, A_o)_e = \frac{\sqrt{2}\,(\sum C_d\, A_o)_F}{\sqrt{1 + \beta^2}}$$

where; $$\beta = \frac{(\sum C_d\, A_o)_F}{(\sum C_d\, A_o)_R}$$

and the subscripts F and R refer to the front and rear faces respectively.

<u>Example 2:</u>

If the building in Example 1 has a front face with 500 ft^2 open and a rear face with 250 ft^2 open

$$\frac{(\sum C_d\, A_o)_e}{A} = \frac{\sqrt{2 \times 500 \times 0.65}}{\sqrt{1 + 2^2}} \times \frac{1}{80 \times 16}$$

$$= 0.161$$

and

$$Q = 16 \times 80 \times 22 \times \frac{0.525 \times .161}{1 + .525 \times .161}$$

$$= 2194\ ft^3/sec.$$

In the computation of the flow Q_I at wind directions near 90° the simple adjustment for the lack of equal open areas on the front and rear faces is not possible. Further, the corrections term $(1/(1 + \sum C_d A_o/A \cdot C_{Qc}))$ introduced to allow for the influence of the internal flows on the pressure field is not necessarily valid since this correction was developed from the studies of cross-flow. Notwithstanding the latter statement, it is suggested that this correction term should be maintained since, at present, no better adjustment is available.

6.0 CONCLUSIONS

6.1 Prediction of Internal Flows From External Pressures Measured on a Sealed ("Solid") Model

The study of the internal flows in model buildings led to the following conclusions:

i) At low values of the internal flow coefficient ($C_Q < 0.1$ or a wall porosity less than about 25% on two opposite faces) the internal flows can be predicted from the external pressure distribution measured on a solid or sealed building provided the openings are on walls. The level of accuracy that can be achieved (given reliable pressure data and reliable estimates of the discharge coefficients) is, typically, 10%.

ii) If a simple correction term is added to account for the influence of the "through-flow" on the pressure field then the internal flows can be predicted with acceptable accuracy (about 10%) for values of C_Q up to about 0.3 which, for openings on two walls, corresponds to a wall porosity of about 70%.

iii) If openings are provided near the ridge line the venting of flow into the wake appears to have a marked influence on the pressure field with the result that internal flows are severely overestimated. This is undoubtedly an area for further study but the results obtained on the two models examined suggest that the actual internal flows generated by ridge vents may only attain 60% to 70% of those predicted from the external pressures measured on a sealed building. It was noted that flow rates corresponding to values of C_Q as low as 0.03 were poorly predicted but that the errors did not increase strongly with increasing C_Q as was observed for wall openings.

6.2 External Pressure Distributions on Low-Rise Buildings

The pressure data gathered in previous studies of wind loads on low-rise buildings was re-organized and presented in a form suited to the computation of internal flows in such structures. The data presented covers typical industrial building geometries with eaves heights from 16' to 32', roof slopes from 1:12 to 12:12 and two levels of terrain roughness.

6.3 The Development of Design Aids for Naturally Ventilated Structures

This final phase of the investigation is still in progress. In the proposal describing the planned study it was noted that progress in this final phase would be limited by the time available for the investigation. A simple approach has been developed for the prediction of the cross-flow in a building with openings in the front and rear walls and the application of this approach has been illustrated with examples. Work in this area will continue with support from other funding sources but the complete results are unlikely to be available before late 1983.

APPENDIX I

TABULATED INTERNAL FLOW MEASUREMENTS

FILE NAME	DESCRIPTION			
	FRONT WALL OPENING	REAR WALL OPENING	RIDGE VENT.	
CAK22	Removed	Removed	NIL	BASIC MODEL
CAK24	4" x 1"	4" x 1"	"	
CAK25	3.2" x 0.8"	3.2" x 0.8"	"	
CAK26	24 @ 3/8"ϕ	24 @ 3/8"ϕ	"	
CAK27	24 @ 1/4"ϕ	24 @ 1/4"ϕ	"	
CAK28	24 @ 3/16"ϕ	24 @ 3/16"ϕ	"	
CAK29	24 @ 1/8"ϕ	24 @ 1/8"ϕ	"	
CAK30	24 @ 3/32"ϕ	24 @ 3/32"ϕ	"	
CAK31	24 @ 1/8"ϕ	NIL	1/8" SLOT	
CAK32	24 @ 3/16"ϕ	"	1/8" SLOT	
CAK33	24 @ 3/16"ϕ	"	1/4" SLOT	
CAK34	24 @ 1/4"ϕ	"	1/4" SLOT	
CAK35	24 @ 1/4"ϕ	"	1/2" SLOT	
CAK36	24 @ 3/8"ϕ	"	1/2" SLOT	
CAK37	Removed	Removed	NIL	WINGS ADDED
CAK38	4" x 1"	4" x 1"	"	
CAK39	3.2" x 0.8"	3.2" x 0.8"	"	
CAK40	24 @ 3/8"ϕ	24 @ 3/8"ϕ	"	
CAK41	24 @ 1/4"ϕ	24 @ 1/4"ϕ	"	
CAK42	24 @ 3/16"ϕ	24 @ 3/16"ϕ	"	
CAK43	24 @ 1/8"ϕ	24 @ 1/8"ϕ	"	
CAK44	24 @ 3/32"ϕ	24 @ 3/32"ϕ	"	
CAK45	24 @ 1/8"ϕ	NIL	1/8" SLOT	
CAK46	24 @ 3/16"ϕ	"	1/8" SLOT	
CAK47	24 @ 3/16"ϕ	"	1/4" SLOT	
CAK48	24 @ 1/4"ϕ	"	1/4" SLOT	
CAK49	24 @ 1/4"ϕ	"	1/2" SLOT	
CAK50	24 @ 3/8"ϕ	"	1/2" SLOT	

FILE CAK23

	Delta P psf(10**-3)	Cd	Q cu.ft/s	CQe	Vg ft/s	Ve ft/s
Azimuth = 0	-383.9600	0.7325	0.3679	0.33292	45.33	28.29
Azimuth = 10	-351.9360	0.7325	0.3499	0.31751	45.21	28.21
Azimuth = 20	-307.3200	0.7320	0.3260	0.29585	45.31	28.27
Azimuth = 30	-231.5280	0.7313	0.3124	0.28345	45.22	28.22
Azimuth = 40	-234.1040	0.7275	0.2834	0.25640	45.35	28.30
Azimuth = 50	-177.3200	0.7225	0.2450	0.22220	45.23	28.23
Azimuth = 60	-92.6640	0.7400	0.1814	0.16459	45.21	28.21
Azimuth = 70	-22.9840	0.7875	0.0961	0.08729	45.18	28.19
Azimuth = 80	-2.0800	0.7150	0.0263	0.02383	45.21	28.21
Azimuth = 90	-0.8320	0.6000	0.0139	0.01264	45.22	28.22

FILE CAK24

	Delta P psf(10**-3)	Cd	Q cu.ft/s	CQe	Vg ft/s	Ve ft/s
Azimuth = 0	-338.5200	0.7325	0.3432	0.31174	45.16	28.18
Azimuth = 10	-300.4560	0.7318	0.3230	0.29425	45.03	28.10
Azimuth = 20	-263.3600	0.7313	0.3056	0.27854	45.01	28.09
Azimuth = 30	-233.4720	0.7288	0.2866	0.26094	45.07	28.13
Azimuth = 40	-186.9830	0.7231	0.2517	0.22911	45.07	28.13
Azimuth = 50	-145.9120	0.7250	0.2230	0.20297	45.07	28.13
Azimuth = 60	-71.8640	0.7500	0.1619	0.14729	45.09	28.14
Azimuth = 70	-22.7760	0.7875	0.0957	0.08712	45.06	28.12
Azimuth = 80	-3.2240	0.7138	0.0326	0.02970	45.08	28.13
Azimuth = 90	-0.5200	0.6400	0.0118	0.01071	45.01	28.09

FILE CAK25

	Delta P psf(10**-3)	Cd	Q cu.ft/s	CQe	Vg ft/s	Ve ft/s
Azimuth = 0	-118.5600	0.7300	0.2024	0.18394	45.14	28.17
Azimuth = 10	-114.6080	0.7313	0.1994	0.18093	45.20	28.21
Azimuth = 20	-113.1520	0.7325	0.1984	0.17999	45.22	28.22
Azimuth = 30	-114.1920	0.7313	0.1990	0.18112	45.07	28.13
Azimuth = 40	-101.1200	0.7350	0.1889	0.17179	45.12	28.16
Azimuth = 50	-80.4960	0.7450	0.1702	0.15498	45.05	28.11
Azimuth = 60	-55.3680	0.7613	0.1455	0.13209	45.20	28.21
Azimuth = 70	-30.7640	0.7875	0.1103	0.10012	45.20	28.21
Azimuth = 80	-5.2400	0.7250	0.0461	0.04195	45.10	28.15
Azimuth = 90	-0.5240	0.6575	0.0132	0.01201	45.16	28.18

FILE CAK26

	Delta P psf(10**-3)	Cd	Q cu.ft/s	CQe	Vg ft/s	Ve ft/s
Azimuth = 0	-114.2960	0.7313	0.1991	0.18088	45.15	28.18
Azimuth = 10	-108.4720	0.7338	0.1946	0.17701	45.10	28.15
Azimuth = 20	-112.0080	0.7325	0.1974	0.17940	45.14	28.17
Azimuth = 30	-103.3760	0.7350	0.1903	0.17308	45.10	28.15
Azimuth = 40	-87.1520	0.7425	0.1765	0.16076	45.04	28.11
Azimuth = 50	-63.3360	0.7313	0.1482	0.13459	45.17	28.19
Azimuth = 60	-38.5840	0.7825	0.1238	0.11243	45.16	28.18
Azimuth = 70	-14.6640	0.7375	0.0719	0.06554	45.01	28.09
Azimuth = 80	-2.4960	0.6075	0.0244	0.02227	45.02	28.10
Azimuth = 90	-0.3120	0.6175	0.0088	0.00800	45.06	28.12

FILE CAK27

	Delta P psf(10**-3)	Cd	Q cu.ft/s	CQe	Vg ft/s	Ve ft/s
Azimuth = 0	-21.4656	0.7375	0.0870	0.07874	45.33	28.29
Azimuth = 10	-19.8016	0.7375	0.0836	0.07571	45.28	28.26
Azimuth = 20	-21.0704	0.7375	0.0862	0.07808	45.29	28.26
Azimuth = 30	-22.2352	0.7375	0.0886	0.08014	45.33	28.29
Azimuth = 40	-21.6736	0.7375	0.0874	0.07926	45.25	28.24
Azimuth = 50	-17.7112	0.7363	0.0789	0.07138	45.35	28.30
Azimuth = 60	-12.2512	0.7375	0.0657	0.05954	45.29	28.26
Azimuth = 70	-6.0944	0.7250	0.0456	0.04127	45.30	28.27
Azimuth = 80	-0.3776	0.6350	0.0172	0.01560	45.34	28.29
Azimuth = 90	0.1248	0.5750	0.0052	0.00469	45.27	28.25

FILE CAK28

	Delta P psf(10**-3)	Cd	Q cu.ft/s	CQe	Vg ft/s	Ve ft/s
Azimuth = 0	-5.9032	0.7250	0.0445	0.04029	45.28	28.26
Azimuth = 10	-5.3976	0.7225	0.0427	0.03869	45.32	28.28
Azimuth = 20	-5.6264	0.7238	0.0437	0.03954	45.36	28.31
Azimuth = 30	-6.3232	0.7263	0.0465	0.04206	45.36	28.31
Azimuth = 40	-6.0632	0.7250	0.0455	0.04124	45.22	28.22
Azimuth = 50	-4.9132	0.7213	0.0407	0.03695	45.23	28.23
Azimuth = 60	-3.3250	0.7150	0.0332	0.03009	45.28	28.26
Azimuth = 70	-2.0696	0.7150	0.0262	0.02374	45.27	28.25
Azimuth = 80	-0.3536	0.6250	0.0075	0.00857	45.30	28.27
Azimuth = 90	0.1248	0.5750	0.0052	0.00468	45.33	28.29

FILE CAK29

	Delta P psf(10**-3)	Cd	Q cu.ft/s	CQe	Vg ft/s	Ve ft/s
Azimuth = 0	-0.8940	0.6775	0.0162	0.01468	45.33	28.29
Azimuth = 10	-0.8320	0.6750	0.0157	0.01419	45.31	28.27
Azimuth = 20	-0.8320	0.6750	0.0157	0.01416	45.41	28.34
Azimuth = 30	-0.6344	0.6575	0.0133	0.01206	45.36	28.31
Azimuth = 40	-0.8424	0.6750	0.0158	0.01429	45.29	28.26
Azimuth = 50	-0.6136	0.6525	0.0130	0.01178	45.34	28.29
Azimuth = 60	-0.3744	0.6250	0.0097	0.00880	45.38	28.32
Azimuth = 70	-0.1040	0.3000	0.0025	0.00223	45.38	28.32
Azimuth = 80	0.1144	0.3000	0.0026	0.00234	45.23	28.23
Azimuth = 90	0.2288	0.6050	0.0074	0.00667	45.32	28.28

FILE CAK30

	Delta P psf(10**-3)	Cd	Q cu.ft/s	CQe	Vg ft/s	Ve ft/s
Azimuth = 0	-0.1352	0.4050	0.0038	0.00343	45.36	28.31
Azimuth = 10	-0.1664	0.4980	0.0052	0.00467	45.40	28.33
Azimuth = 20	-0.2080	0.6025	0.0070	0.00632	45.39	28.32
Azimuth = 30	-0.1976	0.5940	0.0067	0.00608	45.33	28.29
Azimuth = 40	-0.1456	0.4380	0.0043	0.00385	45.39	28.32
Azimuth = 50	-0.0936	0.2820	0.0022	0.00199	45.34	28.29
Azimuth = 60	-0.0312	0.0930	0.0004	0.00038	45.40	28.33
Azimuth = 70	0.1664	0.4980	0.0052	0.00468	45.34	28.29
Azimuth = 80	0.1768	0.5310	0.0057	0.00515	45.33	28.29
Azimuth = 90	0.2288	0.6150	0.0075	0.00677	45.36	28.31

FILE CAK31

	Delta P psf(10**-3)	Cd	Q cu.ft/s	CQe	Vg ft/s	Ve ft/s
Azimuth = 0	-1.3624	0.7025	0.0209	0.01875	45.69	28.51
Azimuth = 10	-1.3104	0.7013	0.0204	0.01833	45.74	28.54
Azimuth = 20	-1.3520	0.7025	0.0208	0.01866	45.73	28.54
Azimuth = 30	-1.5912	0.7100	0.0228	0.02046	45.73	28.53
Azimuth = 40	-1.4768	0.7075	0.0219	0.01967	45.67	28.50
Azimuth = 50	-1.2376	0.7000	0.0198	0.01783	45.62	28.47
Azimuth = 60	-0.9632	0.6750	0.0160	0.01436	45.63	28.47
Azimuth = 70	-0.4264	0.6350	0.0106	0.00948	45.70	28.51
Azimuth = 80	0.0104	0.0310	0.0001	0.00007	45.64	28.48
Azimuth = 90	0.0832	0.2490	0.0018	0.00165	45.59	28.45

FILE CAK32

	Delta P psf(10**-3)	Cd	Q cu.ft/s	CQe	Vg ft/s	Ve ft/s
Azimuth = 0	-3.7336	0.7163	0.0352	0.03165	45.69	28.51
Azimuth = 10	-3.6712	0.7163	0.0349	0.03145	45.59	28.45
Azimuth = 20	-3.7024	0.7113	0.0349	0.03138	45.57	28.43
Azimuth = 30	-4.0768	0.7175	0.0369	0.03318	45.62	28.47
Azimuth = 40	-4.6334	0.7200	0.0395	0.03562	45.48	28.38
Azimuth = 50	-4.2536	0.7188	0.0377	0.03400	45.55	28.42
Azimuth = 60	-3.1720	0.7138	0.0324	0.02918	45.52	28.40
Azimuth = 70	-1.6848	0.7113	0.0235	0.02119	45.51	28.40
Azimuth = 80	-0.1248	0.3744	0.0034	0.00304	45.51	28.40
Azimuth = 90	0.1456	0.4368	0.0042	0.00383	45.44	28.35

FILE CAK33

	Delta P psf(10**-3)	Cd	Q cu.ft/s	CQe	Vg ft/s	Ve ft/s
Azimuth = 0	-6.6040	0.7275	0.0476	0.04293	45.49	28.39
Azimuth = 10	-6.4438	0.7263	0.0470	0.04251	45.39	28.32
Azimuth = 20	-6.2712	0.7258	0.0463	0.04178	45.45	28.36
Azimuth = 30	-6.3856	0.7263	0.0467	0.04215	45.49	28.39
Azimuth = 40	-7.1240	0.7288	0.0495	0.04481	45.35	28.30
Azimuth = 50	-6.4430	0.7263	0.0470	0.04249	45.34	28.29
Azimuth = 60	-4.9296	0.7213	0.0408	0.03683	45.43	28.35
Azimuth = 70	-2.8286	0.7125	0.0305	0.02759	45.37	28.31
Azimuth = 80	-0.5824	0.6500	0.0126	0.01141	45.42	28.34
Azimuth = 90	-0.0936	0.2808	0.0022	0.00198	45.28	28.26

FILE CAK34

	Delta P psf(10**-3)	Cd	Q cu.ft/s	CQe	Vg ft/s	Ve ft/s
Azimuth = 0	-12.6048	0.7375	0.0667	0.06021	45.43	28.35
Azimuth = 10	-12.5632	0.7375	0.0656	0.06024	45.33	28.29
Azimuth = 20	-11.5128	0.7375	0.0637	0.05768	45.32	28.28
Azimuth = 30	-11.9496	0.7375	0.0649	0.05878	45.31	28.27
Azimuth = 40	-13.1632	0.7375	0.0699	0.06335	45.28	28.26
Azimuth = 50	-13.2496	0.7375	0.0684	0.06195	45.27	28.25
Azimuth = 60	-10.7640	0.7363	0.0615	0.05571	45.30	28.27
Azimuth = 70	-5.9592	0.7250	0.0451	0.04084	45.27	28.25
Azimuth = 80	-1.1856	0.6950	0.0193	0.01747	45.26	28.24
Azimuth = 90	-0.1768	0.5304	0.0057	0.00514	45.30	28.27

FILE CAK35

	Delta P psf(10**-3)	Cd	Q cu.ft/s	CQe	Vg ft/s	Ve ft/s
Azimuth = 0	-26.3536	0.7338	0.0959	0.08677	45.35	28.30
Azimuth = 10	-25.6048	0.7338	0.0946	0.08572	45.25	28.24
Azimuth = 20	-23.7432	0.7350	0.0912	0.08253	45.33	28.29
Azimuth = 30	-21.9024	0.7375	0.0879	0.07973	45.22	28.22
Azimuth = 40	-22.5368	0.7375	0.0892	0.08089	45.21	28.21
Azimuth = 50	-21.9648	0.7375	0.0830	0.07976	45.27	28.25
Azimuth = 60	-17.6800	0.7363	0.0788	0.07144	45.27	28.25
Azimuth = 70	-10.2440	0.7363	0.0600	0.05445	45.21	28.21
Azimuth = 80	-2.9392	0.7125	0.0306	0.02778	45.14	28.17
Azimuth = 90	-0.9048	0.6800	0.0165	0.01498	45.09	28.14

FILE CAK36

	Delta P psf(10**-3)	Cd	Q cu.ft/s	CQe	Vg ft/s	Ve ft/s
Azimuth = 0	-62.4000	0.7598	0.1526	0.13877	45.12	28.16
Azimuth = 10	-61.7760	0.7589	0.1519	0.13795	45.16	28.18
Azimuth = 20	-56.7840	0.7613	0.1461	0.13278	45.13	28.16
Azimuth = 30	-50.6440	0.7675	0.1391	0.12670	45.03	28.10
Azimuth = 40	-50.9560	0.7675	0.1394	0.12699	45.02	28.10
Azimuth = 50	-47.4240	0.7700	0.1350	0.12290	45.07	28.13
Azimuth = 60	-35.4640	0.7850	0.1190	0.10856	44.99	28.07
Azimuth = 70	-13.0960	0.7363	0.0798	0.07271	45.00	28.08
Azimuth = 80	-4.5760	0.7200	0.0392	0.03567	45.10	28.15
Azimuth = 90	-0.3320	0.6738	0.0157	0.01429	44.95	28.05

FILE CAK37

	Delta P psf(10**-3)	Cd	Q cu.ft/s	CQe	Vg ft/s	Ve ft/s
Azimuth = 0	-314.0800	0.7325	0.3306	0.30080	45.08	28.13
Azimuth = 10	-283.8160	0.7313	0.3137	0.28535	45.10	28.15
Azimuth = 20	-246.1680	0.7300	0.2917	0.26545	45.07	28.13
Azimuth = 30	-222.4560	0.7263	0.2758	0.25123	45.04	28.11
Azimuth = 40	-186.0560	0.7231	0.2512	0.22845	45.10	28.15
Azimuth = 50	-113.9760	0.7300	0.2028	0.18442	45.10	28.15
Azimuth = 60	-48.3600	0.7700	0.1364	0.12388	45.15	28.18
Azimuth = 70	-13.3320	0.7375	0.0698	0.06354	45.09	28.14
Azimuth = 80	-2.6090	0.7113	0.0292	0.02661	45.03	28.10
Azimuth = 90	-0.7230	0.6563	0.0145	0.01318	45.05	28.11

FILE CAK38

	Delta P psf(10**-3)	Cd	Q cu.ft/s	CQe	Vg ft/s	Ve ft/s
Azimuth = 0	-262.3920	0.7313	0.3016	0.27455	45.07	28.13
Azimuth = 10	-240.4480	0.7288	0.2878	0.26203	45.05	28.11
Azimuth = 20	-203.8720	0.7250	0.2674	0.24391	44.99	28.07
Azimuth = 30	-186.2640	0.7233	0.2514	0.22859	45.11	28.15
Azimuth = 40	-148.0950	0.7248	0.2246	0.20452	45.05	28.11
Azimuth = 50	-102.5560	0.7350	0.1898	0.17330	44.94	28.04
Azimuth = 60	-44.6150	0.7750	0.1318	0.12006	45.04	28.11
Azimuth = 80	-2.6000	0.7113	0.0292	0.02658	45.08	28.13
Azimuth = 90	-0.4160	0.6300	0.0103	0.00943	45.02	28.10

FILE CAK39

	Delta P psf(10**-3)	Cd	Q cu.ft/s	CQe	Vg ft/s	Ve ft/s
Azimuth = 0	-93.9120	0.7388	0.1823	0.16612	45.02	28.10
Azimuth = 10	-94.4320	0.7388	0.1828	0.16643	45.06	28.12
Azimuth = 20	-103.3760	0.7350	0.1903	0.17328	45.05	28.11
Azimuth = 30	-105.8720	0.7338	0.1923	0.17515	45.03	28.10
Azimuth = 40	-97.1360	0.7375	0.1851	0.16887	44.97	28.06
Azimuth = 50	-81.3230	0.7450	0.1711	0.15595	45.00	28.08
Azimuth = 60	-45.2400	0.7750	0.1327	0.12097	45.01	28.09
Azimuth = 70	-15.4950	0.7370	0.0739	0.06731	45.02	28.10
Azimuth = 80	-3.0160	0.7125	0.0315	0.02872	45.00	28.08
Azimuth = 90	-0.5200	0.6425	0.0118	0.01077	44.96	28.05

FILE CAK40

	Delta P psf(10**-3)	Cd	Q cu.ft/s	CQe	Vg ft/s	Ve ft/s
Azimuth = 0	-101.4000	0.7356	0.1886	0.17202	44.99	28.07
Azimuth = 10	-105.5640	0.7338	0.1921	0.17463	45.12	28.16
Azimuth = 20	-106.4960	0.7339	0.1928	0.17562	45.04	28.11
Azimuth = 30	-100.4640	0.7363	0.1879	0.17112	45.05	28.11
Azimuth = 40	-84.7600	0.7425	0.1741	0.15843	45.07	28.13
Azimuth = 50	-61.5630	0.7581	0.1515	0.13802	45.02	28.10
Azimuth = 60	-33.0720	0.7956	0.1150	0.10489	45.00	28.08
Azimuth = 70	-13.2030	0.7375	0.0683	0.06228	44.96	28.05
Azimuth = 80	-2.3920	0.7125	0.0281	0.02559	44.99	28.07
Azimuth = 90	-0.4160	0.6313	0.0104	0.00946	44.99	28.07

FILE CAK41

	Delta P psf(10**-3)	Cd	Q cu.ft/s	CQe	Vg ft/s	Ve ft/s
Azimuth = 0	-19.1568	0.7363	0.0821	0.07423	45.35	28.30
Azimuth = 10	-19.6758	0.7369	0.0832	0.07536	45.31	28.27
Azimuth = 20	-21.0288	0.7375	0.0861	0.07789	45.36	28.31
Azimuth = 30	-21.3236	0.7363	0.0876	0.07935	45.29	28.26
Azimuth = 40	-23.0048	0.7363	0.0899	0.08147	45.28	28.26
Azimuth = 50	-19.7030	0.7363	0.0832	0.07554	45.20	28.21
Azimuth = 60	-13.5032	0.7375	0.0693	0.06263	45.37	28.31
Azimuth = 70	-5.7720	0.7250	0.0444	0.04023	45.23	28.23
Azimuth = 80	-1.2376	0.6975	0.0198	0.01792	45.23	28.23
Azimuth = 90	-0.1768	0.5304	0.0057	0.00514	45.31	28.27

FILE CAK42

	Delta P psf(10**-3)	Cd	Q cu.ft/s	CQe	Vg ft/s	Ve ft/s
Azimuth = 0	-5.4912	0.7231	0.0431	0.03904	45.34	28.29
Azimuth = 10	-5.7408	0.7240	0.0442	0.03998	45.32	28.28
Azimuth = 20	-6.1934	0.7253	0.0460	0.04166	45.31	28.27
Azimuth = 30	-6.3744	0.7275	0.0486	0.04400	45.29	28.26
Azimuth = 40	-7.4256	0.7298	0.0506	0.04598	45.18	28.19
Azimuth = 50	-6.4480	0.7263	0.0470	0.04262	45.23	28.23
Azimuth = 60	-4.7216	0.7205	0.0399	0.03614	45.25	28.24
Azimuth = 70	-1.3760	0.7150	0.0256	0.02317	45.31	28.27
Azimuth = 80	-0.2704	0.6125	0.0081	0.00735	45.27	28.25
Azimuth = 90	-0.1560	0.3432	0.0035	0.00313	45.24	28.23

FILE CAK43

	Delta P psf(10**-3)	Cd	Q cu.ft/s	CQe	Vg ft/s	Ve ft/s
Azimuth = 0	-0.8736	0.6775	0.0161	0.01456	45.43	28.35
Azimuth = 10	-0.8008	0.6725	0.0153	0.01384	45.42	28.34
Azimuth = 20	-0.9360	0.6825	0.0166	0.01521	45.34	28.29
Azimuth = 30	-1.0920	0.6913	0.0184	0.01661	45.44	28.35
Azimuth = 40	-1.1752	0.6963	0.0192	0.01737	45.40	28.33
Azimuth = 50	-1.0296	0.6881	0.0178	0.01608	45.36	28.31
Azimuth = 60	-0.6448	0.6575	0.0134	0.01215	45.40	28.33
Azimuth = 70	-0.1456	0.4368	0.0042	0.00394	45.30	28.27
Azimuth = 80	0.2392	0.6075	0.0076	0.00684	45.36	28.31
Azimuth = 90	0.2912	0.6150	0.0085	0.00765	45.34	28.29

FILE CAK44

	Delta P psf(10**-3)	Cd	Q cu.ft/s	CQe	Vg ft/s	Ve ft/s
Azimuth = 0	-0.1768	0.5304	0.0057	0.00512	45.47	28.37
Azimuth = 10	-0.1664	0.4992	0.0052	0.00467	45.51	28.40
Azimuth = 20	-0.1664	0.4992	0.0052	0.00467	45.58	28.44
Azimuth = 30	-0.2912	0.6150	0.0085	0.00761	45.55	28.42
Azimuth = 40	-0.3120	0.6175	0.0088	0.00791	45.57	28.43
Azimuth = 50	-0.3224	0.6225	0.0090	0.00810	45.57	28.43
Azimuth = 60	-0.1352	0.4056	0.0038	0.00342	45.54	28.42
Azimuth = 70	0.0208	0.0624	0.0002	0.00021	45.57	28.43
Azimuth = 80	0.1768	0.5304	0.0057	0.00512	45.49	28.39
Azimuth = 90	0.2288	0.6025	0.0073	0.00661	45.57	28.43

FILE CAK45

	Delta P psf(10**-3)	Cd	Q cu.ft/s	CQe	Vg ft/s	Ve ft/s
Azimuth = 0	-1.5600	0.7083	0.0225	0.02032	45.52	28.40
Azimuth = 10	-1.6432	0.7109	0.0232	0.02080	45.75	28.55
Azimuth = 20	-1.9240	0.7150	0.0253	0.02267	45.71	28.52
Azimuth = 30	-2.1840	0.7148	0.0269	0.02416	45.68	28.50
Azimuth = 40	-2.5168	0.7100	0.0287	0.02579	45.63	28.47
Azimuth = 50	-2.1944	0.7150	0.0270	0.02429	45.55	28.42
Azimuth = 60	-1.9136	0.7150	0.0252	0.02265	45.63	28.47
Azimuth = 70	-0.3640	0.6850	0.0164	0.01477	45.56	28.43
Azimuth = 80	-0.1768	0.5304	0.0057	0.00512	45.49	28.39
Azimuth = 90	0.0624	0.1872	0.0012	0.00108	45.44	28.35

FILE CAK46

	Delta P psf(10**-3)	Cd	Q cu.ft/s	CQe	Vg ft/s	Ve ft/s
Azimuth = 0	-4.2224	0.7183	0.0376	0.03390	45.48	28.38
Azimuth = 10	-4.4824	0.7200	0.0388	0.03500	45.50	28.39
Azimuth = 20	-4.7632	0.7213	0.0401	0.03624	45.38	28.32
Azimuth = 30	-5.2416	0.7225	0.0421	0.03809	45.36	28.31
Azimuth = 40	-5.7200	0.7240	0.0441	0.03989	45.34	28.29
Azimuth = 50	-5.2416	0.7225	0.0421	0.03814	45.30	28.27
Azimuth = 60	-4.4408	0.7194	0.0386	0.03494	45.33	28.29
Azimuth = 70	-2.0696	0.7145	0.0262	0.02368	45.34	28.29
Azimuth = 80	-0.3120	0.6175	0.0098	0.00795	45.32	28.28
Azimuth = 90	0.0000	0.0000	0.0000	0.00000	45.23	28.23

FILE CAK47

	Delta P psf(10**-3)	Cd	Q cu.ft/s	CQe	Vg ft/s	Ve ft/s
Azimuth = 0	-7.3112	0.7288	0.0502	0.04545	45.29	28.26
Azimuth = 10	-7.7584	0.7300	0.0518	0.04696	45.23	28.23
Azimuth = 20	-8.4448	0.7325	0.0542	0.04905	45.33	28.29
Azimuth = 30	-8.6840	0.7325	0.0550	0.04982	45.26	28.24
Azimuth = 40	-9.4432	0.7345	0.0575	0.05211	45.25	28.24
Azimuth = 50	-8.9336	0.7338	0.0558	0.05069	45.20	28.21
Azimuth = 60	-7.2072	0.7288	0.0498	0.04530	45.12	28.16
Azimuth = 70	-3.9416	0.7175	0.0363	0.03293	45.19	28.20
Azimuth = 80	-0.9360	0.6800	0.0168	0.01521	45.17	28.19
Azimuth = 90	-0.1654	0.4992	0.0052	0.00471	45.19	28.20

FILE CAK48

	Delta P psf(10**-3)	Cd	Q cu.ft/s	CQe	Vg ft/s	Ve ft/s
Azimuth = 0	-13.4056	0.7375	0.0688	0.06234	45.25	28.24
Azimuth = 10	-13.9672	0.7375	0.0702	0.06373	45.18	28.19
Azimuth = 20	-14.4664	0.7375	0.0714	0.06501	45.07	28.13
Azimuth = 30	-14.6016	0.7375	0.0718	0.06520	45.15	28.18
Azimuth = 40	-15.1112	0.7375	0.0730	0.06656	45.00	28.08
Azimuth = 50	-15.4128	0.7375	0.0737	0.06700	45.14	28.17
Azimuth = 60	-11.7208	0.7375	0.0643	0.05852	45.07	28.13
Azimuth = 70	-5.1152	0.7256	0.0457	0.04162	45.03	28.10
Azimuth = 80	-1.6744	0.7113	0.0235	0.02138	45.00	28.08
Azimuth = 90	-0.4254	0.6375	0.0106	0.00964	45.12	28.16

FILE CAK49

	Delta P psf(10**-3)	Cd	Q cu.ft/s	CQe	Vg ft/s	Ve ft/s
Azimuth = 0	-26.8736	0.7325	0.0967	0.08772	45.22	28.22
Azimuth = 10	-26.7488	0.7325	0.0965	0.08753	45.21	28.21
Azimuth = 20	-27.2272	0.7331	0.0974	0.08838	45.21	28.21
Azimuth = 30	-26.3744	0.7325	0.0958	0.08688	45.23	28.23
Azimuth = 40	-25.6464	0.7343	0.0947	0.08607	45.13	28.16
Azimuth = 50	-26.3016	0.7345	0.0959	0.08702	45.22	28.22
Azimuth = 60	-21.9336	0.7375	0.0880	0.07991	45.15	28.18
Azimuth = 70	-12.9688	0.7375	0.0676	0.06141	45.18	28.19
Azimuth = 80	-3.9416	0.7175	0.0363	0.03297	45.13	28.16
Azimuth = 90	-1.3624	0.7025	0.0209	0.01898	45.12	28.16

FILE CAK50

	Delta P psf(10**-3)	Cd	Q cu.ft/s	CQe	Vg ft/s	Ve ft/s
Azimuth = 0	-63.1200	0.7538	0.1584	0.14372	45.22	28.22
Azimuth = 10	-68.0160	0.7538	0.1583	0.14399	45.10	28.15
Azimuth = 20	-67.0800	0.7538	0.1572	0.14284	45.15	28.18
Azimuth = 30	-60.4240	0.7588	0.1502	0.13695	45.00	28.08
Azimuth = 40	-54.9120	0.7625	0.1435	0.13087	45.10	28.15
Azimuth = 50	-49.9200	0.7688	0.1383	0.12578	45.11	28.15
Azimuth = 60	-37.8560	0.7838	0.1228	0.11189	45.02	28.10
Azimuth = 70	-20.1760	0.7363	0.0842	0.07679	45.00	28.08
Azimuth = 80	-5.9280	0.7250	0.0449	0.04095	45.03	28.10
Azimuth = 90	-2.2880	0.7125	0.0274	0.02497	45.08	28.13